



Search for neutral long-lived particles that decay into displaced jets in the ATLAS calorimeter in association with leptons or jets using pp collisions at $\sqrt{s} = 13$ TeV

The ATLAS Collaboration

A search for neutral long-lived particles (LLPs) decaying in the ATLAS hadronic calorimeter using 140 fb^{-1} of proton–proton collisions at $\sqrt{s} = 13$ TeV delivered by the LHC is presented. The analysis is composed of three channels. The first targets pair-produced LLPs, where at least one LLP is produced with sufficiently low boost that its decay products can be resolved as separate jets. The second and third channels target LLPs respectively produced in association with a W or Z boson that decays leptonically. In each channel, different search regions target different kinematic regimes, to cover a broad range of LLP mass hypotheses and models. No excesses of events relative to the background predictions are observed. Higgs boson branching fractions to pairs of hadronically decaying neutral LLPs larger than 1% are excluded at 95% confidence level for proper decay lengths in the range of 30 cm to 4.5 m depending on the LLP mass, a factor of three improvement on previous searches in the hadronic calorimeter. The production of long-lived dark photons in association with a Z boson with cross-sections above 0.1 pb is excluded for dark photon mean proper decay lengths in the range of 20 cm to 50 m, improving previous ATLAS results by an order of magnitude. Finally, long-lived photo-phobic axion-like particle models are probed for the first time by ATLAS, with production cross-sections above 0.1 pb excluded in the 0.1 mm to 10 m range.

Contents

1	Introduction	2
2	The ATLAS detector	4
3	Data and simulated event samples	5
4	Event reconstruction	7
5	Event selection	9
	5.1 CalR+2J channel selection	9
	5.2 CalR+W and CalR+Z channel selections	11
6	Background estimation	14
	6.1 CalR+2J final selection and the ABCDisCo method	15
	6.2 CalR+W and CalR+Z final selections and background estimate	15
7	Systematic uncertainties	17
8	Results and statistical interpretation	19
9	Conclusion	26

1 Introduction

Many extensions to the Standard Model (SM) of particle physics predict new particles whose decays are suppressed by weak coupling constants, small mass differences between particles, or heavy mediators. Such particles can acquire large lifetimes, becoming long-lived particles (LLPs). LLPs are featured in many well-motivated theories including various supersymmetry models [1–6]; neutral naturalness models [7–10] featuring a Hidden Sector (HS) [11–13] that addresses the hierarchy problem; models that seek to incorporate dark matter [14–17], or explain the matter–antimatter asymmetry of the universe [18]; and models including heavy neutrinos [19, 20] that provide an explanation for the origin of light neutrino masses and mixings. Axion-like particles (ALPs), which may help resolve the strong CP problem, are also predicted to be long-lived in some parts of the parameter space [21]. Not only could LLPs provide a novel route to a groundbreaking discovery, but they can also probe regions of common benchmark models [22], such as the two-Higgs doublet model that is widely used to explore dark matter topologies, in regions inaccessible to the wider ATLAS search programme involving prompt particles.

This paper studies electrically neutral LLPs decaying hadronically in the hadronic calorimeter of the ATLAS detector at the Large Hadron Collider (LHC). This corresponds to particles with a lifetime (τ) times the speed of light (c) between a few centimeters and tens of meters. Since the LLPs are neutral, they do not leave any hits in the ATLAS tracking system. Their decay into quarks or gluons, which later hadronise, leads to jets in the calorimeters. For LLPs that decay after the electromagnetic part of the calorimeter, the distribution of energy of the resulting jets differs from that of standard jets, as they have a very low electromagnetic component. This fact can be used to identify displaced jets from SM jets and

other sources of background. The “CalRatio” quantity, representing the ratio of the energy in the hadronic calorimeter to the energy in the electromagnetic calorimeter, can also serve this purpose.

There exist several previous searches for pair-produced neutral LLPs decaying hadronically at the LHC. The search for displaced jets at LHCb in Ref. [23] is sensitive to $c\tau$ values from ~ 1 mm to ~ 0.1 m. The most recent searches by the CMS Collaboration at $\sqrt{s} = 13$ TeV [24–26] involve jets with displaced vertices in the tracking system or muon detectors [27], and are sensitive to $c\tau$ values from ~ 1 mm to ~ 10 m. Previous ATLAS searches at $\sqrt{s} = 13$ TeV looked for displaced vertices in the tracking system [28–30], hadronic calorimeter [31], pairs of reconstructed vertices in the muon spectrometer [32], or the combination of one displaced vertex in the muon spectrometer and one in the inner tracking detector [33]. A search for hadronic decays of LLPs in association with a Z boson was performed by ATLAS in Ref. [34] using early Run 2 data. These ATLAS searches are complementary, and together provide coverage of $c\tau$ values extending from effectively prompt to ~ 200 m.

Previous searches for displaced jets in the calorimeter at ATLAS have found limitations at the level of the trigger. Indeed, if the LLPs are produced without any additional objects (as happens for example for gluon–gluon fusion production of a Higgs boson-like mediator decaying into LLPs), the decay products can often fail to meet minimum energy thresholds required to record the event. This is particularly true in low-mass and low-boost kinematic regimes. The analysis presented in this paper differs from its predecessors insofar as it searches for LLPs decaying into displaced jets in addition to other objects in the event, such as the decay products of W or Z bosons, or resolved jets from another LLP. These differences allow sensitivity to lower decay lengths or to trigger on prompt objects, gaining in trigger efficiency at the cost of a lower production cross-section. The analysis then uses the same displaced jet identification technique as in Ref. [31] to select candidate jets resulting from LLP decays in the calorimeter. These will have large values of the CalRatio variable defined above.

The analysis is split into three channels. The CalRatio + two jets (CalR+2J) channel targets LLPs resulting from gluon–gluon fusion production of the mediator particle in an HS model, leading to two LLPs in the event. One LLP decays in the calorimeter, with its decay products merged into a single displaced jet. The other LLP decays with a short enough decay length and low enough boost to produce two resolved jets from its decay products.

The CalRatio + W boson (CalR+W) and CalRatio + Z boson (CalR+Z) channels target displaced jets produced in association with a SM vector boson. This results, for example, from an HS mediator produced with a SM vector boson or an ALP radiated from a vector boson. In each case, the vector boson’s leptonic decay is exploited.

These different final states require different event selections and triggering strategies. All three channels use the same displaced jet tagger [31]. The main backgrounds for the CalR+2J channel are SM multijets, and non-collision backgrounds (NCBs) such as beam-induced background (BIB) and cosmic rays (although these are ultimately reduced to a negligible level in all channels). The CalR+W and CalR+Z channels have main backgrounds originating from SM processes involving vector bosons produced with jets, and single- or pair-production of top quarks. In all channels, the final background estimate is data-driven (using the likelihood-based ABCD method).

The rest of this document is organised as follows. The ATLAS detector is described in Section 2. The datasets and simulated samples used for the analysis are reported in Section 3. The definitions of the reconstructed objects are provided in Section 4. The selection criteria applied to define each channel are laid out in Section 5. The description of the relevant background sources and how they are evaluated is

available in Section 6. Systematic uncertainties are listed in Section 7. Finally, the statistical analysis and results are reported in Section 8 before the conclusions in Section 9.

2 The ATLAS detector

The ATLAS detector [35] at the LHC covers nearly the entire solid angle around the collision point.¹

It is a multipurpose detector consisting of an inner tracking detector surrounded by a thin superconducting solenoid, electromagnetic and hadronic calorimeters, and a muon spectrometer incorporating three large superconducting toroidal magnets. The inner detector system is immersed in a 2 T axial magnetic field and provides charged-particle tracking in the range of $|\eta| < 2.5$.

The high-granularity silicon pixel detector covers the vertex region and typically provides four measurements per track. The layer closest to the interaction point is known as the insertable B-Layer [36, 37]. The pixel detector is surrounded by the silicon microstrip tracker, which usually provides four three-dimensional measurement points per track. These silicon detectors are complemented by the transition radiation tracker, with coverage up to $|\eta| = 2.0$.

The calorimeter system covers the pseudorapidity range $|\eta| < 4.9$. Within the region $|\eta| < 3.2$, electromagnetic calorimetry is provided by barrel and endcap high-granularity lead/liquid-argon (LAr) electromagnetic calorimeters (together referred to as the ECAL), with an additional thin LAr presampler covering $|\eta| < 1.8$ to correct for energy loss in material upstream of the calorimeters. The ECAL extends from 1.5 m to 2.0 m in radial distance r in the barrel and from 3.6 m to 4.25 m in $|z|$ in the endcaps. Hadronic calorimetry is provided by a steel/scintillator-tile calorimeter (HCAL), segmented into three barrel structures within the range $|\eta| < 1.7$, and two copper/LAr hadronic endcap calorimeters covering $|\eta| > 1.5$. The HCAL covers the region from 2.25 m to 4.25 m in r in the barrel (although the HCAL active material extends only up to 3.9 m) and from 4.3 m to 6.05 m in $|z|$ in the endcaps. The solid angle coverage is completed with forward copper/LAr and tungsten/LAr calorimeter modules optimised for electromagnetic and hadronic measurements, respectively.

The calorimeters have a highly granular lateral and longitudinal segmentation. Including the presamplers, there are seven sampling layers in the combined central calorimeters (the LAr presampler, three in the ECAL barrel and three in the HCAL barrel), and the endcap regions provide up to eight sampling layers (the presampler, three in ECAL endcaps and four in HCAL endcaps). The forward calorimeter modules provide three sampling layers in the forward region. The combined depth of the calorimeters for hadronic energy measurements is more than nine hadronic interaction lengths nearly everywhere across the full detector acceptance.

The muon spectrometer comprises separate trigger and high-precision tracking chambers measuring the deflection of muons in the magnetic field generated by the superconducting air-core toroids. The field integral of the toroids ranges between 2.0 and 6.0 Tm across most of the detector.

¹ ATLAS uses a right-handed coordinate system with its origin at the nominal interaction point (IP) in the centre of the detector and the z -axis along the beam pipe. The x -axis points from the IP to the centre of the LHC ring, and the y -axis points upwards. Polar coordinates (r, ϕ) are used in the transverse plane, ϕ being the azimuthal angle around the z -axis. The pseudorapidity is defined in terms of the polar angle θ as $\eta = -\ln \tan(\theta/2)$ and is equal to the rapidity $y = \frac{1}{2} \ln \left(\frac{E+p_z c}{E-p_z c} \right)$ in the relativistic limit. Angular distance is measured in units of $\Delta R \equiv \sqrt{(\Delta y)^2 + (\Delta \phi)^2}$.

The ATLAS detector records events using a tiered trigger system [38]. The level-1 (L1) trigger is implemented in custom electronics and reduces the event rate from the LHC crossing frequency of 40 MHz to a design value of 100 kHz. The second level, known as the high-level trigger (HLT), is implemented in software running on a commodity PC farm that processes the events and reduces the rate of recorded events to 1 kHz. A software suite [39] is used in data simulation, in the reconstruction and analysis of real and simulated data, in detector operations, and in the trigger and data acquisition systems of the experiment.

3 Data and simulated event samples

The analysed dataset was collected between 2015 and 2018 by the ATLAS detector from proton–proton (pp) collisions at $\sqrt{s} = 13$ TeV at the LHC. The total integrated luminosity of this dataset is 140 fb^{-1} . Data where the LHC beams were not stable or not all subdetectors were operational were excluded [40].

For the CalR+2J channel, dedicated LLP triggers (dubbed “CalRatio triggers” as they exploit the ratio of energy in the electromagnetic and hadronic parts of the calorimeter) were employed. They were detailed Ref. [31], and a short summary is given here. At L1, jets were reconstructed in 0.2×0.2 regions in the $\eta \times \phi$ plane, motivated by the fact that signal jets tend to be narrower than regular SM jets. Events with jets with transverse energy E_T above 60 or 100 GeV (depending on the data-taking period) are selected. In some run periods, triggers were available with the requirement that L1 jet objects were accepted only if there existed no deposit in the electromagnetic calorimeter in the same $\eta - \phi$ position as the jet. This requirement acted as a proxy to the CalRatio quantity, allowing the E_T thresholds to be reduced to 30 GeV. At HLT, the triggering jet was additionally required to satisfy $|\eta| < 2.5$ where tracking information is available. Further, the jet should have a high proportion of its energy in the HCAL, satisfy a modified noise-suppression selection and satisfy a BIB-removal algorithm exploiting, for example, the timing and alignment of deposits in ϕ . In the following, the dataset collected with the CalRatio triggers is referred to as the “main” dataset.

In the remaining channels, single or dilepton triggers [41, 42] were employed, where only triggers running unrescaled for the whole data-taking period in a given year were considered.

Three additional datasets were collected for the study of NCBs and construction of validation and control regions. These datasets are the same as described in Ref. [31] and are summarised briefly here. The BIB dataset was collected from events satisfying all the requirements of the CalRatio triggers but failing to pass the BIB-removal algorithm. The cosmic ray dataset was collected using the same trigger selection but from events recorded during empty bunch crossings. Finally, a dijet dataset was selected using a single-jet-based trigger [43] and vetoing on the CalRatio triggers to make it orthogonal to the main dataset. This dataset is used to test the effect of the modelling in the displaced jet neural network tagger’s output.

The main SM backgrounds are SM multijets in the CalR+2J channel, and W/Z+jets, $t\bar{t}$ and single-top-quark events in the CalR+W and CalR+Z channels. Although data-driven methods are used to do the final background estimations, Monte Carlo (MC) simulated events are needed to train the machine-learning (ML) discriminants and evaluate certain systematic uncertainties. The SM multijet samples were generated at leading order (LO) with PYTHIA 8.186 [44] using the A14 set of tuned parameters (tune) [45] for parton showering and hadronisation. The NNPDF2.3LO parton distribution function (PDF) set [46] was used. Events containing a W or Z boson with jets were simulated with SHERPA v2.2.1 [47, 48]. Next-to-leading-order (NLO) accurate matrix elements for up to two jets, and LO-accurate matrix elements for up to four jets were calculated with the COMIX [49] and OPENLOOPS [50, 51] libraries. The default

SHERPA parton shower [52] was used. The production of $t\bar{t}$ events was modelled using the POWHEG Box v2 [53–56] generator at NLO with the NNPDF3.0NLO PDF set and the hdamp parameter set to 1.5 times the top quark mass [57]. The events were interfaced with PYTHIA 8.230 [58] using the A14 tune and the NNPDF2.3LO PDF set. The NLO $t\bar{t}$ inclusive production cross-section was corrected to the theory prediction at next-to-next-to-leading-order (NNLO) in QCD including the resummation of next-to-next-to-leading logarithmic (NNLL) soft-gluon terms calculated using Top++2.0 [59–65]. Single-top-quark production was modelled using POWHEG Box v2 [54–56, 66] at NLO in QCD in the five-flavour scheme with the NNPDF3.0NLO PDF set [67]. The diagram-removal scheme [68] was employed to address the interference with $t\bar{t}$ production [57]. The events were interfaced with PYTHIA 8.230 using the A14 tune and the NNPDF2.3LO PDF set. The inclusive cross-section was corrected to the theory prediction calculated at NLO in QCD with NNLL soft-gluon corrections [69, 70].

Three types of benchmark signals are considered. The first is the HS model [11, 12, 71, 72], where a scalar boson Φ (the Higgs boson, or a lighter or heavier particle that behaves similarly) acts as mediator between the SM and the HS. The Φ can decay into neutral long-lived scalars, denoted S , which are the LLPs. The scalars decay chiefly into the heaviest kinematically accessible fermion pairs: typically b -quarks in most of the considered signals. This is the same model as studied in Ref. [31]. Events were simulated using MADGRAPH5_AMC@NLO v2.6.2 [73] at LO with the NNPDF2.3LO PDF set. Two production modes for Φ are considered: gluon–gluon fusion production for the CalR+2J channel and associated vector boson (W or Z) production for the CalR+W/Z channels. Vector boson fusion (VBF) is not considered: in the CalR+2J channel all objects that play a role in the selection come from LLP decays. Hence, the efficiencies for events produced from gluon–gluon fusion and VBF productions are expected to be similar. Given the relative cross-sections between these production modes, no sensitive additional contribution is expected from the VBF production. The HS samples produced with a W or Z boson are referred to as WHS and ZHS, respectively. For the gluon–gluon fusion samples, the Φ transverse momentum distribution was reweighted to match NLO predictions using the same event generator. Cross-sections of 48.6 pb for gluon–gluon fusion, 0.45 pb for associated production with a W boson decaying leptonically, and 0.09 pb for associated production with a Z boson decaying leptonically (all extracted from the NNLO calculation [74]) are assumed when normalising results for the case where the mediator is the SM Higgs boson. Several sets of samples were generated, with different assumptions for particle masses, in the range of 60 to 1000 GeV for the mediator, and 5 to 475 GeV for the long-lived scalar. The second type of signal model, considered in the CalR+W/Z channels, contains photo-phobic ALPs [21] that are radiated from vector bosons and decay into gluons. The ALP masses vary between 0.1 and 40 GeV, and the coupling of the ALP to gluons, which determines its lifetime, varies between 10^{-7} and 10^{-2} . In this model, only vector boson decays into electrons or muons are considered. The ALP samples were generated with MADGRAPH5_AMC@NLO v2.9.3 at LO with the NNPDF2.3LO PDF set. The samples are referred to as ZALP and WALP. The third benchmark sample is a long-lived dark photon (Z_d) model [75, 76], where the Z_d is produced with a Z during the decay of a scalar mediator. It is referred to here as the HZZ_d model. This model was studied by ATLAS in Ref. [77]. Mediator masses between 250 and 600 GeV are considered, with dark photon masses ranging between 5 and 400 GeV. The samples were generated with MADGRAPH5_AMC@NLO2.6.7 at LO with the NNPDF2.3LO PDF set. For all signal samples, parton showering and hadronisation were modelled using PYTHIA8 with the A14 tune. This model was last searched for by ATLAS in the Z + displaced jet channel in Ref. [34].

Example Feynman diagrams for these three types of model are shown in Figure 1. For all signal samples, the generated LLP mean proper lifetime (τ_{gen}) was chosen to maximise the fraction of decays in the ATLAS hadronic calorimeter and muon system (these mean proper lifetimes are typically of the order of a few meters, but vary across samples due to time dilation effects). The effect of multiple interactions per

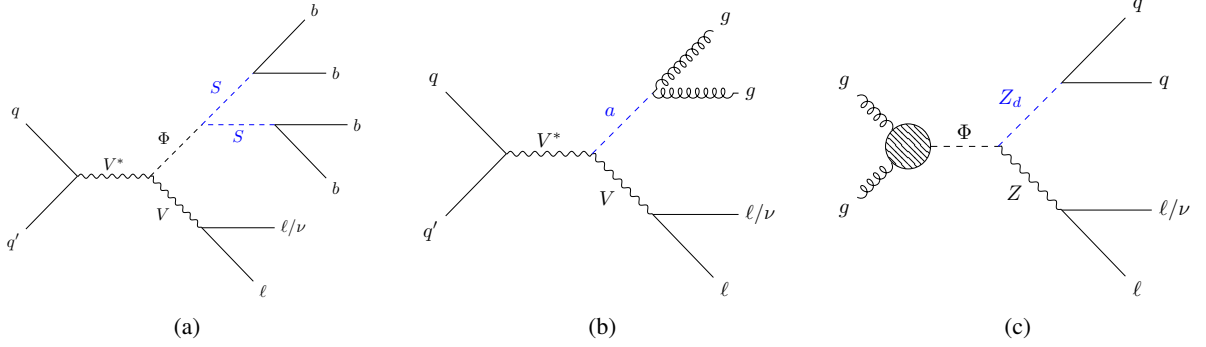


Figure 1: Example Feynman diagrams for the signal processes explored in this paper. (a) Model where the mediator (Φ) is produced in association with a vector boson $V = W$ or Z , and the LLPs S decay into fermions (mainly b -quarks). (b) ALP model where the long-lived ALP a decays into gluons, and is produced in association with a vector boson. (c) Dark photon Z_d model produced with a Z boson from the decay of a mediator Φ .

bunch crossing (pile-up) was modelled by overlaying the simulated hard-scattering event with inelastic pp collision events generated with PYTHIA 8.186 using the NNPDF2.3LO PDF set and the A3 tune [78]. The detector geometry and response were simulated with GEANT4 [79, 80]. The standard ATLAS reconstruction software is used for both the simulation and collision data.

4 Event reconstruction

Three types of reconstructed objects are used: jets, leptons and missing transverse momentum. Hadronically decaying LLPs will form displaced jets, which are the common signature in all the channels. The leptons and missing transverse momentum are exploited to reconstruct W and Z boson candidates in the CalR+W and CalR+Z channels. The formal definitions of each object type are described below.

Jets: Jets are reconstructed using the anti- k_r algorithm [81, 82] with a radius parameter $R = 0.4$ using calorimeter energy clusters only (tracking information is not used). Jets are further calibrated to account for the predicted detector response in MC simulation, and a residual calibration of jets in data is derived through *in situ* measurements [83]. “Clean jets” are defined as those that have transverse momentum (p_T) above 40 GeV, $|\eta| < 2.5$ and satisfy the CalRatio jet cleaning requirement described in Ref. [31]. A “trackless jet” is defined as a clean jet with $\Delta R_{\min} > 0.2$, where ΔR_{\min} represents the angular distance between the jet axis and the closest track with $p_T > 2$ GeV. SM jets, which typically have multiple tracks in their cone, will have small values of this quantity, while anomalous trackless jets will yield large values. The $\sum \Delta R_{\min}$ is defined as the sum of ΔR_{\min} over jets above a certain p_T threshold, which is optimised differently according to the channel: 40 GeV for the CalR+W/Z channels and 50 GeV for the CalR+2J channel. This is a useful discriminant to select events containing displaced jets. This quantity was found to be stable across pile-up values encountered during LHC Run 2. The term “displaced jet” is generically used to refer to jets that originated away from the interaction point: in the context of this analysis, it is taken to mean jets that began in the ATLAS calorimeters. A CalRatio jet candidate must be matched (within a cone of radius 0.2) to an HLT jet that met the criteria of one of the CalRatio triggers. It must also satisfy $\Delta R_{\min}(\text{jet}, \text{track}) > 0.2$ and $\log_{10}(E_H/E_{EM}) > 1.2$, where $\log_{10}(E_H/E_{EM})$ is the base-10 logarithm of their CalRatio value.

All analysis channels make use of a neural network (NN) classifier trained to distinguish signal-like jets (arising from a LLP decay) from BIB-like jets and SM multijets. This displaced NN jet tagger was originally trained for the analysis in Ref. [31], which contains all the details about its architecture, training and performance. Only a brief summary of the key points is included here. The architecture chosen was a set of convolutional layers fed into a long short-term memory (LSTM) layer [84]. An additional adversarial component was added to prevent the network from exploiting mismodelling of some of the features. The inputs to the NN are low-level features of the jets from the tracker (positions, momenta, impact parameter and quality variables of inner-detector tracks that are within $\Delta R = 0.2$ of jets), calorimeters (the fraction of the jet energy deposited in each layer of the ECal and HCal and momenta, timing information and positions of calorimeter topoclusters, i.e. collections of calorimeter cells used in jet reconstruction [85] associated with each jet) and muon system (spatial and timing information for muon track segments within $\Delta\phi = 0.2$ of a jet). The NN was trained on SM multijet MC samples and the BIB dataset, and a combination of HS signal samples. Two trainings were provided: one using signals with mediator masses below or equal to 200 GeV; the other using signal with mediator masses strictly above 200 GeV. These two versions of the NN are referred to as the *low- E_T* and *high- E_T* NNs respectively. Each NN outputs three scores for each jet, which relate to the probability that such a jet would be the result of an LLP decay, a BIB hit, or a non-displaced jet. These scores are referred to as signal-score, BIB-score and multijet-score, and sum to unity. The modelling of the input features is checked using the dijet dataset described in Section 3. A dedicated procedure is used to evaluate the residual uncertainty in the performance of the NN due to potential mis-modelling of the input variables, as described in Section 7. The per-jet NN is then exploited in the three analysis channels, which are described separately in Section 5, selecting the jets with the highest signal-scores.

Leptons: “Baseline” leptons (e or μ) are required to have p_T above 10 GeV, and satisfy $|\eta| < 2.47$ for electrons and $|\eta| < 2.5$ for muons. Electrons in the gap between the barrel and the endcap are excluded. Further, these leptons are expected to meet the standard ATLAS requirements on track-to-vertex association, *Medium* identification and *Tight* isolation conditions, as defined in Refs. [86, 87]. The standard lepton reconstruction efficiency correction factors are used. A procedure is implemented to resolve ambiguities arising from the fact that electrons, muons and jets are identified and reconstructed independently. Only leptons satisfying the baseline selections are considered for this process, and calibrated jets used for the displaced jet identification. First, if two electrons share a track in the inner detector, then the lepton with the lowest p_T is discarded. Next if a muon and electron share a track, then the electron is discarded unless the muon was seeded from calorimeter energy clusters. Any jets within $\Delta R = 0.3$ of electrons or muons are removed from the final state. Then, any selected electrons or muons within $0.2 < \Delta R < 0.4$ of any remaining selected jet are also removed.

Missing transverse momentum and vector bosons: The missing transverse momentum, \vec{p}_T^{miss} , is defined as the negative vector sum of the transverse momenta of all baseline electrons, muons and jets in the event, plus an additional soft term corresponding to tracks not associated with any identified lepton or jet [88]. Its magnitude, E_T^{miss} , is referred to as the missing transverse energy. W boson candidates are formed in events containing exactly one baseline lepton (denoted by ℓ) matched to a lepton trigger object with $p_T > 27$ GeV and $E_T^{\text{miss}} > 30$ GeV. The transverse invariant mass of the system, given by $\sqrt{2E_T^{\text{miss}}p_T^\ell(1 - \cos(\Delta\phi(E_T^{\text{miss}}, \ell)))}$, is required to be above 50 GeV to remove multijet background contamination. Z boson mass are defined in events containing at least one same-flavour opposite-sign pair of baseline leptons, each with the leading and subleading leptons satisfying $p_T > 25$ GeV and $p_T > 10$ GeV respectively. At least one of the selected leptons is required to match to a lepton trigger object. The invariant mass of the dilepton system $m_{\ell\ell}$ is required to be in the range of $60 < m_{\ell\ell} < 120$ GeV. If multiple

lepton pairs are possible, only the pair with the invariant mass closest to the Z boson mass is kept.

5 Event selection

Events are required to first satisfy at least one of the triggers listed in Section 3. In the CalR+W/Z channels, the logical “OR” of the unprescaled triggers with the lowest p_T thresholds is utilised. Adding the CalRatio triggers into the “OR” did not result in a significant gain in signal efficiency, so they were not included. In both the channels, the trigger efficiency increases with lepton p_T , and it reaches a plateau for values of p_T above 50 GeV (in the CalR+Z channel) and 100 GeV (in the CalR+W channel), with similar performance for all benchmark samples. In addition to satisfying a trigger requirement, every event is required to have a primary vertex with at least two tracks with $p_T > 500$ MeV [89]. At least one clean jet is required in the event for all channels.

The three analysis channels (CalR+2J, CalR+W, CalR+Z) exploit different final states but follow the same overall strategy: a per-jet NN provides discrimination between signal-like jets, BIB-like jets and SM multijets. Additional per-event ML algorithms are trained to separate signal from remaining backgrounds at the event level. Some additional selections are applied to ensure consistent behaviour of the remaining population of events. The surviving events are then placed in a plane of two uncorrelated variables, enabling the data-driven ABCD method to be used for the final background estimate as described in Section 6.

5.1 CalR+2J channel selection

The CalR+2J channel targets events containing one displaced jet, and two other jets that may be trackless. Such a signature arises in the HS benchmark models where the mediator is produced by gluon–gluon fusion before decaying into a pair of LLPs. One LLP can decay in the hadronic part of the calorimeter (leading to a displaced jet where both the fermions are collimated into a single jet, with high probability to fulfil the criteria of the CalRatio triggers) and the other LLP can decay with a short enough decay length to produce two separate additional jets (one from each fermion). These jets would likely be reconstructed without associated tracks, and would be delayed relative to activity arriving from the interaction point in a straight line. Events containing mediators produced via vector-boson fusion would also enter this channel, although the additional information from the prompt jets would not be exploited. Hence, no sensitive additional contribution is expected from this production mode given its low cross-section compared with gluon–gluon fusion. A dedicated analysis would be needed to make the most of the vector boson fusion signature. The CalR+2J channel is complementary to the analysis in Ref. [31], which was optimised for the case where both the LLPs led to merged displaced jets. In this analysis, the “merged-resolved” topology (which can account for up to 27% of events in the benchmark HS models) is explored for the first time.

Events entering this channel are required to satisfy a preselection consisting of having at least three clean jets and $\sum \Delta R_{\min}$ being above 0.5, where the sum runs over jets with $p_T > 50$ GeV. This p_T threshold was chosen to be consistent with the previous analysis exploiting a similar topology [31]. The jets with the three highest signal scores from the high- E_T and low- E_T NNs are selected, and one of these must be a CalRatio jet candidate. The two other jets represent the resolved additional jets from a second LLP decay. These jets and the jets with the three highest BIB scores must satisfy additional conditions. The first condition is on jet time, which is the energy-weighted average time of the jet’s constituent energy deposits, relative to the time it would take for a particle to travel at the speed of light directly from the

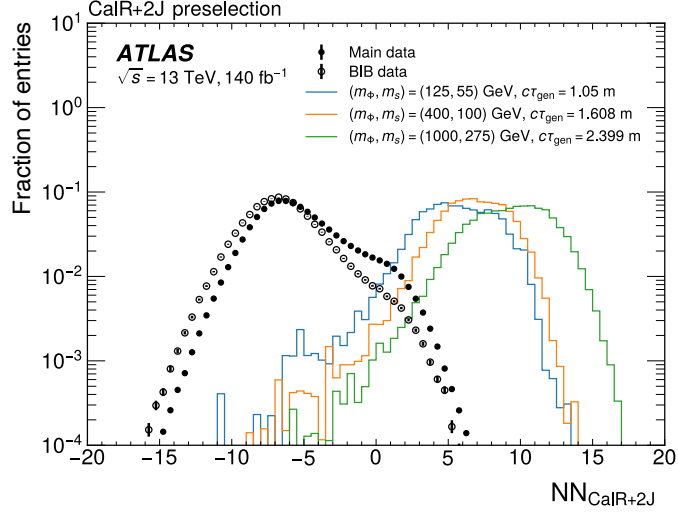


Figure 2: Comparison of the $NN_{\text{CalR+2J}}$ distribution between signal events and background. Only signal events with at least one LLP decaying after the inner detector are shown. The main data, collected with the CalRatio triggers, are dominated by QCD multijet background.

interaction point to the jet’s calorimeter location [85]. All jets should have a time within the range of -3 to 15 ns. This criterion aims to reject BIB jets (which do not need to pass via the interaction point and hence can arrive early) and noise-induced jet candidates (which are uniformly distributed in time), and preserve signal jets from LLPs moving relatively slowly with timings up to 15 ns. Next, these jets should have $\log_{10}(E_H/E_{EM}) > -1.5$. Finally, the jets with the highest signal scores should not be in the barrel-endcap transition regions: $|\eta| \notin (1.45, 1.55)$.

An event-level NN (labelled $NN_{\text{CalR+2J}}$) is trained with the objective of removing all remaining BIB events from the selection, such that the only remaining background is multijet events. This facilitates the use of the ABCD method for the background estimate in Section 6. The input features for the $NN_{\text{CalR+2J}}$ includes jet-level and event-level variables. The jet observables include per-jet NN scores, kinematics, width and time. The event-level variables include the scalar sum hadronic energy of all jets, angular separations between jets, missing transverse energy and related quantities. The $NN_{\text{CalR+2J}}$ is trained on events from the BIB dataset and the HS signal samples after preselection. It was trained to be decorrelated from the $\sum \Delta R_{\min}$ event-level variable, as described in Section 6.1. Figure 2 shows the distribution of the $NN_{\text{CalR+2J}}$ output for the BIB and main datasets and some example signal models. BIB-like events are associated with very small values of the output. Events in the BIB dataset with a $NN_{\text{CalR+2J}}$ output of three or higher do not show the characteristic timing and angular distributions of BIB and are indistinguishable from pure multijet events. Thus events are required to have a $NN_{\text{CalR+2J}}$ score of at least three to be considered in this channel to effectively eliminate BIB-like events. Table 1 lists the full selection criteria.

Table 1: The final selection criteria for the signal region of the CalR+2J channel. Region A is the signal region of the ABCD plane defined in Section 6 and includes all the other requirements listed in the table.

Selection	CalR+2J
Trigger	Satisfy CalRatio trigger
Number of clean jets	≥ 3
$\sum \Delta R_{\min}$	> 0.5
Trigger matching	At least one signal candidate
Signal/BIB jet candidate time	$-3 \text{ ns} < t < 15 \text{ ns}$
Signal/BIB jet candidate $\log_{10}(E_H/E_{EM})$	> -1.5
Signal jet candidate η	$\notin (1.45, 1.55)$
$NN_{\text{CalR+2J}}$	≥ 3
Region A	$\sum \Delta R_{\min} \geq 0.71$ $NN_{\text{CalR+2J}} \geq 7.61$

5.2 CalR+W and CalR+Z channel selections

5.2.1 Preselection

The leptonic channels share a common preselection. At least one trackless jet with $p_T > 40 \text{ GeV}$ is required, and the $\sum \Delta R_{\min}$ is required to be above 0.5, where the sum runs over jets with $p_T > 40 \text{ GeV}$. In both the channels, the jet with the highest low- E_T NN signal-score ($j^{\text{sig}1\ell}$) is required to be trackless and to have $p_T > 50 \text{ GeV}$, $\log_{10}(E_H/E_{EM}) > -1$, a time in the range of $(-3, 15) \text{ ns}$ and not be in the transition regions between the barrel and endcap. The NN signal-score of this jet is required to be above 0.4. Both channels use the low- E_T NN scores to rank jets from most signal-like to least signal-like. As it was already observed in Ref. [31], even for high- E_T input signal samples the low- E_T NN scores provide a better separation from background in cases where the LLP boost is moderate.

5.2.2 CalR+W channel selections

The CalR+W channel targets scenarios where the HS mediator is produced in association with a W boson, where the W boson decays leptonically. While this production mode has a lower expected cross-section than gluon–gluon fusion, the additional lepton from the W boson decay provides a clear signature on which to trigger. It also renders most NCBs negligible, and makes it possible to require only one displaced jet while two were required in Ref. [31]. In addition to the HS models, ALP models also predict events in this topology.

After the application of the preselection, a W boson candidate is required in the event. Events with more than one lepton are rejected, to maintain orthogonality with the CalR+Z channel. The most signal-like jet must be separated in the azimuthal direction from the E_T^{miss} : $\Delta\phi(j^{\text{sig}1\ell}, E_T^{\text{miss}}) > 0.5$. To be orthogonal to the CalR+Z channel, events with more than one baseline lepton are vetoed. Finally, the CalR+W channel exploits a set of Boosted Decision Trees (BDTs) as discriminants. These are trained with XGBoost [90] with the objective of discriminating signal from background events after preselection and W boson identification is applied. Three BDTs are trained corresponding to three input signal sample sets. The first uses a combination of all WALP mass points, in which there is only one LLP in the event. The other two BDTs are trained on low ($m_\Phi \leq 200 \text{ GeV}$) and high ($m_\Phi > 200 \text{ GeV}$) HS mediator mass events with an associated

Table 2: The final selection criteria for the signal regions of the CalR+W channel. Region A is the signal region of the ABCD plane defined in Section 6 and includes all the other requirements listed in the table.

Selection	CalR+W WALP	CalR+W low- E_T	CalR+W high- E_T
Vector boson candidates	0 Z, 1 W	0 Z, 1 W	0 Z, 1 W
BDT score	$\text{BDT}_{\text{CalR+W}}^{\text{ALP}} > 0.82$	$\text{BDT}_{\text{CalR+W}}^{\text{low-}E_T} > 0.92$	$\text{BDT}_{\text{CalR+W}}^{\text{high-}E_T} > 0.89$
$j^{\text{sig}1\ell} \log_{10}(E_H/E_{EM})$	> 1	> 1	–
$j^{\text{sig}1\ell} p_T$	$> 70 \text{ GeV}$	$> 60 \text{ GeV}$	$> 100 \text{ GeV}$
Lepton p_T	–	$> 40 \text{ GeV}$	$> 60 \text{ GeV}$
$\Delta\phi(\text{lepton}, E_T^{\text{miss}})$	< 1.5	–	–
Region A	$\text{BDT}_{\text{CalR+W}}^{\text{ALP}} \geq 0.975$ $\sum \Delta R_{\min} \geq 1.1$	$\text{BDT}_{\text{CalR+W}}^{\text{low-}E_T} \geq 0.985$ $\sum \Delta R_{\min} \geq 1.4$	$\text{BDT}_{\text{CalR+W}}^{\text{high-}E_T} \geq 0.99$ $\sum \Delta R_{\min} \geq 1.1$

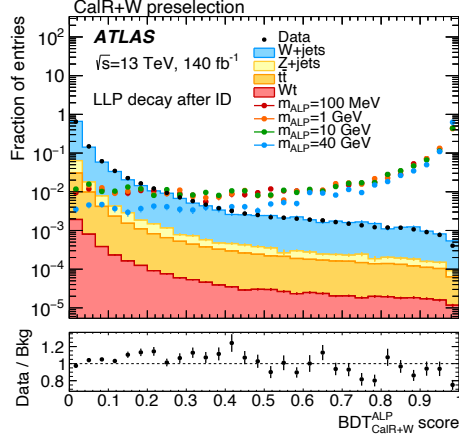
W boson. In all cases, the BDT is trained to discriminate the signal against MC simulated events from all background processes listed in Section 3 for this channel. These three BDTs are hereafter referred to as $\text{BDT}_{\text{CalR+W}}^{\text{ALP}}$, $\text{BDT}_{\text{CalR+W}}^{\text{low-}E_T}$ and $\text{BDT}_{\text{CalR+W}}^{\text{high-}E_T}$. For signal, only events with an odd event number are used for the training, leaving the even numbered events for evaluation. The input variables include information from jets (such as p_T , jet width and per-jet NN scores), leptons (such as p_T and angles between leptons and signal-like jets) and event-level observables (such as missing transverse energy in the event, reconstructed vector boson kinematics).

Figures 3(a), 3(b) and 3(c) show the distribution of $\text{BDT}_{\text{CalR+W}}^{\text{ALP}}$, $\text{BDT}_{\text{CalR+W}}^{\text{low-}E_T}$ and $\text{BDT}_{\text{CalR+W}}^{\text{high-}E_T}$ on four signal models, data and background MC. The simulated background events are shown only for comparison at the preselection stage, and are not used in the final background estimate. Dedicated uncertainties are derived to cover the effect of mis-modelling of input variables on signal efficiency, as detailed in Section 7. Three sets of selection criteria are defined, each exploiting one of these BDTs. The selection criteria are listed in Table 2.

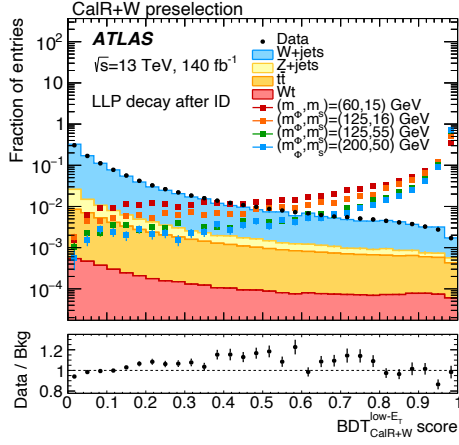
5.2.3 CalR+Z channel selection

The CalR+Z channel targets the topology where the LLP is accompanied by a Z boson decaying into two charged leptons. The motivation is identical to that described in Section 5.2.2. In addition to the benchmark HS and ALP models, this channel considers the study of the long-lived dark photon (Z_d) model described in Section 3.

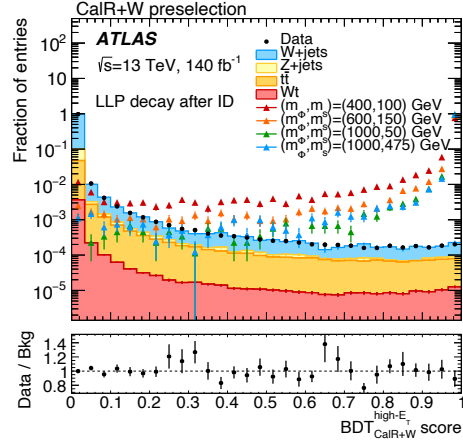
After passing the preselection, events entering the CalR+Z channel must contain a single Z boson candidate. Two different BDTs are trained with XGBoost to discriminate signal from background events. The resulting BDT scores are used for a data-driven background estimate (see Section 6 for details). Each of these BDTs aims at an optimal discrimination in a specific range of masses: the $\text{BDT}_{\text{CalR+Z}}^{\text{low-}E_T}$ is trained with a combination of signal samples including all the ZALP, Z_d and ZHS model with masses of the mediator $m_\Phi \leq 250 \text{ GeV}$; the $\text{BDT}_{\text{CalR+Z}}^{\text{high-}E_T}$ is trained with Z_d and Z+HS samples with $m_\Phi > 250 \text{ GeV}$. In the CalR+Z channel, unlike the CalR+W channel, a dedicated selection targeting ALP models was not needed: this is because the reconstruction of the associated vector boson is more straightforward, permitting a higher signal purity even when the ALP models are targeted together with others using the $\text{BDT}_{\text{CalR+Z}}^{\text{low-}E_T}$. The BDTs are trained to discriminate the signal against the background processes listed in Section 3 for this channel. The input variables are similar those of the CalR+W channel BDTs. Figures 4(a) and 4(b) show



(a)



(b)



(c)

Figure 3: Comparison of the distribution of (a) $\text{BDT}_{\text{CalR+W}}^{\text{ALP}}$, (b) $\text{BDT}_{\text{CalR+W}}^{\text{low-}E_T}$, (c) $\text{BDT}_{\text{CalR+W}}^{\text{high-}E_T}$ scores between signal events and background, after preselection. In all cases, only signal events with at least one LLP decaying after the ID are shown. The simulated background events are shown only for comparison at the preselection stage, and are not used in the final background estimate.

the distributions of the $\text{BDT}_{\text{CalR+Z}}^{\text{low-}E_T}$ and $\text{BDT}_{\text{CalR+Z}}^{\text{high-}E_T}$ on several signal models, on data and background MC. Two selection criteria are defined, one for each BDT, as outlined in Table 3.

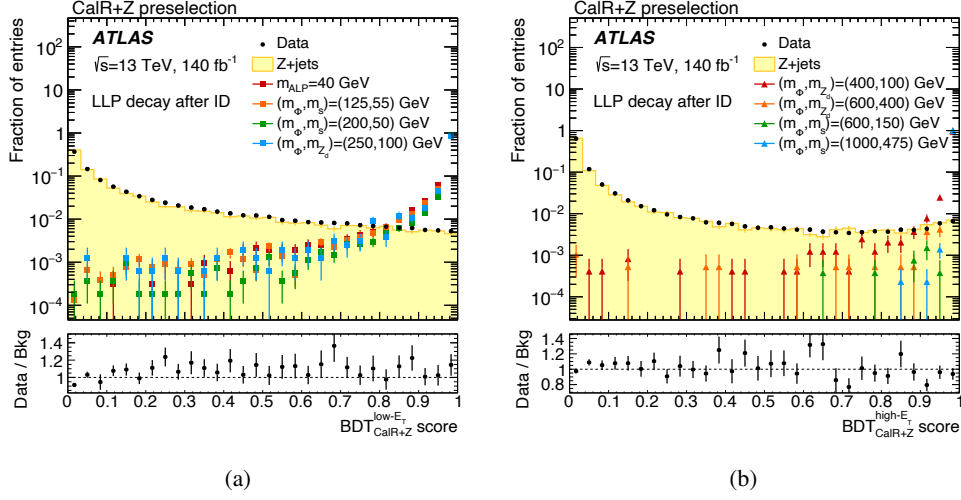


Figure 4: Comparison of the distribution of (a) $\text{BDT}_{\text{CalR+Z}}^{\text{low-}E_T}$ and (b) $\text{BDT}_{\text{CalR+Z}}^{\text{high-}E_T}$ scores between signal events and background, after preselection. In all cases, only signal events with at least one LLP decaying after the ID are shown. The simulated background events are shown only for comparison at the preselection stage, and are not used in the final background estimate.

Table 3: The final selection criteria for the signal regions of the CalR+Z channel. Region A is the signal region of the ABCD plane defined in Section 6 and includes all the other requirements listed in the table.

Selection	CalR+Z low- E_T	CalR+Z high- E_T
Vector boson candidates	1 Z, 0 W	1 Z, 0 W
BDT score	$\text{BDT}_{\text{CalR+Z}}^{\text{low-}E_T}$ score > 0.6	$\text{BDT}_{\text{CalR+Z}}^{\text{high-}E_T}$ score > 0.7
$j^{\text{sig}1\ell} \log_{10}(E_H/E_{EM})$	> 0.8	> 0.8
$j^{\text{sig}1\ell} p_T$	> 80 GeV	> 70 GeV
Lepton p_T	> 70 GeV	> 60 GeV
Region A	$\text{BDT}_{\text{CalR+Z}}^{\text{low-}E_T}$ score > 0.99 $\sum \Delta R_{\min} \geq 0.9$	$\text{BDT}_{\text{CalR+Z}}^{\text{high-}E_T}$ score > 0.985 $\sum \Delta R_{\min} \geq 1$

6 Background estimation

Following the application of the selections, the contributions from cosmic rays and all subdominant SM processes are found to be negligible. Some events from the BIB dataset still pass the selections, but these remaining events show the same behaviour as multijet events. This leaves only one population of background events in each channel, namely multijet events in the CalR+2J channel and W/Z +jets in the CalR+W and CalR+Z channels, respectively. The CalR+W channel contains residual traces of $t\bar{t}$ events, but these show the same behaviour as the dominant background and are therefore grouped as the same population. As these background sources are not well modelled, a data-driven method is used to estimate the background yields in the final signal regions. The data-driven ABCD method is employed to estimate the contribution from the dominant background in each of the final selections. The ABCD method is described extensively in other publications, such as Ref. [31]; the main points are summarised here. In a plane defined by two uncorrelated variables, four regions A, B, C, and D are defined using horizontal and vertical boundaries. When there is one predominant background population (typically

concentrated in regions B, C and D) and a signal population primarily in region A, the background yield in region A (N_A) can be calculated from the yields in the other regions (N_B , N_C and N_D) using the formula $N_A = (N_B \times N_C) / N_D$. Signal leakage into other regions can be accounted for through a simultaneous fit. Leakage of signal into the other regions can be accounted for using a simultaneous fit. All three channels exploit ABCD planes for their background estimates, although the axes are defined differently in each case.

6.1 CalR+2J final selection and the ABCDisCo method

The ABCD plane axes are usually chosen from the list of available variables that separate signal and background well. In cases where it is difficult to find two uncorrelated variables with enough separation power, another approach is to train a ML discriminant, which is required to be uncorrelated to another variable by construction. The CalR+2J channel is such a case: unlike in Ref. [31], the $\sum \Delta R_{\min}$ becomes visibly correlated with displaced jet kinematic information as additional jets from LLP decays are included. A method called ABCDisCo uses the *distance correlation* (DisCo) between the ML discriminant and another event-level variable, and involves adding terms to the loss function of a neural network that penalises the network if these have a large correlation [91]. The ABCDisCo method was employed in the CalR+2J channel to build an ABCD plane constructed from $\sum \Delta R_{\min}$ and the NN output. This is the same NN that is used to eliminate BIB-like events. Even though this NN was only trained with the BIB dataset as background, it has a good discrimination power between signal and multijet events, which are also present in the BIB dataset. The Pearson correlation coefficient for the resulting pair of discriminants is 0.04, small by construction. The final region A is defined by the requirements that $\sum \Delta R_{\min} \geq 0.71$ and $NN_{\text{CalR+2J}} \geq 7.61$. Regions B, C and D are obtained by inverting one or both the requirements, as shown in Figure 5 for the main CalRatio dataset, the BIB dataset and two of the signal samples.

Regions B, C, and D were used to create the validation regions VR_{BD} and VR_{CD} . VR_{BD} consists of the nominal B and D regions combined and is divided into four alternative ABCD regions. The ABCD estimate procedure was tested with these regions and with variations on the cut values in each ABCD plane variable. The predictions are found to be in agreement with the observed number of events within the statistical uncertainties. The same procedure was performed for VR_{CD} , composed of the nominal C and D regions. In VR_{CD} , the observed number of events was consistently about 5% higher than estimated by the ABCD method, which was taken as the systematic uncertainty in the final ABCD prediction in this plane, as discussed in Section 7.

6.2 CalR+W and CalR+Z final selections and background estimate

The standard ABCD method is used to estimate the remaining background contribution in the five signal regions of the CalR+W/Z channels, with the final ABCD planes defined by $\sum \Delta R_{\min}$ and the BDT score relevant to each region. These variables are found to be uncorrelated after preselection, with Pearson correlation coefficients between 0.003 and 0.017 in absolute value in all cases. The ABCDisCo method is not needed in this case because the $\sum \Delta R_{\min}$ is found to be sufficiently well decorrelated to the BDT scores (since the targeted LLP decays always happen outside the tracker). The final ABCD boundaries are set through a selection optimisation procedure performed together with several additional event-level variables (such as kinematic information from the vector boson candidate, angular separations between the jets and leptons, and invariant masses of the possible lepton-jet combinations) to obtain the final selections that maximize sensitivity while reducing the signal leakage in regions B, C and D and keeping the statistical

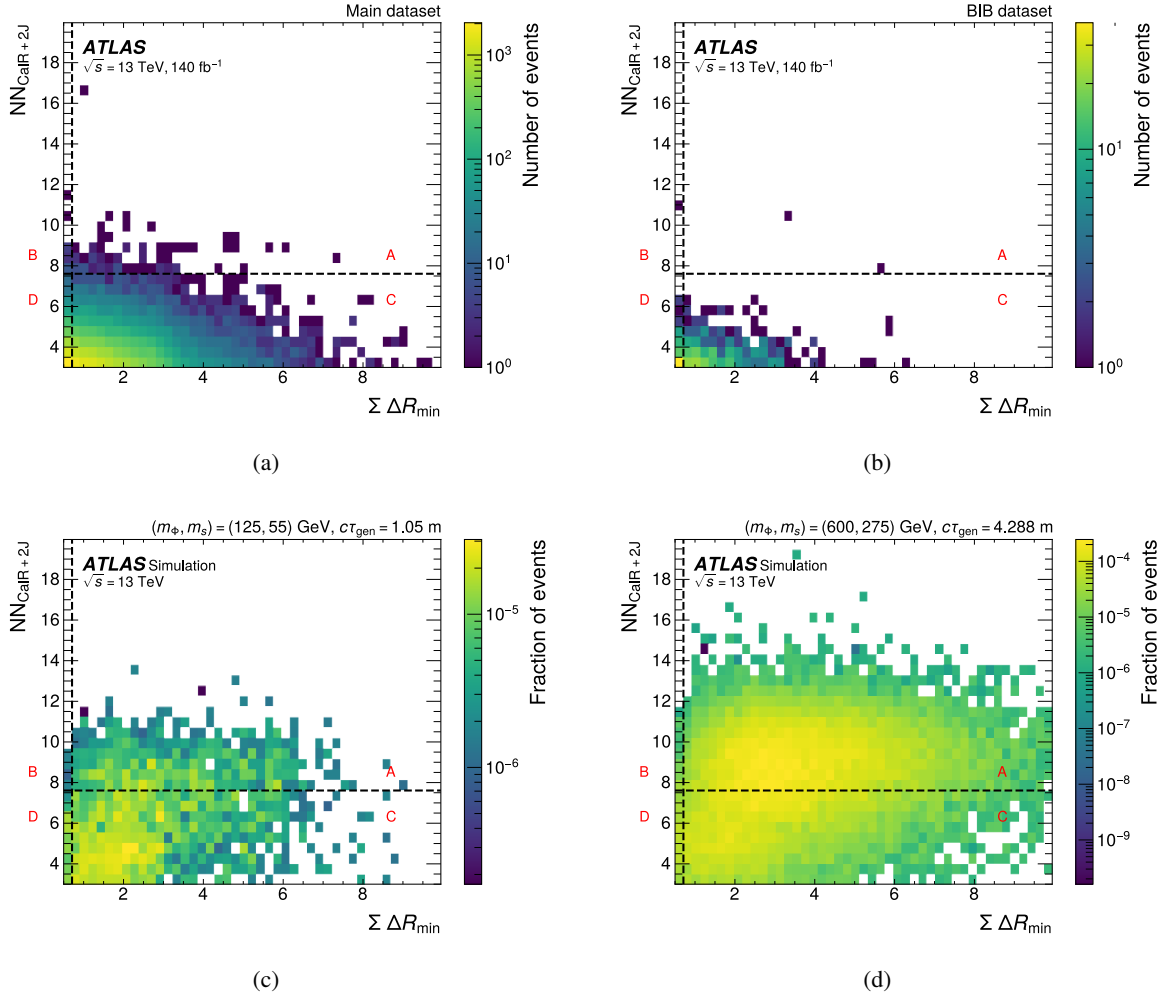


Figure 5: Distribution of events in the two-dimensional plane of $NN_{\text{CalR}+2J}$ vs. $\Sigma \Delta R_{\min}$ in the CalR+2J channel for (a) the main dataset, (b) the BIB datasets, and (c, d) example benchmark signal samples. Final regions A, B, C and D are marked in red.

error on the estimated number of events in A below 35%. These selections, together with the definition of region A, are shown in Tables 2 and 3. The definitions of regions B, C and D can be obtained by inverting one or both the requirements that define region A.

The ABCD method is tested in validation regions that are orthogonal to the signal regions. In the CalR+W channel, validation regions are defined in regions C and D of the main ABCD plane (VR_{CD}), with upper BDT score boundary as close as possible to region A but ensuring a low signal contamination. In the CalR+Z channel, part of regions C and D of the primary ABCD planes are used to define the validation regions. A looser set of criteria was employed for a dedicated validation region (VR_{CD}^{Loose}) to mitigate the significant statistical uncertainty observed in the original region due to limited number of events. In all channels and all validation regions, the agreement between the expected and observed number of events is found to be within statistical uncertainty, and for a wide variety of thresholds on each variable.

Figures 6 and 7 show the ABCD planes for the CalR+W and CalR+Z channels respectively, for data and

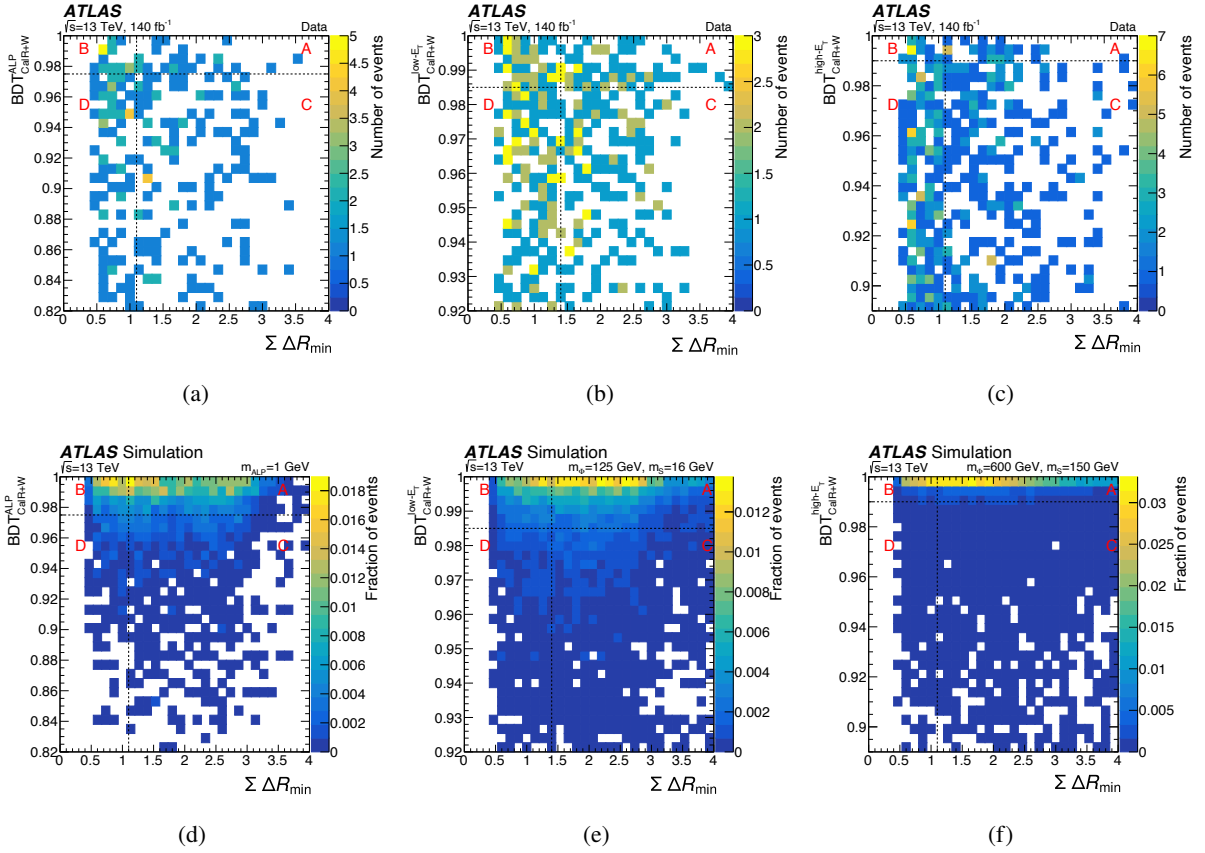


Figure 6: Distribution of events in the two-dimensional plane of $\Sigma \Delta R_{\min}$ vs. BDT score in the CalR+W channel for (a–c) data and (d–f) example benchmark signal samples. Final regions A, B, C and D are marked in red.

for one representative signal sample in each of the analysis selections.

7 Systematic uncertainties

The uncertainty in the integrated luminosity collected by ATLAS during LHC Run 2 is 0.83% [92], obtained using the LUCID-2 detector [93] for the primary luminosity measurement, complemented by measurements using the inner detector and calorimeters. This affects the result during the conversion of the upper limit on the number of allowed signal events given the observed data, into an upper limit on the signal cross-section times branching fraction.

The background estimate is not affected by the typical modelling or experimental uncertainties, as it is data-driven for all three channels. Validation tests for this method were performed in alternative ABCD planes, which were discussed in Section 6. The background estimate uncertainty is found to be negligible for all channels except for CalR+2J, in which it is estimated to be 5%.

All remaining sources of uncertainty affect the signal efficiency estimate. The rest of this section exclusively discusses uncertainties of this type. First, an uncertainty is assigned on the reweighting of events in simulation to match the observed distribution of pile-up in data. The uncertainty in the pile-up reweighting

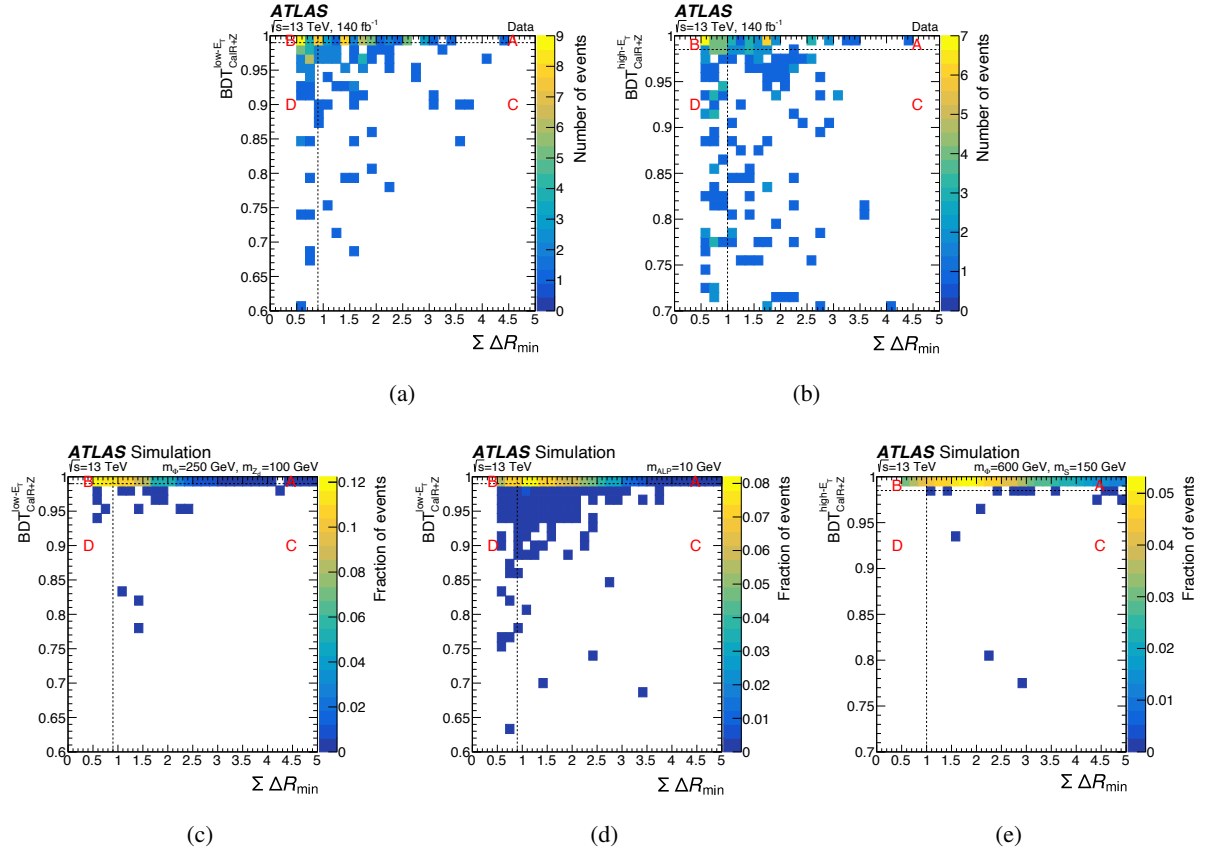


Figure 7: Distribution of events in the two-dimensional plane of $\Sigma \Delta R_{\min}$ vs. BDT score in the CalR+Z channel for data (a, b) and (c–e) example benchmark signal samples. Final regions A, B, C and D are marked in red.

of the reconstructed events in the MC simulation is estimated by comparing the distribution of the number of primary vertices in the MC simulation with the distribution in data as a function of the instantaneous luminosity. Differences between these distributions are reduced by scaling the mean number of interactions per bunch crossing in the MC simulation and $\pm 1\sigma$ uncertainties are assigned to these scaling factors [92, 93]. The effect on the signal event yields varies between 0.3% and 7% depending on the signal model and channel.

Next, the signal efficiency is affected by the jet energy scale (JES) and jet energy resolution (JER). These uncertainties are calculated using the prescription detailed in Ref. [94], and are of the order of 0.1–15% depending on the model. Since the displaced jets used in this analysis are non-standard due to their unusual electromagnetic energy fraction (EMF), the jet energy uncertainties were re-derived as a function of the EMF and η . These additional uncertainties are found to have an effect of up to 4% on the signals efficiencies. They are conservatively taken in quadrature with the standard jet energy uncertainties.

Since LLPs are used for triggering in the CalR+2J channel, an uncertainty is assigned on the signal trigger efficiency by studying the modelling of the key variables in the trigger: the jet energy, the CalRatio and the p_T of the jet’s tracks. The level of agreement between data and the MC simulation for these variables in HLT- and offline-reconstructed quantities is evaluated. A tag-and-probe technique is applied to a pure sample of multijet events obtained using standard jet triggers in both the data and MC simulation.

Scale factors that represent the degree of mismodelling in each variable are derived and then applied in an emulation of the CalRatio triggers. The change in yield relative to the nominal (unscaled) trigger emulation after the full analysis selection is taken as the size of the systematic uncertainty, which has values between 1% and 6% depending on the signal model. In the CalR+W and CalR+Z channels, the triggering is performed using prompt leptons, and the offline selections on the lepton p_T are well above the trigger plateau. The lepton systematic uncertainty's effect on the signal event yields in the ranges from approximately 0.5% to 0.9%, depending on the specific benchmark model. This is small compared with other sources systematic error.

A systematic uncertainty in the machine-learning algorithms used in the analysis is included. Specifically, this uncertainty accounts for potential mismodelling of input variables used in the per-jet NN tagger. It follows the same strategy as in Ref. [31] and is briefly summarised here. In the dijet control regions, the distributions of the inputs of the per-jet NN are studied. The subsequent downstream ML algorithms are also explored in the relevant control regions. In most cases, the agreement is found to be good. Some variables show modelling issues, as show in the Auxiliary Material of Ref. [31]. Examples include longitudinal positions of track impact parameters, and hit and energy deposit timing information. These are caused by the fact that the spread of the beam-crossing time, any instrumental cross-talk and timing offset calibrations are not simulated. The effect of such mismodelling is reduced by the adversarial training of the per-jet NN, which prevents it from exploiting differences between multijet events in simulation and in data. Nevertheless, the following procedure is used to gauge the residual effect on signal efficiency. The mismodelling of problematic variables is encapsulated by a set of transfer factors. In an ensemble of pseudo-experiments, the per-jet NN and downstream ML variables are modulated by random variations sampled from a Gaussian distribution with a mean of zero, and a width determined by the transfer factors determined above. The signal efficiencies in each pseudo-experiment are recalculated with the modulated versions of the NN and ML algorithms. The spread in the signal efficiencies across the ensemble of pseudo-experiments gives the uncertainty associated with this effect, which is estimated to be of the order of 5% or smaller depending on the selection. An alternative method to evaluating the size of this uncertainty was studied. In this alternative method, control regions were defined by inverting the selections that define each signal region. The overall difference agreement of the per-event ML score distributions between data and simulation gave consistent values of the order of 5%.

Small additional uncertainties arise from the electron and muon identification, calibration and reconstruction. The total systematic uncertainty associated with the leptons is below 1% for all models, which is very small compared with all other sources of uncertainty. In the CalR+W, a small uncertainty of up to 1% results from the missing transverse energy calibration.

Finally, an uncertainty due to the NLO-reweighting of the signal samples for the CalR+2J channel is obtained by comparing the NLO MADGRAPH predictions for a 125 GeV mediator mass with predictions at NNLO accuracy in QCD from POWHEG BOX v2. This results in an additional signal efficiency uncertainty of 1% to 6% for most samples. The CalR+Z/W channels are not affected by this uncertainty.

8 Results and statistical interpretation

The data-driven background estimation procedure described in Section 6 is utilised in a simultaneous fit to assess if the data are compatible with the prediction or potential signal events. This approach follows a similar methodology as detailed in Ref. [31], where a successful application of a comparable analysis method was previously demonstrated. An overall profile likelihood function is constructed from the product

of the Poisson probabilities of observing the number of events N_X^{obs} , given an expectation N_X^{exp} in each region X , where $X = A, B, C$ or D . The value of N_X^{exp} in each region is the sum of: the expected signal yield N_X^{sig} , given by the number of simulated signal events entering region X multiplied by the signal strength μ (the parameter of interest); and the expected background yield N_X^{bkg} . In the fit, the expected background yields are constrained to obey the ABCD relation $N_A^{\text{bkg}} = (N_B^{\text{bkg}} \times N_C^{\text{bkg}}) / N_D^{\text{bkg}}$. Since the Poisson constraints only apply to N_X^{obs} relative to N_X^{exp} , it follows that the background prediction may change dynamically in the fit as a function of the signal strength μ . Additional constraint terms in the likelihood are included for the total signal uncertainty nuisance parameter. The likelihood was implemented using the pyhf framework [95, 96].

In the background-only hypothesis, the expected yields can only be adjusted for background components. Initially, without knowing the observed yield in region A, the expected background yields in regions B, C, and D match their observed counterparts, while region A reflects the naive ABCD relation. This initial estimate, known as the *a priori* background estimate, assumes the observed value in region A is unknown, such as before unblinding the data. Once the observed yield in region A is included in the fit, the expected background yields in the other regions may shift away from their observed yields (within statistical uncertainties). This adjustment ensures that the ABCD relation holds for the *expected* yields, even if the *observed* yields deviate due to statistical fluctuations. This is called the *a posteriori* background estimate. It corresponds to the case where the observed yield in region A is known (after unblinding). The introduction of a signal component will dynamically modify the allowed background prediction: for example allowing a potential excess in region A to be explained by a non-zero signal strength. The observed counts and the *a priori* and *a posteriori* results for each channel are summarised in Table 4 for each region.

No significant excess is observed in any of the signal regions. Upper limits on LLP production cross-section times branching fraction are extracted using the CL_s method [97] with the “alternative test statistic” \tilde{q} [98] as implemented in pyhf. The asymptotic approximation is used for all results. The results are obtained for the signal samples, which were generated with a given (arbitrary) LLP proper lifetime. The result can be extrapolated to other lifetimes by reweighting the LLP exponential decay distributions to each lifetime, and re-evaluating the signal efficiency. This procedure is identical to that described in Ref. [31].

Examples of the resulting 95% confidence level (CL) upper limits on the cross-section times branching fraction for HS models based on the CalR+2J channel are shown in Figure 8. Figure 9 shows a selection of limits obtained using the CalR+W channel, constraining the WALP model and the HS model in the associated W boson production mode. The limits derived from the CalR+Z channel are presented in Figure 10 and constrain the ZALP, HZZ_d and ZHS models. For the case of $m_\Phi = 125$ GeV, the limits are scaled to the relevant SM cross-section of Higgs boson production.

The constraints obtained by CalR+2J for HS models are strongest for proper lifetimes $c\tau$ of order of 1–2 m. For the particular case where the SM Higgs boson is the mediator, assuming a production cross-section for gluon–gluon fusion of 48 pb, the branching fraction of Higgs bosons to hadronically decaying scalar LLPs is constrained to below 1% in the mean proper decay length range of 30 cm to 4.5 m, depending on the mass of the LLP. This represents an improvement of a factor of approximately three relative to the results in the previous search [31]. Specifically, this improvement comes from relaxing a requirement on the CalRatio of the two most signal-like jets (which was detrimental to the events featuring the resolved topology but necessary to control backgrounds), and instead exploiting additional jet information, allowing a substantial background reduction while maintaining signal efficiency for low mediator mass samples.

Still considering the HS model, the CalR+Z and CalR+W channels provide the first constraints on hadronically decaying LLPs in the calorimeter where the production of a scalar mediator is in association

Table 4: Application of the modified ABCD method to the final high- E_T and low- E_T selections. The *a priori* estimate refers to the “pre-unblinding” case, where the data in region A are ignored by removing the Poisson constraint in that region and the signal strength is fixed to zero. This matches the simple $N_A^{\text{bkg}} = (N_B^{\text{bkg}} \times N_C^{\text{bkg}}) / N_D^{\text{bkg}}$ relation. The *a posteriori* estimate refers to the “post-unblinding” case, including the observed data in region A in the background-only global fit. As can be seen, the predicted background in region A can increase substantially from the *a priori* case, but only insofar as the adjusted yields in the other regions remain consistent with the observed yields within their statistical uncertainties. Only statistical uncertainties are included in the quoted error on the background.

CalR+2J channel				
	A	B	C	D
Observed data	92	18	25213	4774
Estimated background <i>a priori</i>	95 ± 23	18 ± 4.2	25210 ± 160	4774 ± 69
Fitted background <i>a posteriori</i>	93 ± 10	18 ± 4.2	25210 ± 160	4774 ± 69
CalR+W channel				
W ALP selection	A	B	C	D
Observed data	27	23	122	82
Estimated background <i>a priori</i>	34.2 ± 8.5	23.0 ± 4.8	122 ± 11	82.0 ± 9.1
Fitted background <i>a posteriori</i>	29.3 ± 4.4	20.7 ± 4.5	120 ± 11	84.3 ± 9.2
low- E_T WHS selection	A	B	C	D
Observed data	59	53	155	155
Estimated background <i>a priori</i>	53.0 ± 9.4	53.0 ± 7.3	155 ± 12	155 ± 12
Fitted background <i>a posteriori</i>	56.8 ± 6.0	55.2 ± 7.4	157 ± 13	153 ± 12
high- E_T WHS selection	A	B	C	D
Observed data	33	21	261	220
Estimated background <i>a priori</i>	24.9 ± 5.8	21.0 ± 4.6	261 ± 16	220 ± 15
Fitted background <i>a posteriori</i>	29.6 ± 4.2	24.3 ± 4.9	264 ± 16	217 ± 15
CalR+Z channel				
low- E_T ZHS selection	A	B	C	D
Observed data	36	12	64	43
Estimated background <i>a priori</i>	17.9 ± 6.1	12.0 ± 3.5	64.0 ± 8.0	43.0 ± 6.6
Fitted background <i>a posteriori</i>	31.0 ± 4.8	17.0 ± 3.9	69.0 ± 8.3	38.0 ± 6.2
high- E_T ZHS selection	A	B	C	D
Observed data	32	21	75	52
Estimated background <i>a priori</i>	30.5 ± 8.5	21.0 ± 4.6	75 ± 8.7	52.0 ± 7.2
Fitted background <i>a posteriori</i>	31.6 ± 4.7	21.3 ± 4.6	75.6 ± 8.7	51.4 ± 7.2

with a vector boson. Higgs boson branching fractions to LLPs above 50% in this production mode are excluded for mean proper decay lengths in the cm to m range. While the derived constraints in terms of Higgs boson branching fractions are not as strong as those derived in the CalR+2J channel or in Ref. [31], they provide a complementary constraint in a different production mode. A combination of the HS results between the three channels is not performed, since the gluon–gluon fusion cross-section is overwhelmingly large compared with associated vector boson production cross-section and consequently any combined limit would be fully dominated by the CalR+2J channel results.

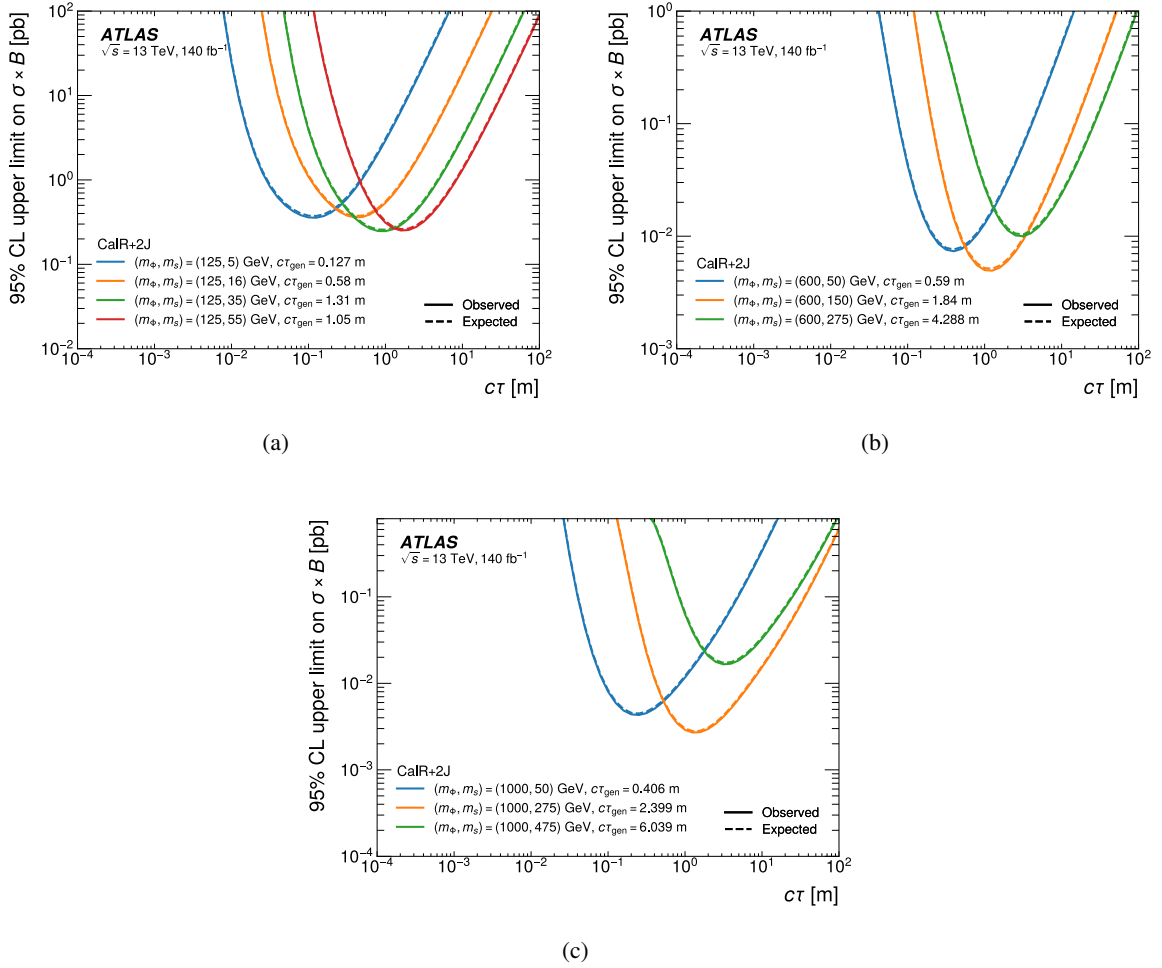


Figure 8: Observed (solid line) and expected (dashed line) upper limits at the 95% CL on the cross-section times branching fraction as a function of $c\tau$ for a selection of HS signal models in the CalR+2J channel for HS models with mediator masses of (a) 125 GeV, (b) 600 GeV and (c) 1000 GeV.

Constraints are set by ATLAS on photophobic ALP models for the first time using the CalR+W and CalR+Z channels, with cross-sections above 0.1 pb excluded in the 0.1 mm–10 m range. ALP exclusion limits in terms of cross-section and proper lifetime can be interpreted for the relevant model parameters. The width of the ALP decay into gluons is given by:

$$\Gamma_{agg} = \frac{2}{\pi f_a^2} C_G^2 m_{\text{ALP}}^3, \quad (1)$$

where f_a is the energy scale of the ALP and m_{ALP} its mass. Therefore, for a given mass and scale, the ALP proper lifetime $c\tau$ depends on the inverse square of the gluon coupling $c\tau \propto C_G^{-2}$. Additionally, the cross-section of the simulated process is determined by the coupling of the ALP with the SM weak-sector. For a photophobic ALP, this implies that $\sigma \propto C_W^2$. The resulting exclusion limits on C_G and C_W are presented in Figure 11. A summary of these results is presented in the plane of ALP mass versus its coupling to gluons in Figure 12, where the coupling to gluons is scaled by the ALP energy scale $g_{agg} = 4C_G/f_a$.

Finally, new constraints on the ZZ_d model are set, which are more sensitive than previous results [34] by an

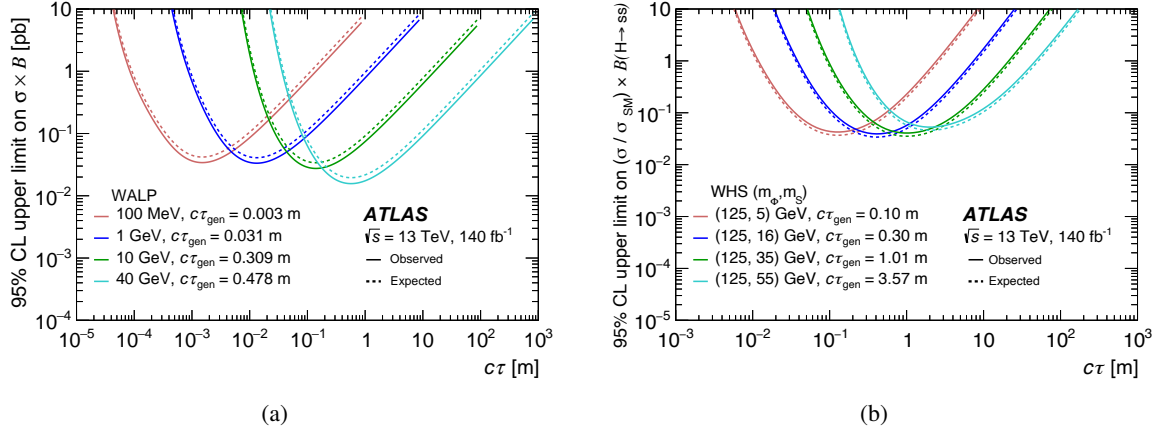


Figure 9: Observed (solid line) and expected (dashed line) upper limits at the 95% CL on the cross-section times branching fraction as a function of $c\tau$ for a selection of models targeted in the CalR+W channel for (a) WALP models and (b) WHS models with a SM Higgs boson mediator.

order of magnitude, with production cross-sections of a dark photon with a Z boson above 0.1 pb excluded for Z_d proper decay lengths in the 20 cm to 50 m range, depending on the mediator and Z_d masses. The improvement comes the fact that this work uses a dataset approximately four times larger than the one studied in Ref. [34], and major improvements in displaced jet identification efficiency and background rejection thanks to the per-jet NN.

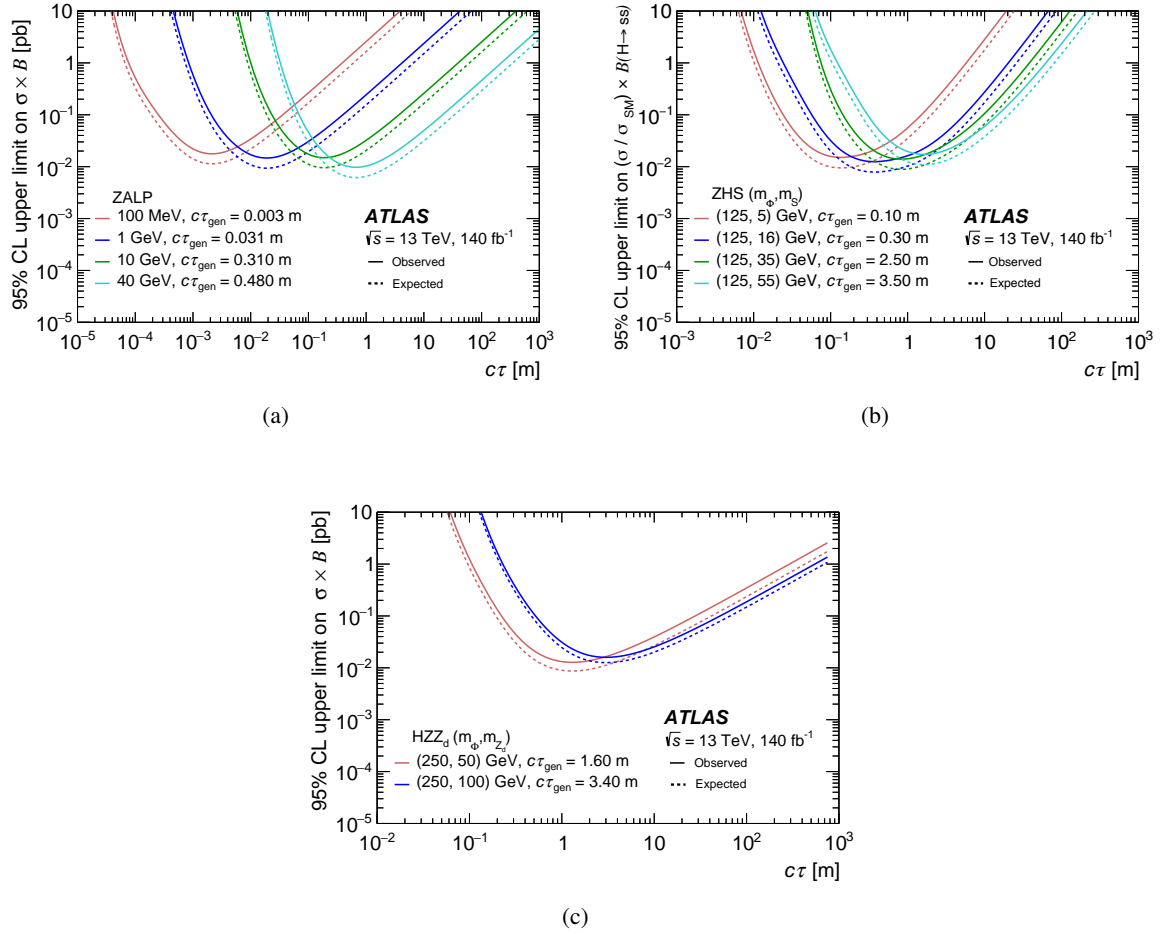


Figure 10: Observed (solid line) and expected (dashed line) upper limits at the 95% CL on the cross-section times branching fraction as a function of $c\tau$ for a variety of models probed by the CalR+Z channel for (a) ZALP models, (b) ZHS models with the SM Higgs boson as a mediator, and (c) HZZ_d models.

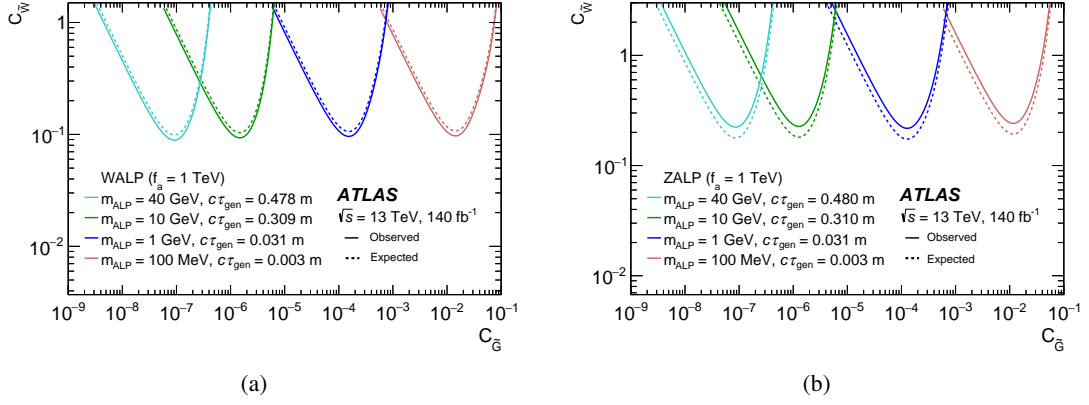


Figure 11: Summary of the observed (solid line) and expected (dashed line) upper limits at the 95% CL on $C_{\tilde{G}}$ as a function of $C_{\tilde{W}}$ for a variety of ALP mass hypotheses probed by the CalR+R and Cal+Z channels for (a) WALP and (b) ZALP models.

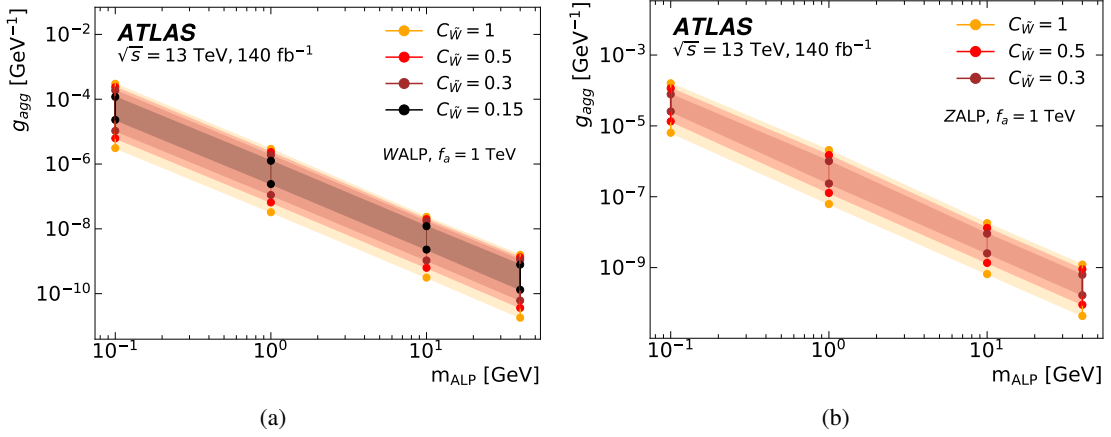


Figure 12: Regions in the ALP mass versus its coupling to gluons scaled by the ALP energy scale $g_{agg} = 4C_{\tilde{G}}/f_a$ excluded at 95% CL, for $C_{\tilde{W}} = 1$, $C_{\tilde{W}} = 0.5$, $C_{\tilde{W}} = 0.3$ and $C_{\tilde{W}} = 0.15$, in the (a) WALP and (b) ZALP models. The contours are obtained by interpolating between the exclusions for different LLP masses considered in the analysis, taking the logical union of the regions excluded for each mass.

9 Conclusion

This paper describes a search for hadronically decaying long-lived particles giving rise to displaced jets in the ATLAS hadronic calorimeter, using the ATLAS Run 2 dataset of 140 fb^{-1} of pp collisions at $\sqrt{s} = 13 \text{ TeV}$. The analysis considers three topologies: pair-produced LLPs, one of which leads to a single displaced jet in the calorimeter, the other, having low boost, yielding two resolved jets; and single- or pair-produced LLPs in association with a W or Z vector boson, which decays leptonically. For all three analysis channels a per-jet neural network is used to distinguish signal-like jets from jets from Standard Model processes or beam-induced backgrounds. Further per-event machine-learning discriminants are then used to define regions sensitive to a variety of LLP signals. In each case, a data-driven background estimate is used. No significant excess of events is observed in any of the channels. Constraints on the production cross-section times branching fraction at 95% confidence level are set for several benchmark models. The results for Hidden Sector models exclude branching fractions of Higgs boson mediators to neutral scalar LLPs above 1% for LLP decay lengths between 30 cm and 4.5 m. These results extend those set by previous ATLAS results, improving the limits by a factor of approximately three, by exploiting additional jet information to more efficiently reject background events. Limits are also set on dark photons produced in association with a Z boson, with production cross-sections above 0.1 pb excluded for proper decay lengths between 20 cm and 50 m. This improves upon previous ATLAS results by an order of magnitude, thanks to a larger dataset and the use of machine-learning discriminants. Finally, constraints are set on photophobic axion-like particle models produced in association with a W or Z boson for the first time, with cross-sections above 0.1 pb excluded in the 10 mm–10 m range. This analysis is part of a wider programme of searches for LLPs with the ATLAS experiment, and has unique sensitivity to LLP laboratory decay lengths of the order of 1 m. It represents the first time that signatures involving neutral hadronically decaying LLPs with prompt objects are targeted in that decay range with the aid of machine-learning discriminants.

Acknowledgements

We thank CERN for the very successful operation of the LHC and its injectors, as well as the support staff at CERN and at our institutions worldwide without whom ATLAS could not be operated efficiently.

The crucial computing support from all WLCG partners is acknowledged gratefully, in particular from CERN, the ATLAS Tier-1 facilities at TRIUMF/SFU (Canada), NDGF (Denmark, Norway, Sweden), CC-IN2P3 (France), KIT/GridKA (Germany), INFN-CNAF (Italy), NL-T1 (Netherlands), PIC (Spain), RAL (UK) and BNL (USA), the Tier-2 facilities worldwide and large non-WLCG resource providers. Major contributors of computing resources are listed in Ref. [99].

We gratefully acknowledge the support of ANPCyT, Argentina; YerPhI, Armenia; ARC, Australia; BMWFW and FWF, Austria; ANAS, Azerbaijan; CNPq and FAPESP, Brazil; NSERC, NRC and CFI, Canada; CERN; ANID, Chile; CAS, MOST and NSFC, China; Minciencias, Colombia; MEYS CR, Czech Republic; DNRF and DNSRC, Denmark; IN2P3-CNRS and CEA-DRF/IRFU, France; SRNSFG, Georgia; BMBF, HGF and MPG, Germany; GSRI, Greece; RGC and Hong Kong SAR, China; ISF and Benozziyo Center, Israel; INFN, Italy; MEXT and JSPS, Japan; CNRST, Morocco; NWO, Netherlands; RCN, Norway; MNiSW, Poland; FCT, Portugal; MNE/IFA, Romania; MESTD, Serbia; MSSR, Slovakia; ARRS and MIZŠ, Slovenia; DSI/NRF, South Africa; MICINN, Spain; SRC and Wallenberg Foundation, Sweden;

SERI, SNSF and Cantons of Bern and Geneva, Switzerland; MOST, Taipei; TENMAK, Türkiye; STFC, United Kingdom; DOE and NSF, United States of America.

Individual groups and members have received support from BCKDF, CANARIE, CRC and DRAC, Canada; CERN-CZ, FORTE and PRIMUS, Czech Republic; COST, ERC, ERDF, Horizon 2020, ICSC-NextGenerationEU and Marie Skłodowska-Curie Actions, European Union; Investissements d'Avenir Labex, Investissements d'Avenir Idex and ANR, France; DFG and AvH Foundation, Germany; Herakleitos, Thales and Aristeia programmes co-financed by EU-ESF and the Greek NSRF, Greece; BSF-NSF and MINERVA, Israel; NCN and NAWA, Poland; La Caixa Banking Foundation, CERCA Programme Generalitat de Catalunya and PROMETEO and GenT Programmes Generalitat Valenciana, Spain; Göran Gustafssons Stiftelse, Sweden; The Royal Society and Leverhulme Trust, United Kingdom.

In addition, individual members wish to acknowledge support from Armenia: Yerevan Physics Institute (FAPERJ); CERN: European Organization for Nuclear Research (CERN PJAS); Chile: Agencia Nacional de Investigación y Desarrollo (FONDECYT 1230812, FONDECYT 1230987, FONDECYT 1240864); China: Chinese Ministry of Science and Technology (MOST-2023YFA1605700), National Natural Science Foundation of China (NSFC - 12175119, NSFC 12275265, NSFC-12075060); Czech Republic: Czech Science Foundation (GACR - 24-11373S), Ministry of Education Youth and Sports (FORTE CZ.02.01.01/00/22_008/0004632), PRIMUS Research Programme (PRIMUS/21/SCI/017); EU: H2020 European Research Council (ERC - 101002463); European Union: European Research Council (ERC - 948254, ERC 101089007), Horizon 2020 Framework Programme (MUCCA - CHIST-ERA-19-XAI-00), European Union, Future Artificial Intelligence Research (FAIR-NextGenerationEU PE00000013), Italian Center for High Performance Computing, Big Data and Quantum Computing (ICSC, NextGenerationEU); France: Agence Nationale de la Recherche (ANR-20-CE31-0013, ANR-21-CE31-0013, ANR-21-CE31-0022), Investissements d'Avenir Labex (ANR-11-LABX-0012); Germany: Baden-Württemberg Stiftung (BW Stiftung-Postdoc Eliteprogramme), Deutsche Forschungsgemeinschaft (DFG - 469666862, DFG - CR 312/5-2); Italy: Istituto Nazionale di Fisica Nucleare (ICSC, NextGenerationEU); Japan: Japan Society for the Promotion of Science (JSPS KAKENHI JP22H01227, JSPS KAKENHI JP22H04944, JSPS KAKENHI JP22KK0227, JSPS KAKENHI JP23KK0245); Netherlands: Netherlands Organisation for Scientific Research (NWO Veni 2020 - VI.Veni.202.179); Norway: Research Council of Norway (RCN-314472); Poland: Polish National Agency for Academic Exchange (PPN/PPO/2020/1/00002/U/00001), Polish National Science Centre (NCN 2021/42/E/ST2/00350, NCN OPUS nr 2022/47/B/ST2/03059, NCN UMO-2019/34/E/ST2/00393, UMO-2020/37/B/ST2/01043, UMO-2021/40/C/ST2/00187, UMO-2022/47/O/ST2/00148, UMO-2023/49/B/ST2/04085, UMO-2023/51/B/ST2/00920); Slovenia: Slovenian Research Agency (ARIS grant J1-3010); Spain: Generalitat Valenciana (Artemisa, FEDER, IDIFEDER/2018/048), Ministry of Science and Innovation (MCIN & NextGenEU PCI2022-135018-2, MICIN & FEDER PID2021-125273NB, RYC2019-028510-I, RYC2020-030254-I, RYC2021-031273-I, RYC2022-038164-I), PROMETEO and GenT Programmes Generalitat Valenciana (CIDEGENT/2019/027); Sweden: Swedish Research Council (Swedish Research Council 2023-04654, VR 2018-00482, VR 2022-03845, VR 2022-04683, VR 2023-03403, VR grant 2021-03651), Knut and Alice Wallenberg Foundation (KAW 2018.0157, KAW 2018.0458, KAW 2019.0447, KAW 2022.0358); Switzerland: Swiss National Science Foundation (SNSF - PCEFP2_194658); United Kingdom: Leverhulme Trust (Leverhulme Trust RPG-2020-004), Royal Society (NIF-R1-231091); United States of America: U.S. Department of Energy (ECA DE-AC02-76SF00515), Neubauer Family Foundation.

References

- [1] N. Arkani-Hamed, A. Gupta, D. E. Kaplan, N. Weiner and T. Zorawski, *Simply Unnatural Supersymmetry*, (2012), arXiv: [1212.6971 \[hep-ph\]](#).
- [2] G. F. Giudice and R. Rattazzi, *Theories with gauge-mediated supersymmetry breaking*, *Phys. Rept.* **322** (1999) 419, arXiv: [hep-ph/9801271 \[hep-ph\]](#).
- [3] R. Barbier et al., *R-Parity-violating supersymmetry*, *Phys. Rept.* **420** (2005) 1, arXiv: [hep-ph/0406039 \[hep-ph\]](#).
- [4] C. Csáki, E. Kuflik, O. Slone and T. Volansky, *Models of dynamical R-parity violation*, *JHEP* **06** (2015) 045, arXiv: [1502.03096 \[hep-ph\]](#).
- [5] J. Fan, M. Reece and J. T. Ruderman, *Stealth supersymmetry*, *JHEP* **11** (2011) 012, arXiv: [1105.5135 \[hep-ph\]](#).
- [6] J. Fan, M. Reece and J. T. Ruderman, *A stealth supersymmetry sampler*, *JHEP* **07** (2012) 196, arXiv: [1201.4875 \[hep-ph\]](#).
- [7] Z. Chacko, D. Curtin and C. B. Verhaaren, *A quirky probe of neutral naturalness*, *Phys. Rev. D* **94** (2016) 011504, arXiv: [1512.05782 \[hep-ph\]](#).
- [8] G. Burdman, Z. Chacko, H.-S. Goh and R. Harnik, *Folded supersymmetry and the LEP paradox*, *JHEP* **02** (2007) 009, arXiv: [hep-ph/0609152 \[hep-ph\]](#).
- [9] H. Cai, H.-C. Cheng and J. Terning, *A quirky little Higgs model*, *JHEP* **05** (2009) 045, arXiv: [0812.0843 \[hep-ph\]](#).
- [10] Z. Chacko, H.-S. Goh and R. Harnik, *Natural Electroweak Breaking from a Mirror Symmetry*, *Phys. Rev. Lett.* **96** (2006) 231802, arXiv: [hep-ph/0506256 \[hep-ph\]](#).
- [11] M. J. Strassler and K. M. Zurek, *Echoes of a hidden valley at hadron colliders*, *Phys. Lett. B* **651** (2007) 374, arXiv: [hep-ph/0604261 \[hep-ph\]](#).
- [12] M. J. Strassler and K. M. Zurek, *Discovering the Higgs through highly-displaced vertices*, *Phys. Lett. B* **661** (2008) 263, arXiv: [hep-ph/0605193 \[hep-ph\]](#).
- [13] Y. F. Chan, M. Low, D. E. Morrissey and A. P. Spray, *LHC Signatures of a Minimal Supersymmetric Hidden Valley*, *JHEP* **05** (2012) 155, arXiv: [1112.2705 \[hep-ph\]](#).
- [14] M. Baumgart, C. Cheung, J. T. Ruderman, L.-T. Wang and I. Yavin, *Non-abelian dark sectors and their collider signatures*, *JHEP* **04** (2009) 014, arXiv: [0901.0283 \[hep-ph\]](#).
- [15] D. E. Kaplan, M. A. Luty and K. M. Zurek, *Asymmetric dark matter*, *Phys. Rev. D* **79** (2009) 115016, arXiv: [0901.4117 \[hep-ph\]](#).
- [16] K. R. Dienes and B. Thomas, *Dynamical dark matter. I. Theoretical overview*, *Phys. Rev. D* **85** (2012) 083523, arXiv: [1106.4546 \[hep-ph\]](#).
- [17] K. R. Dienes, S. Su and B. Thomas, *Distinguishing dynamical dark matter at the LHC*, *Phys. Rev. D* **86** (2012) 054008, arXiv: [1204.4183 \[hep-ph\]](#).
- [18] Y. Cui and B. Shuve, *Probing Baryogenesis with Displaced Vertices at the LHC*, *JHEP* **02** (2015) 049, arXiv: [1409.6729 \[hep-ph\]](#).

- [19] J. C. Helo, S. G. Kovalenko and M. Hirsch, *Heavy neutrino searches at the LHC with displaced vertices*, *Phys. Rev. D* **89** (2014) 073005, arXiv: [1312.2900 \[hep-ph\]](#).
- [20] B. Batell, M. Pospelov and B. Shuve, *Shedding light on neutrino masses with dark forces*, *JHEP* **08** (2016) 052, arXiv: [1604.06099 \[hep-ph\]](#).
- [21] I. Brivio et al., *ALPs Effective Field Theory and Collider Signatures*, *Eur. Phys. J. C* **77** (2017) 572, arXiv: [1701.05379 \[hep-ph\]](#).
- [22] U. Haisch and L. Schnell, *Long-lived particle phenomenology in the 2HDM+a model*, *JHEP* **04** (2023) 134, arXiv: [2302.02735 \[hep-ph\]](#).
- [23] LHCb Collaboration, *Updated search for long-lived particles decaying to jet pairs*, *Eur. Phys. J. C* **77** (2017) 812, arXiv: [1705.07332 \[hep-ex\]](#).
- [24] CMS Collaboration, *Search for long-lived particles using displaced jets in proton–proton collisions at $\sqrt{s} = 13$ TeV*, *Phys. Rev. D* **104** (2021) 012015, arXiv: [2012.01581 \[hep-ex\]](#).
- [25] CMS Collaboration, *Search for long-lived particles produced in association with a Z boson in proton–proton collisions at $\sqrt{s} = 13$ TeV*, *JHEP* **03** (2022) 160, arXiv: [2110.13218 \[hep-ex\]](#).
- [26] CMS Collaboration, *Search for long-lived particles using displaced vertices and missing transverse momentum in proton–proton collisions at $\sqrt{s} = 13$ TeV*, *Phys. Rev. D* **109** (2024) 112005, arXiv: [2402.15804 \[hep-ex\]](#).
- [27] CMS Collaboration, *Search for long-lived particles decaying in the CMS muon detectors in proton–proton collisions at $\sqrt{s} = 13$ TeV*, (2024), arXiv: [2402.01898 \[hep-ex\]](#).
- [28] ATLAS Collaboration, *Search for the Higgs boson produced in association with a vector boson and decaying into two spin-zero particles in the $H \rightarrow aa \rightarrow 4b$ channel in pp collisions at $\sqrt{s} = 13$ TeV with the ATLAS detector*, *JHEP* **10** (2018) 031, arXiv: [1806.07355 \[hep-ex\]](#).
- [29] ATLAS Collaboration, *Search for exotic decays of the Higgs boson into long-lived particles in pp collisions at $\sqrt{s} = 13$ TeV using displaced vertices in the ATLAS inner detector*, *JHEP* **11** (2021) 229, arXiv: [2107.06092 \[hep-ex\]](#).
- [30] ATLAS Collaboration, *Search for light long-lived particles in pp collisions at $\sqrt{s} = 13$ TeV using displaced vertices in the ATLAS inner detector*, (2024), arXiv: [2403.15332 \[hep-ex\]](#).
- [31] ATLAS Collaboration, *Search for neutral long-lived particles in pp collisions at $\sqrt{s} = 13$ TeV that decay into displaced hadronic jets in the ATLAS calorimeter*, *JHEP* **06** (2022) 005, arXiv: [2203.01009 \[hep-ex\]](#).
- [32] ATLAS Collaboration, *Search for long-lived particles produced in pp collisions at $\sqrt{s} = 13$ TeV that decay into displaced hadronic jets in the ATLAS muon spectrometer*, *Phys. Rev. D* **99** (2019) 052005, arXiv: [1811.07370 \[hep-ex\]](#).
- [33] ATLAS Collaboration, *Search for long-lived neutral particles produced in pp collisions at $\sqrt{s} = 13$ TeV decaying into displaced hadronic jets in the ATLAS inner detector and muon spectrometer*, *Phys. Rev. D* **101** (2020) 052013, arXiv: [1911.12575 \[hep-ex\]](#).
- [34] ATLAS Collaboration, *Search for the Production of a Long-Lived Neutral Particle Decaying within the ATLAS Hadronic Calorimeter in Association with a Z Boson from pp Collisions at $\sqrt{s} = 13$ TeV*, *Phys. Rev. Lett.* **122** (2019) 151801, arXiv: [1811.02542 \[hep-ex\]](#).

- [35] ATLAS Collaboration, *The ATLAS Experiment at the CERN Large Hadron Collider*, *JINST* **3** (2008) S08003.
- [36] ATLAS Collaboration, *ATLAS Insertable B-Layer Technical Design Report*, ATLAS-TDR-19; CERN-LHCC-2010-013, 2010, URL: <https://cds.cern.ch/record/1291633>, Addendum: ATLAS-TDR-19-ADD-1; CERN-LHCC-2012-009, 2012, URL: <https://cds.cern.ch/record/1451888>.
- [37] B. Abbott et al., *Production and integration of the ATLAS Insertable B-Layer*, *JINST* **13** (2018) T05008, arXiv: [1803.00844](https://arxiv.org/abs/1803.00844) [[physics.ins-det](#)].
- [38] ATLAS Collaboration, *Performance of the ATLAS trigger system in 2015*, *Eur. Phys. J. C* **77** (2017) 317, arXiv: [1611.09661](https://arxiv.org/abs/1611.09661) [[hep-ex](#)].
- [39] ATLAS Collaboration, *Software and computing for Run 3 of the ATLAS experiment at the LHC*, (2024), arXiv: [2404.06335](https://arxiv.org/abs/2404.06335) [[hep-ex](#)].
- [40] ATLAS Collaboration, *ATLAS data quality operations and performance for 2015–2018 data-taking*, *JINST* **15** (2020) P04003, arXiv: [1911.04632](https://arxiv.org/abs/1911.04632) [[physics.ins-det](#)].
- [41] ATLAS Collaboration, *Performance of electron and photon triggers in ATLAS during LHC Run 2*, *Eur. Phys. J. C* **80** (2020) 47, arXiv: [1909.00761](https://arxiv.org/abs/1909.00761) [[hep-ex](#)].
- [42] ATLAS Collaboration, *Performance of the ATLAS muon triggers in Run 2*, *JINST* **15** (2020) P09015, arXiv: [2004.13447](https://arxiv.org/abs/2004.13447) [[physics.ins-det](#)].
- [43] ATLAS Collaboration, *The performance of the jet trigger for the ATLAS detector during 2011 data taking*, *Eur. Phys. J. C* **76** (2016) 526, arXiv: [1606.07759](https://arxiv.org/abs/1606.07759) [[hep-ex](#)].
- [44] T. Sjöstrand, S. Mrenna and P. Skands, *A brief introduction to PYTHIA 8.1*, *Comput. Phys. Commun.* **178** (2008) 852, arXiv: [0710.3820](https://arxiv.org/abs/0710.3820) [[hep-ph](#)].
- [45] ATLAS Collaboration, *ATLAS Pythia 8 tunes to 7 TeV data*, ATL-PHYS-PUB-2014-021, 2014, URL: <https://cds.cern.ch/record/1966419>.
- [46] NNPDF Collaboration, R. D. Ball et al., *Parton distributions with LHC data*, *Nucl. Phys. B* **867** (2013) 244, arXiv: [1207.1303](https://arxiv.org/abs/1207.1303) [[hep-ph](#)].
- [47] T. Gleisberg et al., *Event generation with SHERPA 1.1*, *JHEP* **02** (2009) 007, arXiv: [0811.4622](https://arxiv.org/abs/0811.4622) [[hep-ph](#)].
- [48] E. Bothmann et al., *Event generation with Sherpa 2.2*, *SciPost Phys.* **7** (2019) 034, arXiv: [1905.09127](https://arxiv.org/abs/1905.09127) [[hep-ph](#)].
- [49] T. Gleisberg and S. Höche, *Comix, a new matrix element generator*, *JHEP* **12** (2008) 039, arXiv: [0808.3674](https://arxiv.org/abs/0808.3674) [[hep-ph](#)].
- [50] F. Cascioli, P. Maierhöfer and S. Pozzorini, *Scattering Amplitudes with Open Loops*, *Phys. Rev. Lett.* **108** (2012) 111601, arXiv: [1111.5206](https://arxiv.org/abs/1111.5206) [[hep-ph](#)].
- [51] A. Denner, S. Dittmaier and L. Hofer, *COLLIER: A fortran-based complex one-loop library in extended regularizations*, *Comput. Phys. Commun.* **212** (2017) 220, arXiv: [1604.06792](https://arxiv.org/abs/1604.06792) [[hep-ph](#)].
- [52] S. Schumann and F. Krauss, *A parton shower algorithm based on Catani–Seymour dipole factorisation*, *JHEP* **03** (2008) 038, arXiv: [0709.1027](https://arxiv.org/abs/0709.1027) [[hep-ph](#)].

- [53] S. Frixione, G. Ridolfi and P. Nason,
A positive-weight next-to-leading-order Monte Carlo for heavy flavour hadroproduction,
JHEP **09** (2007) 126, arXiv: [0707.3088 \[hep-ph\]](#).
- [54] P. Nason, *A new method for combining NLO QCD with shower Monte Carlo algorithms*,
JHEP **11** (2004) 040, arXiv: [hep-ph/0409146](#).
- [55] S. Frixione, P. Nason and C. Oleari,
Matching NLO QCD computations with parton shower simulations: the POWHEG method,
JHEP **11** (2007) 070, arXiv: [0709.2092 \[hep-ph\]](#).
- [56] S. Alioli, P. Nason, C. Oleari and E. Re, *A general framework for implementing NLO calculations in shower Monte Carlo programs: the POWHEG BOX*, *JHEP* **06** (2010) 043,
arXiv: [1002.2581 \[hep-ph\]](#).
- [57] ATLAS Collaboration, *Studies on top-quark Monte Carlo modelling for Top2016*,
ATL-PHYS-PUB-2016-020, 2016, URL: <https://cds.cern.ch/record/2216168>.
- [58] T. Sjöstrand et al., *An introduction to PYTHIA 8.2*, *Comput. Phys. Commun.* **191** (2015) 159,
arXiv: [1410.3012 \[hep-ph\]](#).
- [59] M. Beneke, P. Falgari, S. Klein and C. Schwinn,
Hadronic top-quark pair production with NNLL threshold resummation,
Nucl. Phys. B **855** (2012) 695, arXiv: [1109.1536 \[hep-ph\]](#).
- [60] M. Cacciari, M. Czakon, M. Mangano, A. Mitov and P. Nason, *Top-pair production at hadron colliders with next-to-next-to-leading logarithmic soft-gluon resummation*,
Phys. Lett. B **710** (2012) 612, arXiv: [1111.5869 \[hep-ph\]](#).
- [61] P. Bärnreuther, M. Czakon and A. Mitov, *Percent-Level-Precision Physics at the Tevatron: Next-to-Next-to-Leading Order QCD Corrections to $q\bar{q} \rightarrow t\bar{t} + X$* ,
Phys. Rev. Lett. **109** (2012) 132001, arXiv: [1204.5201 \[hep-ph\]](#).
- [62] M. Czakon and A. Mitov,
NNLO corrections to top-pair production at hadron colliders: the all-fermionic scattering channels,
JHEP **12** (2012) 054, arXiv: [1207.0236 \[hep-ph\]](#).
- [63] M. Czakon and A. Mitov,
NNLO corrections to top pair production at hadron colliders: the quark-gluon reaction,
JHEP **01** (2013) 080, arXiv: [1210.6832 \[hep-ph\]](#).
- [64] M. Czakon, P. Fiedler and A. Mitov,
Total Top-Quark Pair-Production Cross Section at Hadron Colliders Through $O(\alpha_S^4)$,
Phys. Rev. Lett. **110** (2013) 252004, arXiv: [1303.6254 \[hep-ph\]](#).
- [65] M. Czakon and A. Mitov,
Top++: A program for the calculation of the top-pair cross-section at hadron colliders,
Comput. Phys. Commun. **185** (2014) 2930, arXiv: [1112.5675 \[hep-ph\]](#).
- [66] E. Re, *Single-top Wt -channel production matched with parton showers using the POWHEG method*,
Eur. Phys. J. C **71** (2011) 1547, arXiv: [1009.2450 \[hep-ph\]](#).
- [67] NNPDF Collaboration, R. D. Ball et al., *Parton distributions for the LHC run II*,
JHEP **04** (2015) 040, arXiv: [1410.8849 \[hep-ph\]](#).
- [68] S. Frixione, E. Laenen, P. Motylinski, C. White and B. R. Webber,
Single-top hadroproduction in association with a W boson, *JHEP* **07** (2008) 029,
arXiv: [0805.3067 \[hep-ph\]](#).

- [69] M. Aliev et al., *HATHOR – HAdronic Top and Heavy quarks crOss section calculator*, *Comput. Phys. Commun.* **182** (2011) 1034, arXiv: [1007.1327 \[hep-ph\]](#).
- [70] P. Kant et al., *HatHor for single top-quark production: Updated predictions and uncertainty estimates for single top-quark production in hadronic collisions*, *Comput. Phys. Commun.* **191** (2015) 74, arXiv: [1406.4403 \[hep-ph\]](#).
- [71] S. Chang, P. J. Fox and N. Weiner, *Naturalness and Higgs decays in the MSSM with a singlet*, *JHEP* **08** (2006) 068, arXiv: [hep-ph/0511250 \[hep-ph\]](#).
- [72] S. Chang, R. Dermisek, J. F. Gunion and N. Weiner, *Nonstandard Higgs Boson Decays*, *Ann. Rev. Nucl. Part. Sci.* **58** (2008) 75, arXiv: [0801.4554 \[hep-ph\]](#).
- [73] J. Alwall et al., *The automated computation of tree-level and next-to-leading order differential cross sections, and their matching to parton shower simulations*, *JHEP* **07** (2014) 079, arXiv: [1405.0301 \[hep-ph\]](#).
- [74] M. Cepeda et al., *Report from Working Group 2: Higgs Physics at the HL-LHC and HE-LHC*, *CERN Yellow Rep. Monogr.* **7** (2019) 221, ed. by A. Dainese et al., arXiv: [1902.00134 \[hep-ph\]](#).
- [75] H. Davoudiasl, H.-S. Lee and W. J. Marciano, *Dark Z implications for Parity Violation, Rare Meson Decays, and Higgs Physics*, *Phys. Rev. D* **85** (2012) 115019, arXiv: [1203.2947 \[hep-ph\]](#).
- [76] H. Davoudiasl, H.-S. Lee, I. Lewis and W. J. Marciano, *Higgs Decays as a Window into the Dark Sector*, *Phys. Rev. D* **88** (2013) 015022, arXiv: [1304.4935 \[hep-ph\]](#).
- [77] ATLAS Collaboration, *Search for the Production of a Long-Lived Neutral Particle Decaying within the ATLAS Hadronic Calorimeter in Association with a Z Boson from pp Collisions at $\sqrt{s} = 13$ TeV*, *Phys. Rev. Lett.* **122** (2019) 151801, arXiv: [1811.02542 \[hep-ex\]](#).
- [78] ATLAS Collaboration, *The Pythia 8 A3 tune description of ATLAS minimum bias and inelastic measurements incorporating the Donnachie–Landshoff diffractive model*, ATL-PHYS-PUB-2016-017, 2016, URL: <https://cds.cern.ch/record/2206965>.
- [79] ATLAS Collaboration, *The ATLAS Simulation Infrastructure*, *Eur. Phys. J. C* **70** (2010) 823, arXiv: [1005.4568 \[physics.ins-det\]](#).
- [80] S. Agostinelli et al., *GEANT4 - a simulation toolkit*, *Nucl. Instrum. Meth. A* **A506** (2003) 250.
- [81] M. Cacciari, G. P. Salam and G. Soyez, *The anti- k_t jet clustering algorithm*, *JHEP* **04** (2008) 063, arXiv: [0802.1189 \[hep-ph\]](#).
- [82] M. Cacciari, G. P. Salam and G. Soyez, *FastJet user manual*, *Eur. Phys. J. C* **72** (2012) 1896, arXiv: [1111.6097 \[hep-ph\]](#).
- [83] ATLAS Collaboration, *Jet energy scale and resolution measured in proton–proton collisions at $\sqrt{s} = 13$ TeV with the ATLAS detector*, *Eur. Phys. J. C* **81** (2021) 689, arXiv: [2007.02645 \[hep-ex\]](#).
- [84] S. Hochreiter and J. Schmidhuber, *Long Short-Term Memory*, *Neural Comput.* **9** (1997) 1735.
- [85] ATLAS Collaboration, *Topological cell clustering in the ATLAS calorimeters and its performance in LHC Run 1*, *Eur. Phys. J. C* **77** (2017) 490, arXiv: [1603.02934 \[hep-ex\]](#).

- [86] ATLAS Collaboration, *Electron and photon performance measurements with the ATLAS detector using the 2015–2017 LHC proton–proton collision data*, *JINST* **14** (2019) P12006, arXiv: [1908.00005 \[hep-ex\]](#).
- [87] ATLAS Collaboration, *Muon reconstruction and identification efficiency in ATLAS using the full Run 2 pp collision data set at $\sqrt{s} = 13$ TeV*, *Eur. Phys. J. C* **81** (2021) 578, arXiv: [2012.00578 \[hep-ex\]](#).
- [88] ATLAS Collaboration, *The performance of missing transverse momentum reconstruction and its significance with the ATLAS detector using 140fb^{-1} of $\sqrt{s} = 13$ TeV pp collisions*, (2024), arXiv: [2402.05858 \[hep-ex\]](#).
- [89] ATLAS Collaboration, *Vertex Reconstruction Performance of the ATLAS Detector at $\sqrt{s} = 13$ TeV*, ATL-PHYS-PUB-2015-026, 2015, URL: <https://cds.cern.ch/record/2037717>.
- [90] T. Chen and C. Guestrin, *XGBoost: A Scalable Tree Boosting System*, (2016), arXiv: [1603.02754 \[cs.LG\]](#).
- [91] G. Kasieczka, B. Nachman, M. D. Schwartz and D. Shih, *Automating the ABCD method with machine learning*, *Phys. Rev. D* **103** (2021) 035021, arXiv: [2007.14400 \[hep-ph\]](#).
- [92] ATLAS Collaboration, *Luminosity determination in pp collisions at $\sqrt{s} = 13$ TeV using the ATLAS detector at the LHC*, *Eur. Phys. J. C* **83** (2023) 982, arXiv: [2212.09379 \[hep-ex\]](#).
- [93] G. Avoni et al., *The new LUCID-2 detector for luminosity measurement and monitoring in ATLAS*, *JINST* **13** (2018) P07017.
- [94] ATLAS Collaboration, *Jet energy scale measurements and their systematic uncertainties in proton-proton collisions at $\sqrt{s} = 13$ TeV with the ATLAS detector*, *Phys. Rev. D* **96** (2017) 072002, arXiv: [1703.09665 \[hep-ex\]](#).
- [95] L. Heinrich, M. Feickert, G. Stark and K. Cranmer, *pyhf: pure-Python implementation of HistFactory statistical models*, *J. Open Source Softw.* **6** (2021) 2823.
- [96] L. Heinrich, M. Feickert and G. Stark, *pyhf: v0.6.3*, version 0.6.3, <https://github.com/scikit-hep/pyhf/releases/tag/v0.6.3>, URL: <https://doi.org/10.5281/zenodo.1169739>.
- [97] A. L. Read, *Presentation of search results: the CL_s technique*, *J. Phys. G* **28** (2002) 2693.
- [98] G. Cowan, K. Cranmer, E. Gross and O. Vitells, *Asymptotic formulae for likelihood-based tests of new physics*, *Eur. Phys. J. C* **71** (2011) 1554, arXiv: [1007.1727 \[physics.data-an\]](#), Erratum: *Eur. Phys. J. C* **73** (2013) 2501.
- [99] ATLAS Collaboration, *ATLAS Computing Acknowledgements*, ATL-SOFT-PUB-2023-001, 2023, URL: <https://cds.cern.ch/record/2869272>.

The ATLAS Collaboration

G. Aad ¹⁰⁴, E. Aakvaag ¹⁷, B. Abbott ¹²³, S. Abdelhameed ^{119a}, K. Abeling ⁵⁶, N.J. Abicht ⁵⁰, S.H. Abidi ³⁰, M. Aboeela ⁴⁵, A. Aboulhorma ^{36e}, H. Abramowicz ¹⁵⁴, H. Abreu ¹⁵³, Y. Abulaiti ¹²⁰, B.S. Acharya ^{70a,70b,k}, A. Ackermann ^{64a}, C. Adam Bourdarios ⁴, L. Adamczyk ^{87a}, S.V. Addepalli ²⁷, M.J. Addison ¹⁰³, J. Adelman ¹¹⁸, A. Adiguzel ^{22c}, T. Adye ¹³⁷, A.A. Affolder ¹³⁹, Y. Afik ⁴⁰, M.N. Agaras ¹³, J. Agarwala ^{74a,74b}, A. Aggarwal ¹⁰², C. Agheorghiesei ^{28c}, F. Ahmadov ^{39,x}, W.S. Ahmed ¹⁰⁶, S. Ahuja ⁹⁷, X. Ai ^{63e}, G. Aielli ^{77a,77b}, A. Aikot ¹⁶⁶, M. Ait Tamliah ^{36e}, B. Aitbenkikh ^{36a}, M. Akbiyik ¹⁰², T.P.A. Åkesson ¹⁰⁰, A.V. Akimov ³⁸, D. Akiyama ¹⁷¹, N.N. Akolkar ²⁵, S. Aktas ^{22a}, K. Al Houry ⁴², G.L. Alberghi ^{24b}, J. Albert ¹⁶⁸, P. Albicocco ⁵⁴, G.L. Albouy ⁶¹, S. Alderweireldt ⁵³, Z.L. Alegria ¹²⁴, M. Aleksa ³⁷, I.N. Aleksandrov ³⁹, C. Alexa ^{28b}, T. Alexopoulos ¹⁰, F. Alfonsi ^{24b}, M. Algren ⁵⁷, M. Alhroob ¹⁷⁰, B. Ali ¹³⁵, H.M.J. Ali ^{93,r}, S. Ali ³², S.W. Alibocus ⁹⁴, M. Aliev ^{34c}, G. Alimonti ^{72a}, W. Alkahi ⁵⁶, C. Allaire ⁶⁷, B.M.M. Allbrooke ¹⁴⁹, J.F. Allen ⁵³, C.A. Allendes Flores ^{140f}, P.P. Allport ²¹, A. Aloisio ^{73a,73b}, F. Alonso ⁹², C. Alpigiani ¹⁴¹, Z.M.K. Alsolami ⁹³, M. Alvarez Estevez ¹⁰¹, A. Alvarez Fernandez ¹⁰², M. Alves Cardoso ⁵⁷, M.G. Alvigi ^{73a,73b}, M. Aly ¹⁰³, Y. Amaral Coutinho ^{84b}, A. Ambler ¹⁰⁶, C. Amelung ³⁷, M. Amerl ¹⁰³, C.G. Ames ¹¹¹, D. Amidei ¹⁰⁸, B. Amini ⁵⁵, K.J. Amirie ¹⁵⁸, S.P. Amor Dos Santos ^{133a}, K.R. Amos ¹⁶⁶, D. Amperiadou ¹⁵⁵, S. An ⁸⁵, V. Ananiev ¹²⁸, C. Anastopoulos ¹⁴², T. Andeen ¹¹, J.K. Anders ³⁷, A.C. Anderson ⁶⁰, S.Y. Andreato ^{48a,48b}, A. Andreazza ^{72a,72b}, S. Angelidakis ⁹, A. Angerami ⁴², A.V. Anisenkov ³⁸, A. Annovi ^{75a}, C. Antel ⁵⁷, E. Antipov ¹⁴⁸, M. Antonelli ⁵⁴, F. Anulli ^{76a}, M. Aoki ⁸⁵, T. Aoki ¹⁵⁶, M.A. Aparo ¹⁴⁹, L. Aperio Bella ⁴⁹, C. Appelt ¹⁹, A. Apyan ²⁷, S.J. Arbiol Val ⁸⁸, C. Arcangeletti ⁵⁴, A.T.H. Arce ⁵², J-F. Arguin ¹¹⁰, S. Argyropoulos ⁵⁵, J.-H. Arling ⁴⁹, O. Arnaez ⁴, H. Arnold ¹⁴⁸, G. Artoni ^{76a,76b}, H. Asada ¹¹³, K. Asai ¹²¹, S. Asai ¹⁵⁶, N.A. Asbah ³⁷, R.A. Ashby Pickering ¹⁷⁰, K. Assamagan ³⁰, R. Astalos ^{29a}, K.S.V. Astrand ¹⁰⁰, S. Atashi ¹⁶², R.J. Atkin ^{34a}, M. Atkinson ¹⁶⁵, H. Atmani ^{36f}, P.A. Atmasiddha ¹³¹, K. Augsten ¹³⁵, S. Auricchio ^{73a,73b}, A.D. Auriol ²¹, V.A. Austrup ¹⁰³, G. Avolio ³⁷, K. Axiotis ⁵⁷, G. Azuelos ^{110,ac}, D. Babal ^{29b}, H. Bachacou ¹³⁸, K. Bachas ^{155,o}, A. Bachi ³⁵, F. Backman ^{48a,48b}, A. Badea ⁴⁰, T.M. Baer ¹⁰⁸, P. Bagnaia ^{76a,76b}, M. Bahmani ¹⁹, D. Bahner ⁵⁵, K. Bai ¹²⁶, J.T. Baines ¹³⁷, L. Baines ⁹⁶, O.K. Baker ¹⁷⁵, E. Bakos ¹⁶, D. Bakshi Gupta ⁸, L.E. Balabram Filho ^{84b}, V. Balakrishnan ¹²³, R. Balasubramanian ⁴, E.M. Baldin ³⁸, P. Balek ^{87a}, E. Ballabene ^{24b,24a}, F. Balli ¹³⁸, L.M. Baltes ^{64a}, W.K. Balunas ³³, J. Balz ¹⁰², I. Bamwidhi ^{119b}, E. Banas ⁸⁸, M. Bandieramonte ¹³², A. Bandyopadhyay ²⁵, S. Bansal ²⁵, L. Barak ¹⁵⁴, M. Barakat ⁴⁹, E.L. Barberio ¹⁰⁷, D. Barberis ^{58b,58a}, M. Barbero ¹⁰⁴, M.Z. Barel ¹¹⁷, T. Barillari ¹¹², M-S. Barisits ³⁷, T. Barklow ¹⁴⁶, P. Baron ¹²⁵, D.A. Baron Moreno ¹⁰³, A. Baroncelli ^{63a}, A.J. Barr ¹²⁹, J.D. Barr ⁹⁸, F. Barreiro ¹⁰¹, J. Barreiro Guimarães da Costa ¹⁴, U. Barron ¹⁵⁴, M.G. Barros Teixeira ^{133a}, S. Barsov ³⁸, F. Bartels ^{64a}, R. Bartoldus ¹⁴⁶, A.E. Barton ⁹³, P. Bartos ^{29a}, A. Basan ¹⁰², M. Baselga ⁵⁰, A. Bassalat ^{67,b}, M.J. Basso ^{159a}, S. Bataju ⁴⁵, R. Bate ¹⁶⁷, R.L. Bates ⁶⁰, S. Batlamous ¹⁰¹, B. Batool ¹⁴⁴, M. Battaglia ¹³⁹, D. Battulga ¹⁹, M. Baucé ^{76a,76b}, M. Bauer ⁸⁰, P. Bauer ²⁵, L.T. Bazzano Hurrell ³¹, J.B. Beacham ⁵², T. Beau ¹³⁰, J.Y. Beaucamp ⁹², P.H. Beauchemin ¹⁶¹, P. Bechtel ²⁵, H.P. Beck ^{20,n}, K. Becker ¹⁷⁰, A.J. Beddall ⁸³, V.A. Bednyakov ³⁹, C.P. Bee ¹⁴⁸, L.J. Beemster ¹⁶, T.A. Beermann ³⁷, M. Begalli ^{84d}, M. Beger ³⁰, A. Behera ¹⁴⁸, J.K. Behr ⁴⁹, J.F. Beirer ³⁷, F. Beisiegel ²⁵, M. Belfkir ^{119b}, G. Bella ¹⁵⁴, L. Bellagamba ^{24b}, A. Bellerive ³⁵, P. Bellos ²¹, K. Beloborodov ³⁸, D. Benčekroun ^{36a}, F. Bendebba ^{36a}, Y. Benhammou ¹⁵⁴,

K.C. Benkendorfer ⁶², L. Beresford ⁴⁹, M. Beretta ⁵⁴, E. Bergeaas Kuutmann ¹⁶⁴, N. Berger ⁴,
 B. Bergmann ¹³⁵, J. Beringer ^{18a}, G. Bernardi ⁵, C. Bernius ¹⁴⁶, F.U. Bernlochner ²⁵,
 F. Bernon ³⁷, A. Berrocal Guardia ¹³, T. Berry ⁹⁷, P. Berta ¹³⁶, A. Berthold ⁵¹, S. Bethke ¹¹²,
 A. Betti ^{76a,76b}, A.J. Bevan ⁹⁶, N.K. Bhalla ⁵⁵, S. Bhatta ¹⁴⁸, D.S. Bhattacharya ¹⁶⁹,
 P. Bhattarai ¹⁴⁶, K.D. Bhide ⁵⁵, V.S. Bhopatkar ¹²⁴, R.M. Bianchi ¹³², G. Bianco ^{24b,24a},
 O. Biebel ¹¹¹, R. Bielski ¹²⁶, M. Biglietti ^{78a}, C.S. Billingsley ⁴⁵, Y. Bimgdi ^{36f}, M. Bindi ⁵⁶,
 A. Bingul ^{22b}, C. Bini ^{76a,76b}, G.A. Bird ³³, M. Birman ¹⁷², M. Biros ¹³⁶, S. Biryukov ¹⁴⁹,
 T. Bisanz ⁵⁰, E. Bisceglie ^{44b,44a}, J.P. Biswal ¹³⁷, D. Biswas ¹⁴⁴, I. Bloch ⁴⁹, A. Blue ⁶⁰,
 U. Blumenschein ⁹⁶, J. Blumenthal ¹⁰², V.S. Bobrovnikov ³⁸, M. Boehler ⁵⁵, B. Boehm ¹⁶⁹,
 D. Bogavac ³⁷, A.G. Bogdanchikov ³⁸, L.S. Boggia ¹³⁰, C. Bohm ^{48a}, V. Boisvert ⁹⁷,
 P. Bokan ³⁷, T. Bold ^{87a}, M. Bomben ⁵, M. Bona ⁹⁶, M. Boonekamp ¹³⁸, C.D. Booth ⁹⁷,
 A.G. Borbély ⁶⁰, I.S. Bordulev ³⁸, G. Borissov ⁹³, D. Bortoletto ¹²⁹, D. Boscherini ^{24b},
 M. Bosman ¹³, J.D. Bossio Sola ³⁷, K. Bouaouda ^{36a}, N. Bouchhar ¹⁶⁶, L. Boudet ⁴,
 J. Boudreau ¹³², E.V. Bouhova-Thacker ⁹³, D. Boumediene ⁴¹, R. Bouquet ^{58b,58a}, A. Boveia ¹²²,
 J. Boyd ³⁷, D. Boye ³⁰, I.R. Boyko ³⁹, L. Bozianu ⁵⁷, J. Bracinek ²¹, N. Brahimi ⁴,
 G. Brandt ¹⁷⁴, O. Brandt ³³, F. Braren ⁴⁹, B. Brau ¹⁰⁵, J.E. Brau ¹²⁶, R. Brenner ¹⁷²,
 L. Brenner ¹¹⁷, R. Brenner ¹⁶⁴, S. Bressler ¹⁷², G. Brianti ^{79a,79b}, D. Britton ⁶⁰, D. Britzger ¹¹²,
 I. Brock ²⁵, G. Brooijmans ⁴², E.M. Brooks ^{159b}, E. Brost ³⁰, L.M. Brown ¹⁶⁸, L.E. Bruce ⁶²,
 T.L. Bruckler ¹²⁹, P.A. Bruckman de Renstrom ⁸⁸, B. Brüers ⁴⁹, A. Bruni ^{24b}, G. Bruni ^{24b},
 M. Bruschi ^{24b}, N. Bruscinò ^{76a,76b}, T. Buanes ¹⁷, Q. Buat ¹⁴¹, D. Buchin ¹¹², A.G. Buckley ⁶⁰,
 O. Bulekov ³⁸, B.A. Bullard ¹⁴⁶, S. Burdin ⁹⁴, C.D. Burgard ⁵⁰, A.M. Burger ³⁷,
 B. Burghgrave ⁸, O. Burlayenko ⁵⁵, J. Burleson ¹⁶⁵, J.T.P. Burr ³³, J.C. Burzynski ¹⁴⁵,
 E.L. Busch ⁴², V. Büscher ¹⁰², P.J. Bussey ⁶⁰, J.M. Butler ²⁶, C.M. Buttar ⁶⁰,
 J.M. Butterworth ⁹⁸, W. Buttinger ¹³⁷, C.J. Buxo Vazquez ¹⁰⁹, A.R. Buzykaev ³⁸,
 S. Cabrera Urbán ¹⁶⁶, L. Cadamuro ⁶⁷, D. Caforio ⁵⁹, H. Cai ¹³², Y. Cai ^{14,114c}, Y. Cai ^{114a},
 V.M.M. Cairo ³⁷, O. Cakir ^{3a}, N. Calace ³⁷, P. Calafiura ^{18a}, G. Calderini ¹³⁰, P. Calfayan ⁶⁹,
 G. Callea ⁶⁰, L.P. Caloba ^{84b}, D. Calvet ⁴¹, S. Calvet ⁴¹, M. Calvetti ^{75a,75b}, R. Camacho Toro ¹³⁰,
 S. Camarda ³⁷, D. Camarero Munoz ²⁷, P. Camarri ^{77a,77b}, M.T. Camerlingo ^{73a,73b},
 D. Cameron ³⁷, C. Camincher ¹⁶⁸, M. Campanelli ⁹⁸, A. Camplani ⁴³, V. Canale ^{73a,73b},
 A.C. Canbay ^{3a}, E. Canonero ⁹⁷, J. Cantero ¹⁶⁶, Y. Cao ¹⁶⁵, F. Capocasa ²⁷, M. Capua ^{44b,44a},
 A. Carbone ^{72a,72b}, R. Cardarelli ^{77a}, J.C.J. Cardenas ⁸, G. Carducci ^{44b,44a}, T. Carli ³⁷,
 G. Carlino ^{73a}, J.I. Carlotto ¹³, B.T. Carlson ^{132,p}, E.M. Carlson ^{168,159a}, J. Carmignani ⁹⁴,
 L. Carminati ^{72a,72b}, A. Carnelli ¹³⁸, M. Carnesale ^{76a,76b}, S. Caron ¹¹⁶, E. Carquin ^{140f},
 I.B. Carr ¹⁰⁷, S. Carrá ^{72a}, G. Carratta ^{24b,24a}, A.M. Carroll ¹²⁶, M.P. Casado ^{13,h}, M. Caspar ⁴⁹,
 F.L. Castillo ⁴, L. Castillo Garcia ¹³, V. Castillo Gimenez ¹⁶⁶, N.F. Castro ^{133a,133e},
 A. Catinaccio ³⁷, J.R. Catmore ¹²⁸, T. Cavaliere ⁴, V. Cavaliere ³⁰, N. Cavalli ^{24b,24a},
 L.J. Caviedes Betancourt ^{23b}, Y.C. Cekmecelioglu ⁴⁹, E. Celebi ⁸³, S. Cella ³⁷,
 M.S. Centonze ^{71a,71b}, V. Cepaitis ⁵⁷, K. Cerny ¹²⁵, A.S. Cerqueira ^{84a}, A. Cerri ¹⁴⁹,
 L. Cerrito ^{77a,77b}, F. Cerutti ^{18a}, B. Cervato ¹⁴⁴, A. Cervelli ^{24b}, G. Cesarini ⁵⁴, S.A. Cetin ⁸³,
 D. Chakraborty ¹¹⁸, J. Chan ^{18a}, W.Y. Chan ¹⁵⁶, J.D. Chapman ³³, E. Chapon ¹³⁸,
 B. Chargeishvili ^{152b}, D.G. Charlton ²¹, M. Chatterjee ²⁰, C. Chauhan ¹³⁶, Y. Che ^{114a},
 S. Chekanov ⁶, S.V. Chekulaev ^{159a}, G.A. Chelkov ^{39,a}, A. Chen ¹⁰⁸, B. Chen ¹⁵⁴, B. Chen ¹⁶⁸,
 H. Chen ^{114a}, H. Chen ³⁰, J. Chen ^{63c}, J. Chen ¹⁴⁵, M. Chen ¹²⁹, S. Chen ⁸⁹, S.J. Chen ^{114a},
 X. Chen ^{63c}, X. Chen ^{15,ab}, Y. Chen ^{63a}, C.L. Cheng ¹⁷³, H.C. Cheng ^{65a}, S. Cheong ¹⁴⁶,
 A. Cheplakov ³⁹, E. Cheremushkina ⁴⁹, E. Cherepanova ¹¹⁷, R. Cherkaoui El Moursli ^{36e},
 E. Cheu ⁷, K. Cheung ⁶⁶, L. Chevalier ¹³⁸, V. Chiarella ⁵⁴, G. Chiarelli ^{75a}, N. Chiedde ¹⁰⁴,
 G. Chiodini ^{71a}, A.S. Chisholm ²¹, A. Chitan ^{28b}, M. Chitishvili ¹⁶⁶, M.V. Chizhov ³⁹,

K. Choi ¹¹, Y. Chou ¹⁴¹, E.Y.S. Chow ¹¹⁶, K.L. Chu ¹⁷², M.C. Chu ^{65a}, X. Chu ^{14,114c},
 Z. Chubinidze ⁵⁴, J. Chudoba ¹³⁴, J.J. Chwastowski ⁸⁸, D. Cieri ¹¹², K.M. Ciesla ^{87a},
 V. Cindro ⁹⁵, A. Ciocio ^{18a}, F. Cirotto ^{73a,73b}, Z.H. Citron ¹⁷², M. Citterio ^{72a}, D.A. Ciubotaru ^{28b},
 A. Clark ⁵⁷, P.J. Clark ⁵³, N. Clarke Hall ⁹⁸, C. Clarry ¹⁵⁸, J.M. Clavijo Columbie ⁴⁹,
 S.E. Clawson ⁴⁹, C. Clement ^{48a,48b}, Y. Coadou ¹⁰⁴, M. Cobal ^{70a,70c}, A. Coccaro ^{58b},
 R.F. Coelho Barrue ^{133a}, R. Coelho Lopes De Sa ¹⁰⁵, S. Coelli ^{72a}, B. Cole ⁴², J. Collot ⁶¹,
 P. Conde Muiño ^{133a,133g}, M.P. Connell ^{34c}, S.H. Connell ^{34c}, E.I. Conroy ¹²⁹, F. Conventi ^{73a,ad},
 H.G. Cooke ²¹, A.M. Cooper-Sarkar ¹²⁹, F.A. Corchia ^{24b,24a}, A. Cordeiro Oudot Choi ¹³⁰,
 L.D. Corpe ⁴¹, M. Corradi ^{76a,76b}, F. Corriveau ^{106,w}, A. Cortes-Gonzalez ¹⁹, M.J. Costa ¹⁶⁶,
 F. Costanza ⁴, D. Costanzo ¹⁴², B.M. Cote ¹²², J. Couthures ⁴, G. Cowan ⁹⁷, K. Cranmer ¹⁷³,
 L. Cremer ⁵⁰, D. Cremonini ^{24b,24a}, S. Crépé-Renaudin ⁶¹, F. Crescioli ¹³⁰, M. Cristinziani ¹⁴⁴,
 M. Cristoforetti ^{79a,79b}, V. Croft ¹¹⁷, J.E. Crosby ¹²⁴, G. Crosetti ^{44b,44a}, A. Cueto ¹⁰¹, H. Cui ⁹⁸,
 Z. Cui ⁷, W.R. Cunningham ⁶⁰, F. Curcio ¹⁶⁶, J.R. Curran ⁵³, P. Czodrowski ³⁷,
 M.J. Da Cunha Sargedas De Sousa ^{58b,58a}, J.V. Da Fonseca Pinto ^{84b}, C. Da Via ¹⁰³,
 W. Dabrowski ^{87a}, T. Dado ³⁷, S. Dahbi ¹⁵¹, T. Dai ¹⁰⁸, D. Dal Santo ²⁰, C. Dallapiccola ¹⁰⁵,
 M. Dam ⁴³, G. D'amen ³⁰, V. D'Amico ¹¹¹, J. Damp ¹⁰², J.R. Dandoy ³⁵, D. Dannheim ³⁷,
 M. Danninger ¹⁴⁵, V. Dao ¹⁴⁸, G. Darbo ^{58b}, S.J. Das ^{30,ae}, F. Dattola ⁴⁹, S. D'Auria ^{72a,72b},
 A. D'avanzo ^{73a,73b}, C. David ^{34a}, T. Davidek ¹³⁶, I. Dawson ⁹⁶, H.A. Day-hall ¹³⁵, K. De ⁸,
 R. De Asmundis ^{73a}, N. De Biase ⁴⁹, S. De Castro ^{24b,24a}, N. De Groot ¹¹⁶, P. de Jong ¹¹⁷,
 H. De la Torre ¹¹⁸, A. De Maria ^{114a}, A. De Salvo ^{76a}, U. De Sanctis ^{77a,77b}, F. De Santis ^{71a,71b},
 A. De Santo ¹⁴⁹, J.B. De Vivie De Regie ⁶¹, J. Debevc ⁹⁵, D.V. Dedovich ³⁹, J. Degens ⁹⁴,
 A.M. Deiana ⁴⁵, F. Del Corso ^{24b,24a}, J. Del Peso ¹⁰¹, L. Delagrangé ¹³⁰, F. Deliot ¹³⁸,
 C.M. Delitzsch ⁵⁰, M. Della Pietra ^{73a,73b}, D. Della Volpe ⁵⁷, A. Dell'Acqua ³⁷,
 L. Dell'Asta ^{72a,72b}, M. Delmastro ⁴, P.A. Delsart ⁶¹, S. Demers ¹⁷⁵, M. Demichev ³⁹,
 S.P. Denisov ³⁸, L. D'Eramo ⁴¹, D. Derendarz ⁸⁸, F. Derue ¹³⁰, P. Dervan ⁹⁴, K. Desch ²⁵,
 C. Deutsch ²⁵, F.A. Di Bello ^{58b,58a}, A. Di Ciaccio ^{77a,77b}, L. Di Ciaccio ⁴,
 A. Di Domenico ^{76a,76b}, C. Di Donato ^{73a,73b}, A. Di Girolamo ³⁷, G. Di Gregorio ³⁷,
 A. Di Luca ^{79a,79b}, B. Di Micco ^{78a,78b}, R. Di Nardo ^{78a,78b}, K.F. Di Petrillo ⁴⁰,
 M. Diamantopoulou ³⁵, F.A. Dias ¹¹⁷, T. Dias Do Vale ¹⁴⁵, M.A. Diaz ^{140a,140b},
 F.G. Diaz Capriles ²⁵, A.R. Didenko ³⁹, M. Didenko ¹⁶⁶, E.B. Diehl ¹⁰⁸, S. Díez Cornell ⁴⁹,
 C. Díez Pardos ¹⁴⁴, C. Dimitriadi ¹⁶⁴, A. Dimitrievska ²¹, J. Dingfelder ²⁵, T. Dingley ¹²⁹,
 I-M. Dinu ^{28b}, S.J. Dittmeier ^{64b}, F. Dittus ³⁷, M. Divisek ¹³⁶, B. Dixit ⁹⁴, F. Djama ¹⁰⁴,
 T. Djobava ^{152b}, C. Doglioni ^{103,100}, A. Dohalova ^{29a}, J. Dolejsi ¹³⁶, Z. Dolezal ¹³⁶,
 K. Domijan ^{87a}, K.M. Dona ⁴⁰, M. Donadelli ^{84d}, B. Dong ¹⁰⁹, J. Donini ⁴¹,
 A. D'Onofrio ^{73a,73b}, M. D'Onofrio ⁹⁴, J. Dopke ¹³⁷, A. Doria ^{73a}, N. Dos Santos Fernandes ^{133a},
 P. Dougan ¹⁰³, M.T. Dova ⁹², A.T. Doyle ⁶⁰, M.A. Draguet ¹²⁹, M.P. Drescher ⁵⁶, E. Dreyer ¹⁷²,
 I. Drivas-koulouris ¹⁰, M. Drnevich ¹²⁰, M. Drozdova ⁵⁷, D. Du ^{63a}, T.A. du Pree ¹¹⁷,
 F. Dubinin ³⁸, M. Dubovsky ^{29a}, E. Duchovni ¹⁷², G. Duckeck ¹¹¹, O.A. Ducu ^{28b}, D. Duda ⁵³,
 A. Dudarev ³⁷, E.R. Duden ²⁷, M. D'uffizi ¹⁰³, L. Duflot ⁶⁷, M. Dührssen ³⁷, I. Duminica ^{28g},
 A.E. Dumitriu ^{28b}, M. Dunford ^{64a}, S. Dungs ⁵⁰, K. Dunne ^{48a,48b}, A. Duperrin ¹⁰⁴,
 H. Duran Yildiz ^{3a}, M. Düren ⁵⁹, A. Durglishvili ^{152b}, B.L. Dwyer ¹¹⁸, G.I. Dyckes ^{18a},
 M. Dyndal ^{87a}, B.S. Dziedzic ³⁷, Z.O. Earnshaw ¹⁴⁹, G.H. Eberwein ¹²⁹, B. Eckerova ^{29a},
 S. Eggebrecht ⁵⁶, E. Egidio Purcino De Souza ^{84e}, L.F. Ehrke ⁵⁷, G. Eigen ¹⁷, K. Einsweiler ^{18a},
 T. Ekelof ¹⁶⁴, P.A. Ekman ¹⁰⁰, S. El Farkh ^{36b}, Y. El Ghazali ^{63a}, H. El Jarrari ³⁷,
 A. El Moussaouy ^{36a}, V. Ellajosyula ¹⁶⁴, M. Ellert ¹⁶⁴, F. Ellinghaus ¹⁷⁴, N. Ellis ³⁷,
 J. Elmsheuser ³⁰, M. Elsayy ^{119a}, M. Elsing ³⁷, D. Emeliyanov ¹³⁷, Y. Enari ⁸⁵, I. Ene ^{18a},
 S. Epari ¹³, P.A. Erland ⁸⁸, D. Ernani Martins Neto ⁸⁸, M. Errenst ¹⁷⁴, M. Escalier ⁶⁷,

C. Escobar ¹⁶⁶, E. Etzion ¹⁵⁴, G. Evans ^{133a}, H. Evans ⁶⁹, L.S. Evans ⁹⁷, A. Ezhilov ³⁸,
 S. Ezzarqtouni ^{36a}, F. Fabbri ^{24b,24a}, L. Fabbri ^{24b,24a}, G. Facini ⁹⁸, V. Fadeyev ¹³⁹,
 R.M. Fakhrutdinov ³⁸, D. Fakoudis ¹⁰², S. Falciano ^{76a}, L.F. Falda Ulhoa Coelho ³⁷,
 F. Fallavollita ¹¹², G. Falsetti ^{44b,44a}, J. Faltova ¹³⁶, C. Fan ¹⁶⁵, K.Y. Fan ^{65b}, Y. Fan ¹⁴,
 Y. Fang ^{14,114c}, M. Fanti ^{72a,72b}, M. Faraj ^{70a,70b}, Z. Farazpay ⁹⁹, A. Farbin ⁸, A. Farilla ^{78a},
 T. Farooque ¹⁰⁹, S.M. Farrington ⁵³, F. Fassi ^{36e}, D. Fassouliotis ⁹, M. Faucci Giannelli ^{77a,77b},
 W.J. Fawcett ³³, L. Fayard ⁶⁷, P. Federic ¹³⁶, P. Federicova ¹³⁴, O.L. Fedin ^{38,a}, M. Feickert ¹⁷³,
 L. Feligioni ¹⁰⁴, D.E. Fellers ¹²⁶, C. Feng ^{63b}, Z. Feng ¹¹⁷, M.J. Fenton ¹⁶², L. Ferencz ⁴⁹,
 R.A.M. Ferguson ⁹³, S.I. Fernandez Luengo ^{140f}, P. Fernandez Martinez ¹³, M.J.V. Fernoux ¹⁰⁴,
 J. Ferrando ⁹³, A. Ferrari ¹⁶⁴, P. Ferrari ^{117,116}, R. Ferrari ^{74a}, D. Ferrere ⁵⁷, C. Ferretti ¹⁰⁸,
 D. Fiacco ^{76a,76b}, F. Fiedler ¹⁰², P. Fiedler ¹³⁵, A. Filipčić ⁹⁵, E.K. Filmer ^{159a}, F. Filthaut ¹¹⁶,
 M.C.N. Fiolhais ^{133a,133c,c}, L. Fiorini ¹⁶⁶, W.C. Fisher ¹⁰⁹, T. Fitschen ¹⁰³, P.M. Fitzhugh ¹³⁸,
 I. Fleck ¹⁴⁴, P. Fleischmann ¹⁰⁸, T. Flick ¹⁷⁴, M. Flores ^{34d,z}, L.R. Flores Castillo ^{65a},
 L. Flores Sanz De Acedo ³⁷, F.M. Follega ^{79a,79b}, N. Fomin ³³, J.H. Foo ¹⁵⁸, A. Formica ¹³⁸,
 A.C. Forti ¹⁰³, E. Fortin ³⁷, A.W. Fortman ^{18a}, M.G. Foti ^{18a}, L. Fountas ^{9,i}, D. Fournier ⁶⁷,
 H. Fox ⁹³, P. Francavilla ^{75a,75b}, S. Francescato ⁶², S. Franchellucci ⁵⁷, M. Franchini ^{24b,24a},
 S. Franchino ^{64a}, D. Francis ³⁷, L. Franco ¹¹⁶, V. Franco Lima ³⁷, L. Franconi ⁴⁹, M. Franklin ⁶²,
 G. Frattari ²⁷, Y.Y. Frid ¹⁵⁴, J. Friend ⁶⁰, N. Fritzsche ³⁷, A. Froch ⁵⁵, D. Froidevaux ³⁷,
 J.A. Frost ¹²⁹, Y. Fu ^{63a}, S. Fuenzalida Garrido ^{140f}, M. Fujimoto ¹⁰⁴, K.Y. Fung ^{65a},
 E. Furtado De Simas Filho ^{84e}, M. Furukawa ¹⁵⁶, J. Fuster ¹⁶⁶, A. Gaa ⁵⁶, A. Gabrielli ^{24b,24a},
 A. Gabrielli ¹⁵⁸, P. Gadow ³⁷, G. Gagliardi ^{58b,58a}, L.G. Gagnon ^{18a}, S. Gaid ¹⁶³,
 S. Galantzan ¹⁵⁴, J. Gallagher ¹, E.J. Gallas ¹²⁹, B.J. Gallop ¹³⁷, K.K. Gan ¹²², S. Ganguly ¹⁵⁶,
 Y. Gao ⁵³, F.M. Garay Walls ^{140a,140b}, B. Garcia ³⁰, C. García ¹⁶⁶, A. Garcia Alonso ¹¹⁷,
 A.G. Garcia Caffaro ¹⁷⁵, J.E. García Navarro ¹⁶⁶, M. Garcia-Sciveres ^{18a}, G.L. Gardner ¹³¹,
 R.W. Gardner ⁴⁰, N. Garelli ¹⁶¹, D. Garg ⁸¹, R.B. Garg ¹⁴⁶, J.M. Gargan ⁵³, C.A. Garner ¹⁵⁸,
 C.M. Garvey ^{34a}, V.K. Gassmann ¹⁶¹, G. Gaudio ^{74a}, V. Gautam ¹³, P. Gauzzi ^{76a,76b},
 J. Gavranovic ⁹⁵, I.L. Gavrilenko ³⁸, A. Gavriluk ³⁸, C. Gay ¹⁶⁷, G. Gaycken ¹²⁶,
 E.N. Gazis ¹⁰, A.A. Geanta ^{28b}, C.M. Gee ¹³⁹, A. Gekow ¹²², C. Gemme ^{58b}, M.H. Genest ⁶¹,
 A.D. Gentry ¹¹⁵, S. George ⁹⁷, W.F. George ²¹, T. Geralis ⁴⁷, P. Gessinger-Befurt ³⁷,
 M.E. Geyik ¹⁷⁴, M. Ghani ¹⁷⁰, K. Ghorbanian ⁹⁶, A. Ghosal ¹⁴⁴, A. Ghosh ¹⁶², A. Ghosh ⁷,
 B. Giacobbe ^{24b}, S. Giagu ^{76a,76b}, T. Giani ¹¹⁷, A. Giannini ^{63a}, S.M. Gibson ⁹⁷, M. Gignac ¹³⁹,
 D.T. Gil ^{87b}, A.K. Gilbert ^{87a}, B.J. Gilbert ⁴², D. Gillberg ³⁵, G. Gilles ¹¹⁷, L. Ginabat ¹³⁰,
 D.M. Gingrich ^{2,ac}, M.P. Giordani ^{70a,70c}, P.F. Giraud ¹³⁸, G. Giugliarelli ^{70a,70c}, D. Giugni ^{72a},
 F. Giuli ^{77a,77b}, I. Gkialas ^{9,i}, L.K. Gladilin ³⁸, C. Glasman ¹⁰¹, G.R. Gledhill ¹²⁶, G. Glemža ⁴⁹,
 M. Glisic ¹²⁶, I. Gnesi ^{44b}, Y. Go ³⁰, M. Goblirsch-Kolb ³⁷, B. Gocke ⁵⁰, D. Godin ¹¹⁰,
 B. Gokturk ^{22a}, S. Goldfarb ¹⁰⁷, T. Golling ⁵⁷, M.G.D. Gololo ^{34g}, D. Golubkov ³⁸,
 J.P. Gombas ¹⁰⁹, A. Gomes ^{133a,133b}, G. Gomes Da Silva ¹⁴⁴, A.J. Gomez Delegido ¹⁶⁶,
 R. Gonçalves ^{133a}, L. Gonella ²¹, A. Gongadze ^{152c}, F. Gonnella ²¹, J.L. Gonski ¹⁴⁶,
 R.Y. González Andana ⁵³, S. González de la Hoz ¹⁶⁶, R. Gonzalez Lopez ⁹⁴,
 C. Gonzalez Renteria ^{18a}, M.V. Gonzalez Rodrigues ⁴⁹, R. Gonzalez Suarez ¹⁶⁴,
 S. Gonzalez-Sevilla ⁵⁷, L. Goossens ³⁷, B. Gorini ³⁷, E. Gorini ^{71a,71b}, A. Gorišek ⁹⁵,
 T.C. Gosart ¹³¹, A.T. Goshaw ⁵², M.I. Gostkin ³⁹, S. Goswami ¹²⁴, C.A. Gottardo ³⁷,
 S.A. Gotz ¹¹¹, M. Goughri ^{36b}, V. Goumarre ⁴⁹, A.G. Goussiou ¹⁴¹, N. Govender ^{34c},
 R.P. Grabarczyk ¹²⁹, I. Grabowska-Bold ^{87a}, K. Graham ³⁵, E. Gramstad ¹²⁸,
 S. Grancagnolo ^{71a,71b}, C.M. Grant ^{1,138}, P.M. Gravila ^{28f}, F.G. Gravili ^{71a,71b}, H.M. Gray ^{18a},
 M. Greco ^{71a,71b}, M.J. Green ¹, C. Grefe ²⁵, A.S. Grefsrud ¹⁷, I.M. Gregor ⁴⁹, K.T. Greif ¹⁶²,
 P. Grenier ¹⁴⁶, S.G. Grewe ¹¹², A.A. Grillo ¹³⁹, K. Grimm ³², S. Grinstein ^{13,s}, J.-F. Grivaz ⁶⁷,

E. Gross ¹⁷², J. Grosse-Knetter ⁵⁶, L. Guan ¹⁰⁸, J.G.R. Guerrero Rojas ¹⁶⁶, G. Guerrieri ³⁷,
 R. Gugel ¹⁰², J.A.M. Guhit ¹⁰⁸, A. Guida ¹⁹, E. Guilloton ¹⁷⁰, S. Guindon ³⁷, F. Guo ^{14,114c},
 J. Guo ^{63c}, L. Guo ⁴⁹, Y. Guo ¹⁰⁸, A. Gupta ⁵⁰, R. Gupta ¹³², S. Gurbuz ²⁵, S.S. Gurdasani ⁵⁵,
 G. Gustavino ^{76a,76b}, P. Gutierrez ¹²³, L.F. Gutierrez Zagazeta ¹³¹, M. Gutsche ⁵¹, C. Gutschow ⁹⁸,
 C. Gwenlan ¹²⁹, C.B. Gwilliam ⁹⁴, E.S. Haaland ¹²⁸, A. Haas ¹²⁰, M. Habedank ⁶⁰,
 C. Haber ^{18a}, H.K. Hadavand ⁸, A. Haddad ⁴¹, A. Hadeef ⁵¹, S. Hadzic ¹¹², A.I. Hagan ⁹³,
 J.J. Hahn ¹⁴⁴, E.H. Haines ⁹⁸, M. Haleem ¹⁶⁹, J. Haley ¹²⁴, G.D. Hallewell ¹⁰⁴, L. Halser ²⁰,
 K. Hamano ¹⁶⁸, M. Hamer ²⁵, E.J. Hampshire ⁹⁷, J. Han ^{63b}, L. Han ^{114a}, L. Han ^{63a},
 S. Han ^{18a}, Y.F. Han ¹⁵⁸, K. Hanagaki ⁸⁵, M. Hance ¹³⁹, D.A. Hangal ⁴², H. Hanif ¹⁴⁵,
 M.D. Hank ¹³¹, J.B. Hansen ⁴³, P.H. Hansen ⁴³, D. Harada ⁵⁷, T. Harenberg ¹⁷⁴, S. Harkusha ³⁸,
 M.L. Harris ¹⁰⁵, Y.T. Harris ²⁵, J. Harrison ¹³, N.M. Harrison ¹²², P.F. Harrison ¹⁷⁰,
 N.M. Hartman ¹¹², N.M. Hartmann ¹¹¹, R.Z. Hasan ^{97,137}, Y. Hasegawa ¹⁴³, F. Haslbeck ¹²⁹,
 S. Hassan ¹⁷, R. Hauser ¹⁰⁹, C.M. Hawkes ²¹, R.J. Hawkings ³⁷, Y. Hayashi ¹⁵⁶, D. Hayden ¹⁰⁹,
 C. Hayes ¹⁰⁸, R.L. Hayes ¹¹⁷, C.P. Hays ¹²⁹, J.M. Hays ⁹⁶, H.S. Hayward ⁹⁴, F. He ^{63a},
 M. He ^{14,114c}, Y. He ⁴⁹, Y. He ⁹⁸, N.B. Heatley ⁹⁶, V. Hedberg ¹⁰⁰, A.L. Heggelund ¹²⁸,
 N.D. Hehir ^{96,*}, C. Heidegger ⁵⁵, K.K. Heidegger ⁵⁵, J. Heilman ³⁵, S. Heim ⁴⁹, T. Heim ^{18a},
 J.G. Heinlein ¹³¹, J.J. Heinrich ¹²⁶, L. Heinrich ^{112,aa}, J. Hejbal ¹³⁴, A. Held ¹⁷³,
 S. Hellesund ¹⁷, C.M. Helling ¹⁶⁷, S. Hellman ^{48a,48b}, R.C.W. Henderson ⁹³, L. Henkelmann ³³,
 A.M. Henriques Correia ³⁷, H. Herde ¹⁰⁰, Y. Hernández Jiménez ¹⁴⁸, L.M. Herrmann ²⁵,
 T. Herrmann ⁵¹, G. Herten ⁵⁵, R. Hertenberger ¹¹¹, L. Hervas ³⁷, M.E. Hespings ¹⁰²,
 N.P. Hessey ^{159a}, J. Hessler ¹¹², M. Hidaoui ^{36b}, N. Hidic ¹³⁶, E. Hill ¹⁵⁸, S.J. Hillier ²¹,
 J.R. Hinds ¹⁰⁹, F. Hinterkeuser ²⁵, M. Hirose ¹²⁷, S. Hirose ¹⁶⁰, D. Hirschbuehl ¹⁷⁴,
 T.G. Hitchings ¹⁰³, B. Hiti ⁹⁵, J. Hobbs ¹⁴⁸, R. Hobincu ^{28e}, N. Hod ¹⁷², M.C. Hodgkinson ¹⁴²,
 B.H. Hodgkinson ¹²⁹, A. Hoecker ³⁷, D.D. Hofer ¹⁰⁸, J. Hofer ¹⁶⁶, T. Holm ²⁵, M. Holzbock ³⁷,
 L.B.A.H. Hommels ³³, B.P. Honan ¹⁰³, J.J. Hong ⁶⁹, J. Hong ^{63c}, T.M. Hong ¹³²,
 B.H. Hooberman ¹⁶⁵, W.H. Hopkins ⁶, M.C. Hoppesch ¹⁶⁵, Y. Horii ¹¹³, M.E. Horstmann ¹¹²,
 S. Hou ¹⁵¹, A.S. Howard ⁹⁵, J. Howarth ⁶⁰, J. Hoya ⁶, M. Hrabovsky ¹²⁵, A. Hrynevich ⁴⁹,
 T. Hryn'ova ⁴, P.J. Hsu ⁶⁶, S.-C. Hsu ¹⁴¹, T. Hsu ⁶⁷, M. Hu ^{18a}, Q. Hu ^{63a}, S. Huang ³³,
 X. Huang ^{14,114c}, Y. Huang ¹⁴², Y. Huang ¹⁰², Y. Huang ¹⁴, Z. Huang ¹⁰³, Z. Hubacek ¹³⁵,
 M. Huebner ²⁵, F. Huegging ²⁵, T.B. Huffman ¹²⁹, C.A. Hugli ⁴⁹, M. Huhtinen ³⁷,
 S.K. Huiberts ¹⁷, R. Hulsken ¹⁰⁶, N. Huseynov ^{12,f}, J. Huston ¹⁰⁹, J. Huth ⁶², R. Hyneman ¹⁴⁶,
 G. Iacobucci ⁵⁷, G. Iakovidis ³⁰, L. Iconomidou-Fayard ⁶⁷, J.P. Iddon ³⁷, P. Iengo ^{73a,73b},
 R. Iguchi ¹⁵⁶, Y. Iiyama ¹⁵⁶, T. Iizawa ¹²⁹, Y. Ikegami ⁸⁵, N. Ilic ¹⁵⁸, H. Imam ^{84c},
 G. Inacio Goncalves ^{84d}, T. Ingebretsen Carlson ^{48a,48b}, J.M. Inglis ⁹⁶, G. Introzzi ^{74a,74b},
 M. Iodice ^{78a}, V. Ippolito ^{76a,76b}, R.K. Irwin ⁹⁴, M. Ishino ¹⁵⁶, W. Islam ¹⁷³, C. Issever ¹⁹,
 S. Istin ^{22a,ag}, H. Ito ¹⁷¹, R. Iuppa ^{79a,79b}, A. Ivina ¹⁷², J.M. Izen ⁴⁶, V. Izzo ^{73a}, P. Jacka ¹³⁴,
 P. Jackson ¹, C.S. Jagfeld ¹¹¹, G. Jain ^{159a}, P. Jain ⁴⁹, K. Jakobs ⁵⁵, T. Jakoubek ¹⁷²,
 J. Jamieson ⁶⁰, W. Jang ¹⁵⁶, M. Javurkova ¹⁰⁵, P. Jawahar ¹⁰³, L. Jeanty ¹²⁶, J. Jejelava ^{152a,y},
 P. Jenni ^{55,e}, C.E. Jessiman ³⁵, C. Jia ^{63b}, H. Jia ¹⁶⁷, J. Jia ¹⁴⁸, X. Jia ^{14,114c}, Z. Jia ^{114a},
 C. Jiang ⁵³, S. Jiggins ⁴⁹, J. Jimenez Pena ¹³, S. Jin ^{114a}, A. Jinaru ^{28b}, O. Jinnouchi ¹⁵⁷,
 P. Johansson ¹⁴², K.A. Johns ⁷, J.W. Johnson ¹³⁹, F.A. Jolly ⁴⁹, D.M. Jones ¹⁴⁹, E. Jones ⁴⁹,
 K.S. Jones ⁸, P. Jones ³³, R.W.L. Jones ⁹³, T.J. Jones ⁹⁴, H.L. Joos ^{56,37}, R. Joshi ¹²²,
 J. Jovicevic ¹⁶, X. Ju ^{18a}, J.J. Junggeburth ¹⁰⁵, T. Junkermann ^{64a}, A. Juste Rozas ^{13,s},
 M.K. Juzek ⁸⁸, S. Kabana ^{140e}, A. Kaczmarska ⁸⁸, M. Kado ¹¹², H. Kagan ¹²², M. Kagan ¹⁴⁶,
 A. Kahn ¹³¹, C. Kahra ¹⁰², T. Kaji ¹⁵⁶, E. Kajomovitz ¹⁵³, N. Kakati ¹⁷², I. Kalaitzidou ⁵⁵,
 C.W. Kalderon ³⁰, N.J. Kang ¹³⁹, D. Kar ^{34g}, K. Karava ¹²⁹, M.J. Kareem ^{159b}, E. Karentzos ⁵⁵,
 O. Karkout ¹¹⁷, S.N. Karpov ³⁹, Z.M. Karpova ³⁹, V. Kartvelishvili ⁹³, A.N. Karyukhin ³⁸,

E. Kasimi ¹⁵⁵, J. Katzy ⁴⁹, S. Kaur ³⁵, K. Kawade ¹⁴³, M.P. Kawale ¹²³, C. Kawamoto ⁸⁹, T. Kawamoto ^{63a}, E.F. Kay ³⁷, F.I. Kaya ¹⁶¹, S. Kazakos ¹⁰⁹, V.F. Kazanin ³⁸, Y. Ke ¹⁴⁸, J.M. Keaveney ^{34a}, R. Keeler ¹⁶⁸, G.V. Kehris ⁶², J.S. Keller ³⁵, J.J. Kempster ¹⁴⁹, O. Kepka ¹³⁴, B.P. Kerridge ¹³⁷, S. Kersten ¹⁷⁴, B.P. Kerševan ⁹⁵, L. Keszeghova ^{29a}, S. Ketabchi Haghighat ¹⁵⁸, R.A. Khan ¹³², A. Khanov ¹²⁴, A.G. Kharlamov ³⁸, T. Kharlamova ³⁸, E.E. Khoda ¹⁴¹, M. Kholodenko ^{133a}, T.J. Khoo ¹⁹, G. Khorauli ¹⁶⁹, J. Khubua ^{152b,*}, Y.A.R. Khwaira ¹³⁰, B. Kibirige ^{34g}, D. Kim ⁶, D.W. Kim ^{48a,48b}, Y.K. Kim ⁴⁰, N. Kimura ⁹⁸, M.K. Kingston ⁵⁶, A. Kirchhoff ⁵⁶, C. Kirfel ²⁵, F. Kirfel ²⁵, J. Kirk ¹³⁷, A.E. Kiryunin ¹¹², S. Kita ¹⁶⁰, C. Kitsaki ¹⁰, O. Kivernyk ²⁵, M. Klassen ¹⁶¹, C. Klein ³⁵, L. Klein ¹⁶⁹, M.H. Klein ⁴⁵, S.B. Klein ⁵⁷, U. Klein ⁹⁴, A. Klimentov ³⁰, T. Klioutchnikova ³⁷, P. Kluit ¹¹⁷, S. Kluth ¹¹², E. Kneringer ⁸⁰, T.M. Knight ¹⁵⁸, A. Knue ⁵⁰, D. Kobylanski ¹⁷², S.F. Koch ¹²⁹, M. Kocian ¹⁴⁶, P. Kodyš ¹³⁶, D.M. Koeck ¹²⁶, P.T. Koenig ²⁵, T. Koffas ³⁵, O. Kolay ⁵¹, I. Koletsou ⁴, T. Komarek ⁸⁸, K. Köneke ⁵⁵, A.X.Y. Kong ¹, T. Kono ¹²¹, N. Konstantinidis ⁹⁸, P. Kontaxakis ⁵⁷, B. Konya ¹⁰⁰, R. Kopeliansky ⁴², S. Koperny ^{87a}, K. Korcyl ⁸⁸, K. Kordas ^{155,d}, A. Korn ⁹⁸, S. Korn ⁵⁶, I. Korolkov ¹³, N. Korotkova ³⁸, B. Kortman ¹¹⁷, O. Kortner ¹¹², S. Kortner ¹¹², W.H. Kostecka ¹¹⁸, V.V. Kostyukhin ¹⁴⁴, A. Kotsokechagia ³⁷, A. Kotwal ⁵², A. Koulouris ³⁷, A. Kourkoumeli-Charalampidi ^{74a,74b}, C. Kourkoumelis ⁹, E. Kourlitis ^{112,aa}, O. Kovanda ¹²⁶, R. Kowalewski ¹⁶⁸, W. Kozanecki ¹²⁶, A.S. Kozhin ³⁸, V.A. Kramarenko ³⁸, G. Kramberger ⁹⁵, P. Kramer ¹⁰², M.W. Krasny ¹³⁰, A. Krasznahorkay ³⁷, A.C. Kraus ¹¹⁸, J.W. Kraus ¹⁷⁴, J.A. Kremer ⁴⁹, T. Kresse ⁵¹, L. Kretschmann ¹⁷⁴, J. Kretschmar ⁹⁴, K. Kreul ¹⁹, P. Krieger ¹⁵⁸, M. Krivos ¹³⁶, K. Krizka ²¹, K. Kroeninger ⁵⁰, H. Kroha ¹¹², J. Kroll ¹³⁴, J. Kroll ¹³¹, K.S. Krowpman ¹⁰⁹, U. Kruchonak ³⁹, H. Krüger ²⁵, N. Krumnack ⁸², M.C. Kruse ⁵², O. Kuchinskaja ³⁸, S. Kудay ^{3a}, S. Kuehn ³⁷, R. Kuesters ⁵⁵, T. Kuhl ⁴⁹, V. Kukhtin ³⁹, Y. Kulchitsky ^{38,a}, S. Kuleshov ^{140d,140b}, M. Kumar ^{34g}, N. Kumari ⁴⁹, P. Kumari ^{159b}, A. Kupco ¹³⁴, T. Kupfer ⁵⁰, A. Kupich ³⁸, O. Kuprash ⁵⁵, H. Kurashige ⁸⁶, L.L. Kurchaninov ^{159a}, O. Kurdysh ⁶⁷, Y.A. Kurochkin ³⁸, A. Kurova ³⁸, M. Kuze ¹⁵⁷, A.K. Kvam ¹⁰⁵, J. Kvita ¹²⁵, T. Kwan ¹⁰⁶, N.G. Kyriacou ¹⁰⁸, L.A.O. Laatu ¹⁰⁴, C. Lacasta ¹⁶⁶, F. Lacava ^{76a,76b}, H. Lacker ¹⁹, D. Lacour ¹³⁰, N.N. Lad ⁹⁸, E. Ladygin ³⁹, A. Lafarge ⁴¹, B. Laforge ¹³⁰, T. Lagouri ¹⁷⁵, F.Z. Lahbabi ^{36a}, S. Lai ⁵⁶, J.E. Lambert ¹⁶⁸, S. Lammers ⁶⁹, W. Lampl ⁷, C. Lampoudis ^{155,d}, G. Lamprinoudis ¹⁰², A.N. Lancaster ¹¹⁸, E. Lançon ³⁰, U. Landgraf ⁵⁵, M.P.J. Landon ⁹⁶, V.S. Lang ⁵⁵, O.K.B. Langrekken ¹²⁸, A.J. Lankford ¹⁶², F. Lanni ³⁷, K. Lantzsch ²⁵, A. Lanza ^{74a}, M. Lanzac Berrocal ¹⁶⁶, J.F. Laporte ¹³⁸, T. Lari ^{72a}, F. Lasagni Manghi ^{24b}, M. Lassnig ³⁷, V. Latonova ¹³⁴, A. Laurier ¹⁵³, S.D. Lawlor ¹⁴², Z. Lawrence ¹⁰³, R. Lazaridou ¹⁷⁰, M. Lazzaroni ^{72a,72b}, B. Le ¹⁰³, H.D.M. Le ¹⁰⁹, E.M. Le Boulicaut ¹⁷⁵, L.T. Le Pottier ^{18a}, B. Leban ^{24b,24a}, A. Lebedev ⁸², M. LeBlanc ¹⁰³, F. Ledroit-Guillon ⁶¹, S.C. Lee ¹⁵¹, S. Lee ^{48a,48b}, T.F. Lee ⁹⁴, L.L. Leeuw ^{34c}, H.P. Lefebvre ⁹⁷, M. Lefebvre ¹⁶⁸, C. Leggett ^{18a}, G. Lehmann Miotto ³⁷, M. Leigh ⁵⁷, W.A. Leight ¹⁰⁵, W. Leinonen ¹¹⁶, A. Leisos ^{155,q}, M.A.L. Leite ^{84c}, C.E. Leitgeb ¹⁹, R. Leitner ¹³⁶, K.J.C. Leney ⁴⁵, T. Lenz ²⁵, S. Leone ^{75a}, C. Leonidopoulos ⁵³, A. Leopold ¹⁴⁷, R. Les ¹⁰⁹, C.G. Lester ³³, M. Levchenko ³⁸, J. Levêque ⁴, L.J. Levinson ¹⁷², G. Levrimi ^{24b,24a}, M.P. Lewicki ⁸⁸, C. Lewis ¹⁴¹, D.J. Lewis ⁴, L. Lewitt ¹⁴², A. Li ³⁰, B. Li ^{63b}, C. Li ^{63a}, C-Q. Li ¹¹², H. Li ^{63a}, H. Li ^{63b}, H. Li ^{114a}, H. Li ¹⁵, H. Li ^{63b}, J. Li ^{63c}, K. Li ¹⁴, L. Li ^{63c}, M. Li ^{14,114c}, S. Li ^{14,114c}, S. Li ^{63d,63c}, T. Li ⁵, X. Li ¹⁰⁶, Z. Li ¹⁵⁶, Z. Li ^{14,114c}, Z. Li ^{63a}, S. Liang ^{14,114c}, Z. Liang ¹⁴, M. Liberatore ¹³⁸, B. Liberti ^{77a}, K. Lie ^{65c}, J. Lieber Marin ^{84e}, H. Lien ⁶⁹, H. Lin ¹⁰⁸, K. Lin ¹⁰⁹, R.E. Lindley ⁷, J.H. Lindon ², J. Ling ⁶², E. Lipeles ¹³¹, A. Lipniacka ¹⁷, A. Lister ¹⁶⁷, J.D. Little ⁶⁹, B. Liu ¹⁴, B.X. Liu ^{114b}, D. Liu ^{63d,63c}, E.H.L. Liu ²¹, J.B. Liu ^{63a}, J.K.K. Liu ³³, K. Liu ^{63d}, K. Liu ^{63d,63c}, M. Liu ^{63a}, M.Y. Liu ^{63a},

P. Liu ¹⁴, Q. Liu ^{63d,141,63c}, X. Liu ^{63a}, X. Liu ^{63b}, Y. Liu ^{114b,114c}, Y.L. Liu ^{63b}, Y.W. Liu ^{63a},
 S.L. Lloyd ⁹⁶, E.M. Lobodzinska ⁴⁹, P. Loch ⁷, E. Lodhi ¹⁵⁸, T. Lohse ¹⁹, K. Lohwasser ¹⁴²,
 E. Loiacono ⁴⁹, M. Lokajicek ^{134,*}, J.D. Lomas ²¹, J.D. Long ⁴², I. Longarini ¹⁶², R. Longo ¹⁶⁵,
 I. Lopez Paz ⁶⁸, A. Lopez Solis ⁴⁹, N.A. Lopez-canelas ⁷, N. Lorenzo Martinez ⁴, A.M. Lory ¹¹¹,
 M. Losada ^{119a}, G. Löschcke Centeno ¹⁴⁹, O. Loseva ³⁸, X. Lou ^{48a,48b}, X. Lou ^{14,114c},
 A. Lounis ⁶⁷, P.A. Love ⁹³, G. Lu ^{14,114c}, M. Lu ⁶⁷, S. Lu ¹³¹, Y.J. Lu ⁶⁶, H.J. Lubatti ¹⁴¹,
 C. Luci ^{76a,76b}, F.L. Lucio Alves ^{114a}, F. Luehring ⁶⁹, O. Lukianchuk ⁶⁷, B.S. Lunday ¹³¹,
 O. Lundberg ¹⁴⁷, B. Lund-Jensen ^{147,*}, N.A. Luongo ⁶, M.S. Lutz ³⁷, A.B. Lux ²⁶, D. Lynn ³⁰,
 R. Lysak ¹³⁴, E. Lytken ¹⁰⁰, V. Lyubushkin ³⁹, T. Lyubushkina ³⁹, M.M. Lyukova ¹⁴⁸,
 M.Firdaus M. Soberi ⁵³, H. Ma ³⁰, K. Ma ^{63a}, L.L. Ma ^{63b}, W. Ma ^{63a}, Y. Ma ¹²⁴,
 J.C. MacDonald ¹⁰², P.C. Machado De Abreu Farias ^{84e}, R. Madar ⁴¹, T. Madula ⁹⁸, J. Maeda ⁸⁶,
 T. Maeno ³⁰, H. Maguire ¹⁴², V. Maiboroda ¹³⁸, A. Maio ^{133a,133b,133d}, K. Maj ^{87a},
 O. Majersky ⁴⁹, S. Majewski ¹²⁶, N. Makovec ⁶⁷, V. Maksimovic ¹⁶, B. Malaescu ¹³⁰,
 Pa. Malecki ⁸⁸, V.P. Maleev ³⁸, F. Malek ^{61,m}, M. Mali ⁹⁵, D. Malito ⁹⁷, U. Mallik ⁸¹,
 S. Maltezos¹⁰, S. Malyukov³⁹, J. Mamuzic ¹³, G. Mancini ⁵⁴, M.N. Mancini ²⁷, G. Manco ^{74a,74b},
 J.P. Mandalia ⁹⁶, S.S. Mandarray ¹⁴⁹, I. Mandić ⁹⁵, L. Manhaes de Andrade Filho ^{84a},
 I.M. Maniatis ¹⁷², J. Manjarres Ramos ⁹¹, D.C. Mankad ¹⁷², A. Mann ¹¹¹, S. Manzoni ³⁷,
 L. Mao ^{63c}, X. Mapekula ^{34c}, A. Marantis ^{155,q}, G. Marchiori ⁵, M. Marcisovsky ¹³⁴,
 C. Marcon ^{72a}, M. Marinescu ²¹, S. Marium ⁴⁹, M. Marjanovic ¹²³, A. Markhoos ⁵⁵,
 M. Markovitch ⁶⁷, E.J. Marshall ⁹³, Z. Marshall ^{18a}, S. Marti-Garcia ¹⁶⁶, J. Martin ⁹⁸,
 T.A. Martin ¹³⁷, V.J. Martin ⁵³, B. Martin dit Latour ¹⁷, L. Martinelli ^{76a,76b}, M. Martinez ^{13,s},
 P. Martinez Agullo ¹⁶⁶, V.I. Martinez Outschoorn ¹⁰⁵, P. Martinez Suarez ¹³, S. Martin-Haugh ¹³⁷,
 G. Martinovicova ¹³⁶, V.S. Martoiu ^{28b}, A.C. Martyniuk ⁹⁸, A. Marzin ³⁷, D. Mascione ^{79a,79b},
 L. Masetti ¹⁰², J. Masik ¹⁰³, A.L. Maslennikov ³⁸, P. Massarotti ^{73a,73b}, P. Mastrandrea ^{75a,75b},
 A. Mastroberardino ^{44b,44a}, T. Masubuchi ¹²⁷, T.T. Mathew ¹²⁶, T. Mathisen ¹⁶⁴, J. Matousek ¹³⁶,
 D.M. Mattern ⁵⁰, J. Maurer ^{28b}, T. Maurin ⁶⁰, A.J. Maury ⁶⁷, B. Maček ⁹⁵, D.A. Maximov ³⁸,
 A.E. May ¹⁰³, R. Mazini ¹⁵¹, I. Maznas ¹¹⁸, M. Mazza ¹⁰⁹, S.M. Mazza ¹³⁹, E. Mazzeo ^{72a,72b},
 C. Mc Ginn ³⁰, J.P. Mc Gowan ¹⁶⁸, S.P. Mc Kee ¹⁰⁸, C.A. Mc Lean ⁶, C.C. McCracken ¹⁶⁷,
 E.F. McDonald ¹⁰⁷, A.E. McDougall ¹¹⁷, J.A. Mcfayden ¹⁴⁹, R.P. McGovern ¹³¹,
 R.P. Mckenzie ^{34g}, T.C. Mclachlan ⁴⁹, D.J. Mclaughlin ⁹⁸, S.J. McMahon ¹³⁷,
 C.M. Mcpartland ⁹⁴, R.A. McPherson ^{168,w}, S. Mehlhase ¹¹¹, A. Mehta ⁹⁴, D. Melini ¹⁶⁶,
 B.R. Mellado Garcia ^{34g}, A.H. Melo ⁵⁶, F. Meloni ⁴⁹, A.M. Mendes Jacques Da Costa ¹⁰³,
 H.Y. Meng ¹⁵⁸, L. Meng ⁹³, S. Menke ¹¹², M. Mentink ³⁷, E. Meoni ^{44b,44a}, G. Mercado ¹¹⁸,
 S. Merianos ¹⁵⁵, C. Merlassino ^{70a,70c}, L. Merola ^{73a,73b}, C. Meroni ^{72a,72b}, J. Metcalfe ⁶,
 A.S. Mete ⁶, E. Meuser ¹⁰², C. Meyer ⁶⁹, J-P. Meyer ¹³⁸, R.P. Middleton ¹³⁷, L. Mijović ⁵³,
 G. Mikenberg ¹⁷², M. Mikesstikova ¹³⁴, M. Mikuž ⁹⁵, H. Mildner ¹⁰², A. Milic ³⁷,
 D.W. Miller ⁴⁰, E.H. Miller ¹⁴⁶, L.S. Miller ³⁵, A. Milov ¹⁷², D.A. Milstead^{48a,48b}, T. Min^{114a},
 A.A. Minaenko ³⁸, I.A. Minashvili ^{152b}, L. Mince ⁶⁰, A.I. Mincer ¹²⁰, B. Mindur ^{87a},
 M. Mineev ³⁹, Y. Mino ⁸⁹, L.M. Mir ¹³, M. Miralles Lopez ⁶⁰, M. Mironova ^{18a},
 M.C. Missio ¹¹⁶, A. Mitra ¹⁷⁰, V.A. Mitsou ¹⁶⁶, Y. Mitsumori ¹¹³, O. Miu ¹⁵⁸,
 P.S. Miyagawa ⁹⁶, T. Mkrtchyan ^{64a}, M. Mlinarevic ⁹⁸, T. Mlinarevic ⁹⁸, M. Mlynarikova ³⁷,
 S. Mobius ²⁰, P. Mogg ¹¹¹, M.H. Mohamed Farook ¹¹⁵, A.F. Mohammed ^{14,114c}, S. Mohapatra ⁴²,
 G. Mokgatitwane ^{34g}, L. Moleri ¹⁷², B. Mondal ¹⁴⁴, S. Mondal ¹³⁵, K. Mönig ⁴⁹,
 E. Monnier ¹⁰⁴, L. Monsonis Romero¹⁶⁶, J. Montejo Berlingen ¹³, A. Montella ^{48a,48b},
 M. Montella ¹²², F. Montekali ^{78a,78b}, F. Monticelli ⁹², S. Monzani ^{70a,70c}, A. Morancho Tarda ⁴³,
 N. Morange ⁶⁷, A.L. Moreira De Carvalho ⁴⁹, M. Moreno Llácer ¹⁶⁶, C. Moreno Martinez ⁵⁷,
 J.M. Moreno Perez^{23b}, P. Morettini ^{58b}, S. Morgenstern ³⁷, M. Morii ⁶², M. Morinaga ¹⁵⁶,

M. Moritsu [ID⁹⁰](#), F. Morodei [ID^{76a,76b}](#), P. Moschovakos [ID³⁷](#), B. Moser [ID¹²⁹](#), M. Mosidze [ID^{152b}](#),
T. Moskalets [ID⁴⁵](#), P. Moskvitina [ID¹¹⁶](#), J. Moss [ID^{32j}](#), P. Moszkowicz [ID^{37a}](#), A. Moussa [ID^{36d}](#),
E.J.W. Moyse [ID¹⁰⁵](#), O. Mtintsilana [ID^{34g}](#), S. Muanza [ID¹⁰⁴](#), J. Mueller [ID¹³²](#), D. Muenstermann [ID⁹³](#),
R. Müller [ID³⁷](#), G.A. Mullier [ID¹⁶⁴](#), A.J. Mullin³³, J.J. Mullin¹³¹, A.E. Mulski [ID⁶²](#), D.P. Mungo [ID¹⁵⁸](#),
D. Munoz Perez [ID¹⁶⁶](#), F.J. Munoz Sanchez [ID¹⁰³](#), M. Murin [ID¹⁰³](#), W.J. Murray [ID^{170,137}](#), M. Muškinja [ID⁹⁵](#),
C. Mwewa [ID³⁰](#), A.G. Myagkov [ID^{38,a}](#), A.J. Myers [ID⁸](#), G. Myers [ID¹⁰⁸](#), M. Myska [ID¹³⁵](#),
B.P. Nachman [ID^{18a}](#), O. Nackenhorst [ID⁵⁰](#), K. Nagai [ID¹²⁹](#), K. Nagano [ID⁸⁵](#), J.L. Nagle [ID^{30,ae}](#), E. Nagy [ID¹⁰⁴](#),
A.M. Nairz [ID³⁷](#), Y. Nakahama [ID⁸⁵](#), K. Nakamura [ID⁸⁵](#), K. Nakkalil [ID⁵](#), H. Nanjo [ID¹²⁷](#),
E.A. Narayanan [ID¹¹⁵](#), I. Naryshkin [ID³⁸](#), L. Nasella [ID^{72a,72b}](#), M. Naseri [ID³⁵](#), S. Nasri [ID^{119b}](#), C. Nass [ID²⁵](#),
G. Navarro [ID^{23a}](#), J. Navarro-Gonzalez [ID¹⁶⁶](#), R. Nayak [ID¹⁵⁴](#), A. Nayaz [ID¹⁹](#), P.Y. Nechaeva [ID³⁸](#),
S. Nechaeva [ID^{24b,24a}](#), F. Nechansky [ID¹³⁴](#), L. Nedic [ID¹²⁹](#), T.J. Neep [ID²¹](#), A. Negri [ID^{74a,74b}](#),
M. Negrini [ID^{24b}](#), C. Nellist [ID¹¹⁷](#), C. Nelson [ID¹⁰⁶](#), K. Nelson [ID¹⁰⁸](#), S. Nemecek [ID¹³⁴](#), M. Nessi [ID^{37,g}](#),
M.S. Neubauer [ID¹⁶⁵](#), F. Neuhaus [ID¹⁰²](#), J. Neundorf [ID⁴⁹](#), J. Newell [ID⁹⁴](#), P.R. Newman [ID²¹](#), C.W. Ng [ID¹³²](#),
Y.W.Y. Ng [ID⁴⁹](#), B. Ngair [ID^{119a}](#), H.D.N. Nguyen [ID¹¹⁰](#), R.B. Nickerson [ID¹²⁹](#), R. Nicolaidou [ID¹³⁸](#),
J. Nielsen [ID¹³⁹](#), M. Niemeyer [ID⁵⁶](#), J. Niermann [ID⁵⁶](#), N. Nikiforou [ID³⁷](#), V. Nikolaenko [ID^{38,a}](#),
I. Nikolic-Audit [ID¹³⁰](#), K. Nikolopoulos [ID²¹](#), P. Nilsson [ID³⁰](#), I. Ninca [ID⁴⁹](#), G. Ninio [ID¹⁵⁴](#), A. Nisati [ID^{76a}](#),
N. Nishu [ID²](#), R. Nisius [ID¹¹²](#), N. Nitika [ID^{70a,70c}](#), J-E. Nitschke [ID⁵¹](#), E.K. Nkadimeng [ID^{34g}](#), T. Nobe [ID¹⁵⁶](#),
T. Nommensen [ID¹⁵⁰](#), M.B. Norfolk [ID¹⁴²](#), B.J. Norman [ID³⁵](#), M. Noury [ID^{36a}](#), J. Novak [ID⁹⁵](#), T. Novak [ID⁹⁵](#),
L. Novotny [ID¹³⁵](#), R. Novotny [ID¹¹⁵](#), L. Nozka [ID¹²⁵](#), K. Ntekas [ID¹⁶²](#), N.M.J. Nunes De Moura Junior [ID^{84b}](#),
J. Ocariz [ID¹³⁰](#), A. Ochi [ID⁸⁶](#), I. Ochoa [ID^{133a}](#), S. Oerdek [ID^{49,t}](#), J.T. Offermann [ID⁴⁰](#), A. Ogrodnik [ID¹³⁶](#),
A. Oh [ID¹⁰³](#), C.C. Ohm [ID¹⁴⁷](#), H. Oide [ID⁸⁵](#), R. Oishi [ID¹⁵⁶](#), M.L. Ojeda [ID³⁷](#), Y. Okumura [ID¹⁵⁶](#),
L.F. Oleiro Seabra [ID^{133a}](#), I. Oleksiyuk [ID⁵⁷](#), S.A. Olivares Pino [ID^{140d}](#), G. Oliveira Correa [ID¹³](#),
D. Oliveira Damazio [ID³⁰](#), J.L. Oliver [ID¹⁶²](#), Ö.O. Öncel [ID⁵⁵](#), A.P. O'Neill [ID²⁰](#), A. Onofre [ID^{133a,133e}](#),
P.U.E. Onyisi [ID¹¹](#), M.J. Oreglia [ID⁴⁰](#), G.E. Orellana [ID⁹²](#), D. Orestano [ID^{78a,78b}](#), N. Orlando [ID¹³](#),
R.S. Orr [ID¹⁵⁸](#), L.M. Osojnak [ID¹³¹](#), R. Ospanov [ID^{63a}](#), G. Otero y Garzon [ID³¹](#), H. Otono [ID⁹⁰](#), P.S. Ott [ID^{64a}](#),
G.J. Ottino [ID^{18a}](#), M. Ouchrif [ID^{36d}](#), F. Ould-Saada [ID¹²⁸](#), T. Ovsianikova [ID¹⁴¹](#), M. Owen [ID⁶⁰](#),
R.E. Owen [ID¹³⁷](#), V.E. Ozcan [ID^{22a}](#), F. Ozturk [ID⁸⁸](#), N. Ozturk [ID⁸](#), S. Ozturk [ID⁸³](#), H.A. Pacey [ID¹²⁹](#),
A. Pacheco Pages [ID¹³](#), C. Padilla Aranda [ID¹³](#), G. Padovano [ID^{76a,76b}](#), S. Pagan Griso [ID^{18a}](#),
G. Palacino [ID⁶⁹](#), A. Palazzo [ID^{71a,71b}](#), J. Pampel [ID²⁵](#), J. Pan [ID¹⁷⁵](#), T. Pan [ID^{65a}](#), D.K. Panchal [ID¹¹](#),
C.E. Pandini [ID¹¹⁷](#), J.G. Panduro Vazquez [ID¹³⁷](#), H.D. Pandya [ID¹](#), H. Pang [ID¹⁵](#), P. Pani [ID⁴⁹](#),
G. Panizzo [ID^{70a,70c}](#), L. Panwar [ID¹³⁰](#), L. Paolozzi [ID⁵⁷](#), S. Parajuli [ID¹⁶⁵](#), A. Paramonov [ID⁶](#),
C. Paraskevopoulos [ID⁵⁴](#), D. Paredes Hernandez [ID^{65b}](#), A. Pareti [ID^{74a,74b}](#), K.R. Park [ID⁴²](#), T.H. Park [ID¹⁵⁸](#),
M.A. Parker [ID³³](#), F. Parodi [ID^{58b,58a}](#), E.W. Parrish [ID¹¹⁸](#), V.A. Parrish [ID⁵³](#), J.A. Parsons [ID⁴²](#),
U. Parzefall [ID⁵⁵](#), B. Pascual Dias [ID¹¹⁰](#), L. Pascual Dominguez [ID¹⁰¹](#), E. Pasqualucci [ID^{76a}](#),
S. Passaggio [ID^{58b}](#), F. Pastore [ID⁹⁷](#), P. Patel [ID⁸⁸](#), U.M. Patel [ID⁵²](#), J.R. Pater [ID¹⁰³](#), T. Pauly [ID³⁷](#),
F. Pauwels¹³⁶, C.I. Pazos [ID¹⁶¹](#), M. Pedersen [ID¹²⁸](#), R. Pedro [ID^{133a}](#), S.V. Peleganchuk [ID³⁸](#), O. Penc [ID³⁷](#),
E.A. Pender [ID⁵³](#), S. Peng¹⁵, G.D. Penn [ID¹⁷⁵](#), K.E. Penski [ID¹¹¹](#), M. Penzin [ID³⁸](#), B.S. Peralva [ID^{84d}](#),
A.P. Pereira Peixoto [ID¹⁴¹](#), L. Pereira Sanchez [ID¹⁴⁶](#), D.V. Perepelitsa [ID^{30,ae}](#), G. Perera [ID¹⁰⁵](#),
E. Perez Codina [ID^{159a}](#), M. Perganti [ID¹⁰](#), H. Pernegger [ID³⁷](#), S. Perrella [ID^{76a,76b}](#), O. Perrin [ID⁴¹](#),
K. Peters [ID⁴⁹](#), R.F.Y. Peters [ID¹⁰³](#), B.A. Petersen [ID³⁷](#), T.C. Petersen [ID⁴³](#), E. Petit [ID¹⁰⁴](#), V. Petousis [ID¹³⁵](#),
C. Petridou [ID^{155,d}](#), T. Petru [ID¹³⁶](#), A. Petrukhin [ID¹⁴⁴](#), M. Pettee [ID^{18a}](#), A. Petukhov [ID³⁸](#), K. Petukhova [ID³⁷](#),
R. Pezoa [ID^{140f}](#), L. Pezzotti [ID³⁷](#), G. Pezzullo [ID¹⁷⁵](#), A.J. Pflieger [ID³⁷](#), T.M. Pham [ID¹⁷³](#), T. Pham [ID¹⁰⁷](#),
P.W. Phillips [ID¹³⁷](#), G. Piacquadio [ID¹⁴⁸](#), E. Pianori [ID^{18a}](#), F. Piazza [ID¹²⁶](#), R. Piegai [ID³¹](#), D. Pietreanu [ID^{28b}](#),
A.D. Pilkington [ID¹⁰³](#), M. Pinamonti [ID^{70a,70c}](#), J.L. Pinfeld [ID²](#), B.C. Pinheiro Pereira [ID^{133a}](#),
J. Pinol Bel [ID¹³](#), A.E. Pinto Pinoargote [ID^{138,138}](#), L. Pintucci [ID^{70a,70c}](#), K.M. Piper [ID¹⁴⁹](#), A. Pirttikoski [ID⁵⁷](#),
D.A. Pizzi [ID³⁵](#), L. Pizzimento [ID^{65b}](#), A. Pizzini [ID¹¹⁷](#), M.-A. Pleier [ID³⁰](#), V. Pleskot [ID¹³⁶](#), E. Plotnikova³⁹,
G. Poddar [ID⁹⁶](#), R. Poettgen [ID¹⁰⁰](#), L. Poggioli [ID¹³⁰](#), I. Pokharel [ID⁵⁶](#), S. Polacek [ID¹³⁶](#), G. Polesello [ID^{74a}](#),

A. Poley ^{145,159a}, A. Polini ^{24b}, C.S. Pollard ¹⁷⁰, Z.B. Pollock ¹²², E. Pompa Pacchi ^{76a,76b},
 N.I. Pond ⁹⁸, D. Ponomarenko ⁶⁹, L. Pontecorvo ³⁷, S. Popa ^{28a}, G.A. Popeneciu ^{28d},
 A. Poreba ³⁷, D.M. Portillo Quintero ^{159a}, S. Pospisil ¹³⁵, M.A. Postill ¹⁴², P. Postolache ^{28c},
 K. Potamianos ¹⁷⁰, P.A. Potepa ^{87a}, I.N. Potrap ³⁹, C.J. Potter ³³, H. Potti ¹⁵⁰, J. Poveda ¹⁶⁶,
 M.E. Pozo Astigarraga ³⁷, A. Prades Ibanez ^{77a,77b}, J. Pretel ¹⁶⁸, D. Price ¹⁰³, M. Primavera ^{71a},
 L. Primomo ^{70a,70c}, M.A. Principe Martin ¹⁰¹, R. Privara ¹²⁵, T. Procter ⁶⁰, M.L. Proffitt ¹⁴¹,
 N. Proklova ¹³¹, K. Prokofiev ^{65c}, G. Proto ¹¹², J. Proudfoot ⁶, M. Przybycien ^{87a},
 W.W. Przygoda ^{87b}, A. Psallidas ⁴⁷, J.E. Puddefoot ¹⁴², D. Pudzha ⁵⁵, D. Pyatiizbyantseva ³⁸,
 J. Qian ¹⁰⁸, D. Qichen ¹⁰³, Y. Qin ¹³, T. Qiu ⁵³, A. Quadt ⁵⁶, M. Queitsch-Maitland ¹⁰³,
 G. Quetant ⁵⁷, R.P. Quinn ¹⁶⁷, G. Rabanal Bolanos ⁶², D. Rafanoharana ⁵⁵, F. Raffaelli ^{77a,77b},
 F. Ragusa ^{72a,72b}, J.L. Rainbolt ⁴⁰, J.A. Raine ⁵⁷, S. Rajagopalan ³⁰, E. Ramakoti ³⁸,
 L. Rambelli ^{58b,58a}, I.A. Ramirez-Berend ³⁵, K. Ran ^{49,114c}, D.S. Rankin ¹³¹, N.P. Rapheeha ^{34g},
 H. Rasheed ^{28b}, V. Raskina ¹³⁰, D.F. Rassloff ^{64a}, A. Rastogi ^{18a}, S. Rave ¹⁰², S. Ravera ^{58b,58a},
 B. Ravina ⁵⁶, I. Ravinovich ¹⁷², M. Raymond ³⁷, A.L. Read ¹²⁸, N.P. Readioff ¹⁴²,
 D.M. Rebuzzi ^{74a,74b}, G. Redlinger ³⁰, A.S. Reed ¹¹², K. Reeves ²⁷, J.A. Reidelsturz ¹⁷⁴,
 D. Reikher ¹²⁶, A. Rej ⁵⁰, C. Rembser ³⁷, M. Renda ^{28b}, F. Renner ⁴⁹, A.G. Rennie ¹⁶²,
 A.L. Rescia ⁴⁹, S. Resconi ^{72a}, M. Ressegotti ^{58b,58a}, S. Rettie ³⁷, J.G. Reyes Rivera ¹⁰⁹,
 E. Reynolds ^{18a}, O.L. Rezanova ³⁸, P. Reznicek ¹³⁶, H. Riani ^{36d}, N. Ribaric ⁵², E. Ricci ^{79a,79b},
 R. Richter ¹¹², S. Richter ^{48a,48b}, E. Richter-Was ^{87b}, M. Ridel ¹³⁰, S. Ridouani ^{36d}, P. Rieck ¹²⁰,
 P. Riedler ³⁷, E.M. Riefel ^{48a,48b}, J.O. Rieger ¹¹⁷, M. Rijssenbeek ¹⁴⁸, M. Rimoldi ³⁷,
 L. Rinaldi ^{24b,24a}, P. Rincke ^{56,164}, T.T. Rinn ³⁰, M.P. Rinnagel ¹¹¹, G. Ripellino ¹⁶⁴, I. Riu ¹³,
 J.C. Rivera Vergara ¹⁶⁸, F. Rizatdinova ¹²⁴, E. Rizvi ⁹⁶, B.R. Roberts ^{18a}, S.S. Roberts ¹³⁹,
 S.H. Robertson ^{106,w}, D. Robinson ³³, M. Robles Manzano ¹⁰², A. Robson ⁶⁰, A. Rocchi ^{77a,77b},
 C. Roda ^{75a,75b}, S. Rodriguez Bosca ³⁷, Y. Rodriguez Garcia ^{23a}, A. Rodriguez Rodriguez ⁵⁵,
 A.M. Rodríguez Vera ¹¹⁸, S. Roe ³⁷, J.T. Roemer ³⁷, A.R. Roepe-Gier ¹³⁹, O. Røhne ¹²⁸,
 R.A. Rojas ¹⁰⁵, C.P.A. Roland ¹³⁰, J. Roloff ³⁰, A. Romaniouk ³⁸, E. Romano ^{74a,74b},
 M. Romano ^{24b}, A.C. Romero Hernandez ¹⁶⁵, N. Rompotis ⁹⁴, L. Roos ¹³⁰, S. Rosati ^{76a},
 B.J. Rosser ⁴⁰, E. Rossi ¹²⁹, E. Rossi ^{73a,73b}, L.P. Rossi ⁶², L. Rossini ⁵⁵, R. Rosten ¹²²,
 M. Rotaru ^{28b}, B. Rottler ⁵⁵, C. Rougier ⁹¹, D. Rousseau ⁶⁷, D. Rousso ⁴⁹, A. Roy ¹⁶⁵,
 S. Roy-Garand ¹⁵⁸, A. Rozanov ¹⁰⁴, Z.M.A. Rozario ⁶⁰, Y. Rozen ¹⁵³, A. Rubio Jimenez ¹⁶⁶,
 A.J. Ruby ⁹⁴, V.H. Ruelas Rivera ¹⁹, T.A. Ruggeri ¹, A. Ruggiero ¹²⁹, A. Ruiz-Martinez ¹⁶⁶,
 A. Rummler ³⁷, Z. Rurikova ⁵⁵, N.A. Rusakovich ³⁹, H.L. Russell ¹⁶⁸, G. Russo ^{76a,76b},
 J.P. Rutherford ⁷, S. Rutherford Colmenares ³³, M. Rybar ¹³⁶, E.B. Rye ¹²⁸, A. Ryzhov ⁴⁵,
 J.A. Sabater Iglesias ⁵⁷, H.F.W. Sadrozinski ¹³⁹, F. Safai Tehrani ^{76a}, B. Safarzadeh Samani ¹³⁷,
 S. Saha ¹, M. Sahinsoy ⁸³, A. Saibel ¹⁶⁶, M. Saimpert ¹³⁸, M. Saito ¹⁵⁶, T. Saito ¹⁵⁶,
 A. Sala ^{72a,72b}, D. Salamani ³⁷, A. Salnikov ¹⁴⁶, J. Salt ¹⁶⁶, A. Salvador Salas ¹⁵⁴,
 D. Salvatore ^{44b,44a}, F. Salvatore ¹⁴⁹, A. Salzburger ³⁷, D. Sammel ⁵⁵, E. Sampson ⁹³,
 D. Sampsonidis ^{155,d}, D. Sampsonidou ¹²⁶, J. Sánchez ¹⁶⁶, V. Sanchez Sebastian ¹⁶⁶,
 H. Sandaker ¹²⁸, C.O. Sander ⁴⁹, J.A. Sandesara ¹⁰⁵, M. Sandhoff ¹⁷⁴, C. Sandoval ^{23b},
 L. Sanfilippo ^{64a}, D.P.C. Sankey ¹³⁷, T. Sano ⁸⁹, A. Sansoni ⁵⁴, L. Santi ^{37,76b}, C. Santoni ⁴¹,
 H. Santos ^{133a,133b}, A. Santra ¹⁷², E. Sanzani ^{24b,24a}, K.A. Saoucha ¹⁶³, J.G. Saraiva ^{133a,133d},
 J. Sardain ⁷, O. Sasaki ⁸⁵, K. Sato ¹⁶⁰, C. Sauer ^{64b}, E. Sauvan ⁴, P. Savard ^{158,ac}, R. Sawada ¹⁵⁶,
 C. Sawyer ¹³⁷, L. Sawyer ⁹⁹, C. Sbarra ^{24b}, A. Sbrizzi ^{24b,24a}, T. Scanlon ⁹⁸,
 J. Schaarschmidt ¹⁴¹, U. Schäfer ¹⁰², A.C. Schaffer ^{67,45}, D. Schaile ¹¹¹, R.D. Schamberger ¹⁴⁸,
 C. Scharf ¹⁹, M.M. Schefer ²⁰, V.A. Schegelsky ³⁸, D. Scheirich ¹³⁶, M. Schernau ¹⁶²,
 C. Scheulen ⁵⁶, C. Schiavi ^{58b,58a}, M. Schioppa ^{44b,44a}, B. Schlag ^{146,1}, S. Schlenker ³⁷,
 J. Schmeing ¹⁷⁴, M.A. Schmidt ¹⁷⁴, K. Schmieden ¹⁰², C. Schmitt ¹⁰², N. Schmitt ¹⁰²,

S. Schmitt ⁴⁹, L. Schoeffel ¹³⁸, A. Schoening ^{64b}, P.G. Scholer ³⁵, E. Schopf ¹²⁹, M. Schott ²⁵,
 J. Schovancova ³⁷, S. Schramm ⁵⁷, T. Schroer ⁵⁷, H-C. Schultz-Coulon ^{64a}, M. Schumacher ⁵⁵,
 B.A. Schumm ¹³⁹, Ph. Schune ¹³⁸, A.J. Schuy ¹⁴¹, H.R. Schwartz ¹³⁹, A. Schwartzman ¹⁴⁶,
 T.A. Schwarz ¹⁰⁸, Ph. Schwemling ¹³⁸, R. Schwienhorst ¹⁰⁹, F.G. Sciacca ²⁰, A. Sciandra ³⁰,
 G. Sciolla ²⁷, F. Scuri ^{75a}, C.D. Sebastiani ⁹⁴, K. Sedlaczek ¹¹⁸, S.C. Seidel ¹¹⁵, A. Seiden ¹³⁹,
 B.D. Seidlitz ⁴², C. Seitz ⁴⁹, J.M. Seixas ^{84b}, G. Sekhniaidze ^{73a}, L. Selem ⁶¹,
 N. Semprini-Cesari ^{24b,24a}, D. Sengupta ⁵⁷, V. Senthilkumar ¹⁶⁶, L. Serin ⁶⁷, M. Sessa ^{77a,77b},
 H. Severini ¹²³, F. Sforza ^{58b,58a}, A. Sfyrta ⁵⁷, Q. Sha ¹⁴, E. Shabalina ⁵⁶, A.H. Shah ³³,
 R. Shaheen ¹⁴⁷, J.D. Shahinian ¹³¹, D. Shaked Renous ¹⁷², L.Y. Shan ¹⁴, M. Shapiro ^{18a},
 A. Sharma ³⁷, A.S. Sharma ¹⁶⁷, P. Sharma ⁸¹, P.B. Shatalov ³⁸, K. Shaw ¹⁴⁹, S.M. Shaw ¹⁰³,
 Q. Shen ^{63c}, D.J. Sheppard ¹⁴⁵, P. Sherwood ⁹⁸, L. Shi ⁹⁸, X. Shi ¹⁴, S. Shimizu ⁸⁵,
 C.O. Shimmin ¹⁷⁵, J.D. Shinner ⁹⁷, I.P.J. Shipsey ¹²⁹, S. Shirabe ⁹⁰, M. Shiyakova ^{39,u},
 M.J. Shochet ⁴⁰, D.R. Shope ¹²⁸, B. Shrestha ¹²³, S. Shrestha ^{122,af}, M.J. Shroff ¹⁶⁸,
 P. Sicho ¹³⁴, A.M. Sickles ¹⁶⁵, E. Sideras Haddad ^{34g}, A.C. Sidley ¹¹⁷, A. Sidoti ^{24b},
 F. Siegert ⁵¹, Dj. Sijacki ¹⁶, F. Sili ⁹², J.M. Silva ⁵³, I. Silva Ferreira ^{84b}, M.V. Silva Oliveira ³⁰,
 S.B. Silverstein ^{48a}, S. Simion ⁶⁷, R. Simoniello ³⁷, E.L. Simpson ¹⁰³, H. Simpson ¹⁴⁹,
 L.R. Simpson ¹⁰⁸, S. Simsek ⁸³, S. Sindhu ⁵⁶, P. Sinervo ¹⁵⁸, S. Singh ¹⁵⁸, S. Sinha ⁴⁹,
 S. Sinha ¹⁰³, M. Sioli ^{24b,24a}, I. Siral ³⁷, E. Sitnikova ⁴⁹, J. Sjölin ^{48a,48b}, A. Skaf ⁵⁶,
 E. Skorda ²¹, P. Skubic ¹²³, M. Slawinska ⁸⁸, V. Smakhtin ¹⁷², B.H. Smart ¹³⁷, S.Yu. Smirnov ³⁸,
 Y. Smirnov ³⁸, L.N. Smirnova ^{38,a}, O. Smirnova ¹⁰⁰, A.C. Smith ⁴², D.R. Smith ¹⁶², E.A. Smith ⁴⁰,
 J.L. Smith ¹⁰³, R. Smith ¹⁴⁶, M. Smizanska ⁹³, K. Smolek ¹³⁵, A.A. Snesarev ³⁸, H.L. Snoek ¹¹⁷,
 S. Snyder ³⁰, R. Sobie ^{168,w}, A. Soffer ¹⁵⁴, C.A. Solans Sanchez ³⁷, E.Yu. Soldatov ³⁸,
 U. Soldevila ¹⁶⁶, A.A. Solodkov ³⁸, S. Solomon ²⁷, A. Soloshenko ³⁹, K. Solovieva ⁵⁵,
 O.V. Solovyanov ⁴¹, P. Sommer ⁵¹, A. Sonay ¹³, W.Y. Song ^{159b}, A. Sopczak ¹³⁵, A.L. Sopio ⁵³,
 F. Sopkova ^{29b}, J.D. Sorenson ¹¹⁵, I.R. Sotarriva Alvarez ¹⁵⁷, V. Sothilingam ^{64a},
 O.J. Soto Sandoval ^{140c,140b}, S. Sottocornola ⁶⁹, R. Soualah ¹⁶³, Z. Soumami ^{36e}, D. South ⁴⁹,
 N. Soybelman ¹⁷², S. Spagnolo ^{71a,71b}, M. Spalla ¹¹², D. Sperlich ⁵⁵, G. Spigo ³⁷,
 B. Spisso ^{73a,73b}, D.P. Spiteri ⁶⁰, M. Spousta ¹³⁶, E.J. Staats ³⁵, R. Stamen ^{64a}, A. Stampekis ²¹,
 E. Stanecka ⁸⁸, W. Stanek-Maslouska ⁴⁹, M.V. Stange ⁵¹, B. Stanislaus ^{18a}, M.M. Stanitzki ⁴⁹,
 B. Stapf ⁴⁹, E.A. Starchenko ³⁸, G.H. Stark ¹³⁹, J. Stark ⁹¹, P. Staroba ¹³⁴, P. Starovoitov ^{64a},
 S. Stärz ¹⁰⁶, R. Staszewski ⁸⁸, G. Stavropoulos ⁴⁷, P. Steinberg ³⁰, B. Stelzer ^{145,159a},
 H.J. Stelzer ¹³², O. Stelzer-Chilton ^{159a}, H. Stenzel ⁵⁹, T.J. Stevenson ¹⁴⁹, G.A. Stewart ³⁷,
 J.R. Stewart ¹²⁴, M.C. Stockton ³⁷, G. Stoicea ^{28b}, M. Stolarski ^{133a}, S. Stonjek ¹¹²,
 A. Straessner ⁵¹, J. Strandberg ¹⁴⁷, S. Strandberg ^{48a,48b}, M. Stratmann ¹⁷⁴, M. Strauss ¹²³,
 T. Streblner ¹⁰⁴, P. Strizenec ^{29b}, R. Ströhmer ¹⁶⁹, D.M. Strom ¹²⁶, R. Stroynowski ⁴⁵,
 A. Strubig ^{48a,48b}, S.A. Stucci ³⁰, B. Stugu ¹⁷, J. Stupak ¹²³, N.A. Styles ⁴⁹, D. Su ¹⁴⁶,
 S. Su ^{63a}, W. Su ^{63d}, X. Su ^{63a}, D. Suchy ^{29a}, K. Sugizaki ¹⁵⁶, V.V. Sulin ³⁸, M.J. Sullivan ⁹⁴,
 D.M.S. Sultan ¹²⁹, L. Sultanaliev ³⁸, S. Sultansoy ^{3b}, T. Sumida ⁸⁹, S. Sun ¹⁷³,
 O. Sunneborn Gudnadottir ¹⁶⁴, N. Sur ¹⁰⁴, M.R. Sutton ¹⁴⁹, H. Suzuki ¹⁶⁰, M. Svatos ¹³⁴,
 M. Swiatlowski ^{159a}, T. Swirski ¹⁶⁹, I. Sykora ^{29a}, M. Sykora ¹³⁶, T. Sykora ¹³⁶, D. Ta ¹⁰²,
 K. Tackmann ^{49,t}, A. Taffard ¹⁶², R. Tafirout ^{159a}, J.S. Tafoya Vargas ⁶⁷, Y. Takubo ⁸⁵,
 M. Talby ¹⁰⁴, A.A. Talyshv ³⁸, K.C. Tam ^{65b}, N.M. Tamir ¹⁵⁴, A. Tanaka ¹⁵⁶, J. Tanaka ¹⁵⁶,
 R. Tanaka ⁶⁷, M. Tanasini ¹⁴⁸, Z. Tao ¹⁶⁷, S. Tapia Araya ^{140f}, S. Tapprogge ¹⁰²,
 A. Tarek Abouelfadl Mohamed ¹⁰⁹, S. Tarem ¹⁵³, K. Tariq ¹⁴, G. Tarna ^{28b}, G.F. Tartarelli ^{72a},
 M.J. Tartarin ⁹¹, P. Tas ¹³⁶, M. Tasevsky ¹³⁴, E. Tassi ^{44b,44a}, A.C. Tate ¹⁶⁵, G. Tateno ¹⁵⁶,
 Y. Tayalati ^{36e,v}, G.N. Taylor ¹⁰⁷, W. Taylor ^{159b}, R. Teixeira De Lima ¹⁴⁶, P. Teixeira-Dias ⁹⁷,
 J.J. Teoh ¹⁵⁸, K. Terashi ¹⁵⁶, J. Terron ¹⁰¹, S. Terzo ¹³, M. Testa ⁵⁴, R.J. Teuscher ^{158,w},

A. Thaler ⁸⁰, O. Theiner ⁵⁷, T. Theveneaux-Pelzer ¹⁰⁴, O. Thielmann ¹⁷⁴, D.W. Thomas ⁹⁷,
 J.P. Thomas ²¹, E.A. Thompson ^{18a}, P.D. Thompson ²¹, E. Thomson ¹³¹, R.E. Thornberry ⁴⁵,
 C. Tian ^{63a}, Y. Tian ⁵⁷, V. Tikhomirov ^{38,a}, Yu.A. Tikhonov ³⁸, S. Timoshenko ³⁸,
 D. Timoshyn ¹³⁶, E.X.L. Ting ¹, P. Tipton ¹⁷⁵, A. Tishelman-Charny ³⁰, S.H. Tlou ^{34g},
 K. Todome ¹⁵⁷, S. Todorova-Nova ¹³⁶, S. Todt ⁵¹, L. Toffolin ^{70a,70c}, M. Togawa ⁸⁵, J. Tojo ⁹⁰,
 S. Tokár ^{29a}, K. Tokushuku ⁸⁵, O. Toldaiev ⁶⁹, M. Tomoto ^{85,113}, L. Tompkins ^{146,1},
 K.W. Topolnicki ^{87b}, E. Torrence ¹²⁶, H. Torres ⁹¹, E. Torró Pastor ¹⁶⁶, M. Toscani ³¹,
 C. Toscirì ⁴⁰, M. Tost ¹¹, D.R. Tovey ¹⁴², I.S. Trandafir ^{28b}, T. Trefzger ¹⁶⁹, A. Tricoli ³⁰,
 I.M. Trigger ^{159a}, S. Trincaz-Duvoid ¹³⁰, D.A. Trischuk ²⁷, B. Trocmé ⁶¹, A. Tropina ³⁹,
 L. Truong ^{34c}, M. Trzebinski ⁸⁸, A. Trzupiek ⁸⁸, F. Tsai ¹⁴⁸, M. Tsai ¹⁰⁸, A. Tsiamis ¹⁵⁵,
 P.V. Tsiareshka ³⁸, S. Tsigaridas ^{159a}, A. Tsirigotis ^{155,q}, V. Tsiskaridze ¹⁵⁸, E.G. Tskhadadze ^{152a},
 M. Tsopoulou ¹⁵⁵, Y. Tsujikawa ⁸⁹, I.I. Tsukerman ³⁸, V. Tsulaia ^{18a}, S. Tsuno ⁸⁵, K. Tsurii ¹²¹,
 D. Tsybychev ¹⁴⁸, Y. Tu ^{65b}, A. Tudorache ^{28b}, V. Tudorache ^{28b}, A.N. Tuna ⁶²,
 S. Turchikhin ^{58b,58a}, I. Turk Cakir ^{3a}, R. Turra ^{72a}, T. Turtuvshin ³⁹, P.M. Tuts ⁴²,
 S. Tzamarias ^{155,d}, E. Tzovara ¹⁰², F. Ukegawa ¹⁶⁰, P.A. Ulloa Poblete ^{140c,140b}, E.N. Umaka ³⁰,
 G. Unal ³⁷, A. Undrus ³⁰, G. Unel ¹⁶², J. Urban ^{29b}, P. Urrejola ^{140a}, G. Usai ⁸, R. Ushioda ¹⁵⁷,
 M. Usman ¹¹⁰, F. Ustuner ⁵³, Z. Uysal ⁸³, V. Vacek ¹³⁵, B. Vachon ¹⁰⁶, T. Vafeiadis ³⁷,
 A. Vaitkus ⁹⁸, C. Valderanis ¹¹¹, E. Valdes Santurio ^{48a,48b}, M. Valente ^{159a}, S. Valentinetti ^{24b,24a},
 A. Valero ¹⁶⁶, E. Valiente Moreno ¹⁶⁶, A. Vallier ⁹¹, J.A. Valls Ferrer ¹⁶⁶, D.R. Van Arneman ¹¹⁷,
 T.R. Van Daalen ¹⁴¹, A. Van Der Graaf ⁵⁰, P. Van Gemmeren ⁶, M. Van Rijnbach ³⁷,
 S. Van Stroud ⁹⁸, I. Van Vulpen ¹¹⁷, P. Vana ¹³⁶, M. Vanadia ^{77a,77b}, U.M. Vande Voorde ¹⁴⁷,
 W. Vandelli ³⁷, E.R. Vandewall ¹²⁴, D. Vannicola ¹⁵⁴, L. Vannoli ⁵⁴, R. Vari ^{76a}, E.W. Varnes ⁷,
 C. Varni ^{18b}, T. Varol ¹⁵¹, D. Varouchas ⁶⁷, L. Varriale ¹⁶⁶, K.E. Varvell ¹⁵⁰, M.E. Vasile ^{28b},
 L. Vaslin ⁸⁵, G.A. Vasquez ¹⁶⁸, A. Vasyukov ³⁹, L.M. Vaughan ¹²⁴, R. Vavricka ¹⁰²,
 T. Vazquez Schroeder ³⁷, J. Veatch ³², V. Vecchio ¹⁰³, M.J. Veen ¹⁰⁵, I. Veliscek ³⁰,
 L.M. Veloce ¹⁵⁸, F. Veloso ^{133a,133c}, S. Veneziano ^{76a}, A. Ventura ^{71a,71b}, S. Ventura Gonzalez ¹³⁸,
 A. Verbytskyi ¹¹², M. Verducci ^{75a,75b}, C. Vergis ⁹⁶, M. Verissimo De Araujo ^{84b},
 W. Verkerke ¹¹⁷, J.C. Vermeulen ¹¹⁷, C. Vernieri ¹⁴⁶, M. Vessella ¹⁰⁵, M.C. Vetterli ^{145,ac},
 A. Vgenopoulos ¹⁰², N. Viaux Maira ^{140f}, T. Vickey ¹⁴², O.E. Vickey Boeriu ¹⁴²,
 G.H.A. Viehhauser ¹²⁹, L. Vigani ^{64b}, M. Vigil ¹¹², M. Villa ^{24b,24a}, M. Villaplana Perez ¹⁶⁶,
 E.M. Villhauer ⁵³, E. Vilucchi ⁵⁴, M.G. Vincter ³⁵, A. Visibile ¹¹⁷, C. Vittori ³⁷, I. Vivarelli ^{24b,24a},
 E. Voevodina ¹¹², F. Vogel ¹¹¹, J.C. Voigt ⁵¹, P. Vokac ¹³⁵, Yu. Volkotrub ^{87b}, E. Von Toerne ²⁵,
 B. Vormwald ³⁷, V. Vorobel ¹³⁶, K. Vorobev ³⁸, M. Vos ¹⁶⁶, K. Voss ¹⁴⁴, M. Vozak ¹¹⁷,
 L. Vozdecky ¹²³, N. Vranjes ¹⁶, M. Vranjes Milosavljevic ¹⁶, M. Vreeswijk ¹¹⁷, N.K. Vu ^{63d,63c},
 R. Vuillermet ³⁷, O. Vujinovic ¹⁰², I. Vukotic ⁴⁰, I.K. Vyas ³⁵, S. Wada ¹⁶⁰, C. Wagner ¹⁴⁶,
 J.M. Wagner ^{18a}, W. Wagner ¹⁷⁴, S. Wahdan ¹⁷⁴, H. Wahlberg ⁹², C.H. Waits ¹²³, J. Walder ¹³⁷,
 R. Walker ¹¹¹, W. Walkowiak ¹⁴⁴, A. Wall ¹³¹, E.J. Wallin ¹⁰⁰, T. Wamorkar ⁶, A.Z. Wang ¹³⁹,
 C. Wang ¹⁰², C. Wang ¹¹, H. Wang ^{18a}, J. Wang ^{65c}, P. Wang ⁹⁸, R. Wang ⁶², R. Wang ⁶,
 S.M. Wang ¹⁵¹, S. Wang ^{63b}, S. Wang ¹⁴, T. Wang ^{63a}, T. Wang ^{63a}, W.T. Wang ⁸¹, W. Wang ¹⁴,
 X. Wang ^{114a}, X. Wang ¹⁶⁵, X. Wang ^{63c}, Y. Wang ^{63d}, Y. Wang ^{114a}, Y. Wang ^{63a},
 Z. Wang ¹⁰⁸, Z. Wang ^{63d,52,63c}, Z. Wang ¹⁰⁸, A. Warburton ¹⁰⁶, R.J. Ward ²¹, N. Warrack ⁶⁰,
 S. Waterhouse ⁹⁷, A.T. Watson ²¹, H. Watson ⁵³, M.F. Watson ²¹, E. Watton ^{60,137}, G. Watts ¹⁴¹,
 B.M. Waugh ⁹⁸, J.M. Webb ⁵⁵, C. Weber ³⁰, H.A. Weber ¹⁹, M.S. Weber ²⁰, S.M. Weber ^{64a},
 C. Wei ^{63a}, Y. Wei ⁵⁵, A.R. Weidberg ¹²⁹, E.J. Weik ¹²⁰, J. Weingarten ⁵⁰, C. Weiser ⁵⁵,
 C.J. Wells ⁴⁹, T. Wenaus ³⁰, B. Wendland ⁵⁰, T. Wengler ³⁷, N.S. Wenke ¹¹², N. Wermes ²⁵,
 M. Wessels ^{64a}, A.M. Wharton ⁹³, A.S. White ⁶², A. White ⁸, M.J. White ¹, D. Whiteson ¹⁶²,
 L. Wickremasinghe ¹²⁷, W. Wiedenmann ¹⁷³, M. Wielers ¹³⁷, C. Wiglesworth ⁴³, D.J. Wilbern ¹²³,

H.G. Wilkens ³⁷, J.J.H. Wilkinson ³³, D.M. Williams ⁴², H.H. Williams ¹³¹, S. Williams ³³, S. Willocq ¹⁰⁵, B.J. Wilson ¹⁰³, P.J. Windischhofer ⁴⁰, F.I. Winkel ³¹, F. Winklmeier ¹²⁶, B.T. Winter ⁵⁵, J.K. Winter ¹⁰³, M. Wittgen ¹⁴⁶, M. Wobisch ⁹⁹, T. Wojtkowski ⁶¹, Z. Wolffs ¹¹⁷, J. Wollrath ¹⁶², M.W. Wolter ⁸⁸, H. Wolters ^{133a,133c}, M.C. Wong ¹³⁹, E.L. Woodward ⁴², S.D. Worm ⁴⁹, B.K. Wosiek ⁸⁸, K.W. Woźniak ⁸⁸, S. Wozniewski ⁵⁶, K. Wraight ⁶⁰, C. Wu ²¹, M. Wu ^{114b}, M. Wu ¹¹⁶, S.L. Wu ¹⁷³, X. Wu ⁵⁷, Y. Wu ^{63a}, Z. Wu ⁴, J. Wuerzinger ^{112,aa}, T.R. Wyatt ¹⁰³, B.M. Wynne ⁵³, S. Xella ⁴³, L. Xia ^{114a}, M. Xia ¹⁵, M. Xie ^{63a}, S. Xin ^{14,114c}, A. Xiong ¹²⁶, J. Xiong ^{18a}, D. Xu ¹⁴, H. Xu ^{63a}, L. Xu ^{63a}, R. Xu ¹³¹, T. Xu ¹⁰⁸, Y. Xu ¹⁵, Z. Xu ⁵³, Z. Xu ^{114a}, B. Yabsley ¹⁵⁰, S. Yacoub ^{34a}, Y. Yamaguchi ⁸⁵, E. Yamashita ¹⁵⁶, H. Yamauchi ¹⁶⁰, T. Yamazaki ^{18a}, Y. Yamazaki ⁸⁶, S. Yan ⁶⁰, Z. Yan ¹⁰⁵, H.J. Yang ^{63c,63d}, H.T. Yang ^{63a}, S. Yang ^{63a}, T. Yang ^{65c}, X. Yang ³⁷, X. Yang ¹⁴, Y. Yang ⁴⁵, Y. Yang ^{63a}, Z. Yang ^{63a}, W.-M. Yao ^{18a}, H. Ye ^{114a}, H. Ye ⁵⁶, J. Ye ¹⁴, S. Ye ³⁰, X. Ye ^{63a}, Y. Yeh ⁹⁸, I. Yeletsikh ³⁹, B.K. Yeo ^{18b}, M.R. Yexley ⁹⁸, T.P. Yildirim ¹²⁹, P. Yin ⁴², K. Yorita ¹⁷¹, S. Younas ^{28b}, C.J.S. Young ³⁷, C. Young ¹⁴⁶, C. Yu ^{14,114c}, Y. Yu ^{63a}, J. Yuan ^{14,114c}, M. Yuan ¹⁰⁸, R. Yuan ^{63d,63c}, L. Yue ⁹⁸, M. Zaazoua ^{63a}, B. Zabinski ⁸⁸, E. Zaid ⁵³, Z.K. Zak ⁸⁸, T. Zakareishvili ¹⁶⁶, S. Zambito ⁵⁷, J.A. Zamora Saa ^{140d,140b}, J. Zang ¹⁵⁶, D. Zanzi ⁵⁵, O. Zaplatilek ¹³⁵, C. Zeitnitz ¹⁷⁴, H. Zeng ¹⁴, J.C. Zeng ¹⁶⁵, D.T. Zenger Jr ²⁷, O. Zenin ³⁸, T. Ženiš ^{29a}, S. Zenz ⁹⁶, S. Zerradi ^{36a}, D. Zerwas ⁶⁷, M. Zhai ^{14,114c}, D.F. Zhang ¹⁴², J. Zhang ^{63b}, J. Zhang ⁶, K. Zhang ^{14,114c}, L. Zhang ^{63a}, L. Zhang ^{114a}, P. Zhang ^{14,114c}, R. Zhang ¹⁷³, S. Zhang ¹⁰⁸, S. Zhang ⁹¹, T. Zhang ¹⁵⁶, X. Zhang ^{63c}, X. Zhang ^{63b}, Y. Zhang ^{63c}, Y. Zhang ⁹⁸, Y. Zhang ^{114a}, Z. Zhang ^{18a}, Z. Zhang ^{63b}, Z. Zhang ⁶⁷, H. Zhao ¹⁴¹, T. Zhao ^{63b}, Y. Zhao ¹³⁹, Z. Zhao ^{63a}, Z. Zhao ^{63a}, A. Zhemchugov ³⁹, J. Zheng ^{114a}, K. Zheng ¹⁶⁵, X. Zheng ^{63a}, Z. Zheng ¹⁴⁶, D. Zhong ¹⁶⁵, B. Zhou ¹⁰⁸, H. Zhou ⁷, N. Zhou ^{63c}, Y. Zhou ¹⁵, Y. Zhou ^{114a}, Y. Zhou ⁷, C.G. Zhu ^{63b}, J. Zhu ¹⁰⁸, X. Zhu ^{63d}, Y. Zhu ^{63c}, Y. Zhu ^{63a}, X. Zhuang ¹⁴, K. Zhukov ⁶⁹, N.I. Zimine ³⁹, J. Zinsser ^{64b}, M. Ziolkowski ¹⁴⁴, L. Živković ¹⁶, A. Zoccoli ^{24b,24a}, K. Zoch ⁶², T.G. Zorbas ¹⁴², O. Zormpa ⁴⁷, W. Zou ⁴², L. Zwalinski ³⁷.

¹Department of Physics, University of Adelaide, Adelaide; Australia.

²Department of Physics, University of Alberta, Edmonton AB; Canada.

³(^a)Department of Physics, Ankara University, Ankara;(^b)Division of Physics, TOBB University of Economics and Technology, Ankara; Türkiye.

⁴LAPP, Université Savoie Mont Blanc, CNRS/IN2P3, Annecy; France.

⁵APC, Université Paris Cité, CNRS/IN2P3, Paris; France.

⁶High Energy Physics Division, Argonne National Laboratory, Argonne IL; United States of America.

⁷Department of Physics, University of Arizona, Tucson AZ; United States of America.

⁸Department of Physics, University of Texas at Arlington, Arlington TX; United States of America.

⁹Physics Department, National and Kapodistrian University of Athens, Athens; Greece.

¹⁰Physics Department, National Technical University of Athens, Zografou; Greece.

¹¹Department of Physics, University of Texas at Austin, Austin TX; United States of America.

¹²Institute of Physics, Azerbaijan Academy of Sciences, Baku; Azerbaijan.

¹³Institut de Física d'Altes Energies (IFAE), Barcelona Institute of Science and Technology, Barcelona; Spain.

¹⁴Institute of High Energy Physics, Chinese Academy of Sciences, Beijing; China.

¹⁵Physics Department, Tsinghua University, Beijing; China.

¹⁶Institute of Physics, University of Belgrade, Belgrade; Serbia.

¹⁷Department for Physics and Technology, University of Bergen, Bergen; Norway.

- ¹⁸(*a*) Physics Division, Lawrence Berkeley National Laboratory, Berkeley CA; (*b*) University of California, Berkeley CA; United States of America.
- ¹⁹Institut für Physik, Humboldt Universität zu Berlin, Berlin; Germany.
- ²⁰Albert Einstein Center for Fundamental Physics and Laboratory for High Energy Physics, University of Bern, Bern; Switzerland.
- ²¹School of Physics and Astronomy, University of Birmingham, Birmingham; United Kingdom.
- ²²(*a*) Department of Physics, Bogazici University, Istanbul; (*b*) Department of Physics Engineering, Gaziantep University, Gaziantep; (*c*) Department of Physics, Istanbul University, Istanbul; Türkiye.
- ²³(*a*) Facultad de Ciencias y Centro de Investigaciones, Universidad Antonio Nariño, Bogotá; (*b*) Departamento de Física, Universidad Nacional de Colombia, Bogotá; Colombia.
- ²⁴(*a*) Dipartimento di Fisica e Astronomia A. Righi, Università di Bologna, Bologna; (*b*) INFN Sezione di Bologna; Italy.
- ²⁵Physikalisches Institut, Universität Bonn, Bonn; Germany.
- ²⁶Department of Physics, Boston University, Boston MA; United States of America.
- ²⁷Department of Physics, Brandeis University, Waltham MA; United States of America.
- ²⁸(*a*) Transilvania University of Brasov, Brasov; (*b*) Horia Hulubei National Institute of Physics and Nuclear Engineering, Bucharest; (*c*) Department of Physics, Alexandru Ioan Cuza University of Iasi, Iasi; (*d*) National Institute for Research and Development of Isotopic and Molecular Technologies, Physics Department, Cluj-Napoca; (*e*) National University of Science and Technology Politehnica, Bucharest; (*f*) West University in Timisoara, Timisoara; (*g*) Faculty of Physics, University of Bucharest, Bucharest; Romania.
- ²⁹(*a*) Faculty of Mathematics, Physics and Informatics, Comenius University, Bratislava; (*b*) Department of Subnuclear Physics, Institute of Experimental Physics of the Slovak Academy of Sciences, Kosice; Slovak Republic.
- ³⁰Physics Department, Brookhaven National Laboratory, Upton NY; United States of America.
- ³¹Universidad de Buenos Aires, Facultad de Ciencias Exactas y Naturales, Departamento de Física, y CONICET, Instituto de Física de Buenos Aires (IFIBA), Buenos Aires; Argentina.
- ³²California State University, CA; United States of America.
- ³³Cavendish Laboratory, University of Cambridge, Cambridge; United Kingdom.
- ³⁴(*a*) Department of Physics, University of Cape Town, Cape Town; (*b*) iThemba Labs, Western Cape; (*c*) Department of Mechanical Engineering Science, University of Johannesburg, Johannesburg; (*d*) National Institute of Physics, University of the Philippines Diliman (Philippines); (*e*) University of South Africa, Department of Physics, Pretoria; (*f*) University of Zululand, KwaDlangezwa; (*g*) School of Physics, University of the Witwatersrand, Johannesburg; South Africa.
- ³⁵Department of Physics, Carleton University, Ottawa ON; Canada.
- ³⁶(*a*) Faculté des Sciences Ain Chock, Réseau Universitaire de Physique des Hautes Energies - Université Hassan II, Casablanca; (*b*) Faculté des Sciences, Université Ibn-Tofail, Kénitra; (*c*) Faculté des Sciences Semlalia, Université Cadi Ayyad, LPHEA-Marrakech; (*d*) LPMR, Faculté des Sciences, Université Mohamed Premier, Oujda; (*e*) Faculté des sciences, Université Mohammed V, Rabat; (*f*) Institute of Applied Physics, Mohammed VI Polytechnic University, Ben Guerir; Morocco.
- ³⁷CERN, Geneva; Switzerland.
- ³⁸Affiliated with an institute covered by a cooperation agreement with CERN.
- ³⁹Affiliated with an international laboratory covered by a cooperation agreement with CERN.
- ⁴⁰Enrico Fermi Institute, University of Chicago, Chicago IL; United States of America.
- ⁴¹LPC, Université Clermont Auvergne, CNRS/IN2P3, Clermont-Ferrand; France.
- ⁴²Nevis Laboratory, Columbia University, Irvington NY; United States of America.
- ⁴³Niels Bohr Institute, University of Copenhagen, Copenhagen; Denmark.
- ⁴⁴(*a*) Dipartimento di Fisica, Università della Calabria, Rende; (*b*) INFN Gruppo Collegato di Cosenza,

Laboratori Nazionali di Frascati; Italy.

⁴⁵Physics Department, Southern Methodist University, Dallas TX; United States of America.

⁴⁶Physics Department, University of Texas at Dallas, Richardson TX; United States of America.

⁴⁷National Centre for Scientific Research "Demokritos", Agia Paraskevi; Greece.

⁴⁸(^a) Department of Physics, Stockholm University; (^b) Oskar Klein Centre, Stockholm; Sweden.

⁴⁹Deutsches Elektronen-Synchrotron DESY, Hamburg and Zeuthen; Germany.

⁵⁰Fakultät Physik, Technische Universität Dortmund, Dortmund; Germany.

⁵¹Institut für Kern- und Teilchenphysik, Technische Universität Dresden, Dresden; Germany.

⁵²Department of Physics, Duke University, Durham NC; United States of America.

⁵³SUPA - School of Physics and Astronomy, University of Edinburgh, Edinburgh; United Kingdom.

⁵⁴INFN e Laboratori Nazionali di Frascati, Frascati; Italy.

⁵⁵Physikalisches Institut, Albert-Ludwigs-Universität Freiburg, Freiburg; Germany.

⁵⁶II. Physikalisches Institut, Georg-August-Universität Göttingen, Göttingen; Germany.

⁵⁷Département de Physique Nucléaire et Corpusculaire, Université de Genève, Genève; Switzerland.

⁵⁸(^a) Dipartimento di Fisica, Università di Genova, Genova; (^b) INFN Sezione di Genova; Italy.

⁵⁹II. Physikalisches Institut, Justus-Liebig-Universität Giessen, Giessen; Germany.

⁶⁰SUPA - School of Physics and Astronomy, University of Glasgow, Glasgow; United Kingdom.

⁶¹LPSC, Université Grenoble Alpes, CNRS/IN2P3, Grenoble INP, Grenoble; France.

⁶²Laboratory for Particle Physics and Cosmology, Harvard University, Cambridge MA; United States of America.

⁶³(^a) Department of Modern Physics and State Key Laboratory of Particle Detection and Electronics, University of Science and Technology of China, Hefei; (^b) Institute of Frontier and Interdisciplinary Science and Key Laboratory of Particle Physics and Particle Irradiation (MOE), Shandong University, Qingdao; (^c) School of Physics and Astronomy, Shanghai Jiao Tong University, Key Laboratory for Particle Astrophysics and Cosmology (MOE), SKLPPC, Shanghai; (^d) Tsung-Dao Lee Institute, Shanghai; (^e) School of Physics and Microelectronics, Zhengzhou University; China.

⁶⁴(^a) Kirchhoff-Institut für Physik, Ruprecht-Karls-Universität Heidelberg, Heidelberg; (^b) Physikalisches Institut, Ruprecht-Karls-Universität Heidelberg, Heidelberg; Germany.

⁶⁵(^a) Department of Physics, Chinese University of Hong Kong, Shatin, N.T., Hong Kong; (^b) Department of Physics, University of Hong Kong, Hong Kong; (^c) Department of Physics and Institute for Advanced Study, Hong Kong University of Science and Technology, Clear Water Bay, Kowloon, Hong Kong; China.

⁶⁶Department of Physics, National Tsing Hua University, Hsinchu; Taiwan.

⁶⁷IJCLab, Université Paris-Saclay, CNRS/IN2P3, 91405, Orsay; France.

⁶⁸Centro Nacional de Microelectrónica (IMB-CNM-CSIC), Barcelona; Spain.

⁶⁹Department of Physics, Indiana University, Bloomington IN; United States of America.

⁷⁰(^a) INFN Gruppo Collegato di Udine, Sezione di Trieste, Udine; (^b) ICTP, Trieste; (^c) Dipartimento Politecnico di Ingegneria e Architettura, Università di Udine, Udine; Italy.

⁷¹(^a) INFN Sezione di Lecce; (^b) Dipartimento di Matematica e Fisica, Università del Salento, Lecce; Italy.

⁷²(^a) INFN Sezione di Milano; (^b) Dipartimento di Fisica, Università di Milano, Milano; Italy.

⁷³(^a) INFN Sezione di Napoli; (^b) Dipartimento di Fisica, Università di Napoli, Napoli; Italy.

⁷⁴(^a) INFN Sezione di Pavia; (^b) Dipartimento di Fisica, Università di Pavia, Pavia; Italy.

⁷⁵(^a) INFN Sezione di Pisa; (^b) Dipartimento di Fisica E. Fermi, Università di Pisa, Pisa; Italy.

⁷⁶(^a) INFN Sezione di Roma; (^b) Dipartimento di Fisica, Sapienza Università di Roma, Roma; Italy.

⁷⁷(^a) INFN Sezione di Roma Tor Vergata; (^b) Dipartimento di Fisica, Università di Roma Tor Vergata, Roma; Italy.

⁷⁸(^a) INFN Sezione di Roma Tre; (^b) Dipartimento di Matematica e Fisica, Università Roma Tre, Roma; Italy.

- ^{79(a)}INFN-TIFPA;^(b)Università degli Studi di Trento, Trento; Italy.
- ⁸⁰Universität Innsbruck, Department of Astro and Particle Physics, Innsbruck; Austria.
- ⁸¹University of Iowa, Iowa City IA; United States of America.
- ⁸²Department of Physics and Astronomy, Iowa State University, Ames IA; United States of America.
- ⁸³Istinye University, Sariyer, Istanbul; Türkiye.
- ^{84(a)}Departamento de Engenharia Elétrica, Universidade Federal de Juiz de Fora (UFJF), Juiz de Fora;^(b)Universidade Federal do Rio De Janeiro COPPE/EE/IF, Rio de Janeiro;^(c)Instituto de Física, Universidade de São Paulo, São Paulo;^(d)Rio de Janeiro State University, Rio de Janeiro;^(e)Federal University of Bahia, Bahia; Brazil.
- ⁸⁵KEK, High Energy Accelerator Research Organization, Tsukuba; Japan.
- ⁸⁶Graduate School of Science, Kobe University, Kobe; Japan.
- ^{87(a)}AGH University of Krakow, Faculty of Physics and Applied Computer Science, Krakow;^(b)Marian Smoluchowski Institute of Physics, Jagiellonian University, Krakow; Poland.
- ⁸⁸Institute of Nuclear Physics Polish Academy of Sciences, Krakow; Poland.
- ⁸⁹Faculty of Science, Kyoto University, Kyoto; Japan.
- ⁹⁰Research Center for Advanced Particle Physics and Department of Physics, Kyushu University, Fukuoka ; Japan.
- ⁹¹L2IT, Université de Toulouse, CNRS/IN2P3, UPS, Toulouse; France.
- ⁹²Instituto de Física La Plata, Universidad Nacional de La Plata and CONICET, La Plata; Argentina.
- ⁹³Physics Department, Lancaster University, Lancaster; United Kingdom.
- ⁹⁴Oliver Lodge Laboratory, University of Liverpool, Liverpool; United Kingdom.
- ⁹⁵Department of Experimental Particle Physics, Jožef Stefan Institute and Department of Physics, University of Ljubljana, Ljubljana; Slovenia.
- ⁹⁶School of Physics and Astronomy, Queen Mary University of London, London; United Kingdom.
- ⁹⁷Department of Physics, Royal Holloway University of London, Egham; United Kingdom.
- ⁹⁸Department of Physics and Astronomy, University College London, London; United Kingdom.
- ⁹⁹Louisiana Tech University, Ruston LA; United States of America.
- ¹⁰⁰Fysiska institutionen, Lunds universitet, Lund; Sweden.
- ¹⁰¹Departamento de Física Teórica C-15 and CIAFF, Universidad Autónoma de Madrid, Madrid; Spain.
- ¹⁰²Institut für Physik, Universität Mainz, Mainz; Germany.
- ¹⁰³School of Physics and Astronomy, University of Manchester, Manchester; United Kingdom.
- ¹⁰⁴CPPM, Aix-Marseille Université, CNRS/IN2P3, Marseille; France.
- ¹⁰⁵Department of Physics, University of Massachusetts, Amherst MA; United States of America.
- ¹⁰⁶Department of Physics, McGill University, Montreal QC; Canada.
- ¹⁰⁷School of Physics, University of Melbourne, Victoria; Australia.
- ¹⁰⁸Department of Physics, University of Michigan, Ann Arbor MI; United States of America.
- ¹⁰⁹Department of Physics and Astronomy, Michigan State University, East Lansing MI; United States of America.
- ¹¹⁰Group of Particle Physics, University of Montreal, Montreal QC; Canada.
- ¹¹¹Fakultät für Physik, Ludwig-Maximilians-Universität München, München; Germany.
- ¹¹²Max-Planck-Institut für Physik (Werner-Heisenberg-Institut), München; Germany.
- ¹¹³Graduate School of Science and Kobayashi-Maskawa Institute, Nagoya University, Nagoya; Japan.
- ^{114(a)}Department of Physics, Nanjing University, Nanjing;^(b)School of Science, Shenzhen Campus of Sun Yat-sen University;^(c)University of Chinese Academy of Science (UCAS), Beijing; China.
- ¹¹⁵Department of Physics and Astronomy, University of New Mexico, Albuquerque NM; United States of America.
- ¹¹⁶Institute for Mathematics, Astrophysics and Particle Physics, Radboud University/Nikhef, Nijmegen;

Netherlands.

¹¹⁷Nikhef National Institute for Subatomic Physics and University of Amsterdam, Amsterdam; Netherlands.

¹¹⁸Department of Physics, Northern Illinois University, DeKalb IL; United States of America.

¹¹⁹(^a)New York University Abu Dhabi, Abu Dhabi;(^b)United Arab Emirates University, Al Ain; United Arab Emirates.

¹²⁰Department of Physics, New York University, New York NY; United States of America.

¹²¹Ochanomizu University, Otsuka, Bunkyo-ku, Tokyo; Japan.

¹²²Ohio State University, Columbus OH; United States of America.

¹²³Homer L. Dodge Department of Physics and Astronomy, University of Oklahoma, Norman OK; United States of America.

¹²⁴Department of Physics, Oklahoma State University, Stillwater OK; United States of America.

¹²⁵Palacký University, Joint Laboratory of Optics, Olomouc; Czech Republic.

¹²⁶Institute for Fundamental Science, University of Oregon, Eugene, OR; United States of America.

¹²⁷Graduate School of Science, Osaka University, Osaka; Japan.

¹²⁸Department of Physics, University of Oslo, Oslo; Norway.

¹²⁹Department of Physics, Oxford University, Oxford; United Kingdom.

¹³⁰LPNHE, Sorbonne Université, Université Paris Cité, CNRS/IN2P3, Paris; France.

¹³¹Department of Physics, University of Pennsylvania, Philadelphia PA; United States of America.

¹³²Department of Physics and Astronomy, University of Pittsburgh, Pittsburgh PA; United States of America.

¹³³(^a)Laboratório de Instrumentação e Física Experimental de Partículas - LIP, Lisboa;(^b)Departamento de Física, Faculdade de Ciências, Universidade de Lisboa, Lisboa;(^c)Departamento de Física, Universidade de Coimbra, Coimbra;(^d)Centro de Física Nuclear da Universidade de Lisboa, Lisboa;(^e)Departamento de Física, Universidade do Minho, Braga;(^f)Departamento de Física Teórica y del Cosmos, Universidad de Granada, Granada (Spain);(^g)Departamento de Física, Instituto Superior Técnico, Universidade de Lisboa, Lisboa; Portugal.

¹³⁴Institute of Physics of the Czech Academy of Sciences, Prague; Czech Republic.

¹³⁵Czech Technical University in Prague, Prague; Czech Republic.

¹³⁶Charles University, Faculty of Mathematics and Physics, Prague; Czech Republic.

¹³⁷Particle Physics Department, Rutherford Appleton Laboratory, Didcot; United Kingdom.

¹³⁸IRFU, CEA, Université Paris-Saclay, Gif-sur-Yvette; France.

¹³⁹Santa Cruz Institute for Particle Physics, University of California Santa Cruz, Santa Cruz CA; United States of America.

¹⁴⁰(^a)Departamento de Física, Pontificia Universidad Católica de Chile, Santiago;(^b)Millennium Institute for Subatomic physics at high energy frontier (SAPHIR), Santiago;(^c)Instituto de Investigación Multidisciplinario en Ciencia y Tecnología, y Departamento de Física, Universidad de La Serena;(^d)Universidad Andres Bello, Department of Physics, Santiago;(^e)Instituto de Alta Investigación, Universidad de Tarapacá, Arica;(^f)Departamento de Física, Universidad Técnica Federico Santa María, Valparaíso; Chile.

¹⁴¹Department of Physics, University of Washington, Seattle WA; United States of America.

¹⁴²Department of Physics and Astronomy, University of Sheffield, Sheffield; United Kingdom.

¹⁴³Department of Physics, Shinshu University, Nagano; Japan.

¹⁴⁴Department Physik, Universität Siegen, Siegen; Germany.

¹⁴⁵Department of Physics, Simon Fraser University, Burnaby BC; Canada.

¹⁴⁶SLAC National Accelerator Laboratory, Stanford CA; United States of America.

¹⁴⁷Department of Physics, Royal Institute of Technology, Stockholm; Sweden.

- ¹⁴⁸Departments of Physics and Astronomy, Stony Brook University, Stony Brook NY; United States of America.
- ¹⁴⁹Department of Physics and Astronomy, University of Sussex, Brighton; United Kingdom.
- ¹⁵⁰School of Physics, University of Sydney, Sydney; Australia.
- ¹⁵¹Institute of Physics, Academia Sinica, Taipei; Taiwan.
- ¹⁵²^(a)E. Andronikashvili Institute of Physics, Iv. Javakhishvili Tbilisi State University, Tbilisi;^(b)High Energy Physics Institute, Tbilisi State University, Tbilisi;^(c)University of Georgia, Tbilisi; Georgia.
- ¹⁵³Department of Physics, Technion, Israel Institute of Technology, Haifa; Israel.
- ¹⁵⁴Raymond and Beverly Sackler School of Physics and Astronomy, Tel Aviv University, Tel Aviv; Israel.
- ¹⁵⁵Department of Physics, Aristotle University of Thessaloniki, Thessaloniki; Greece.
- ¹⁵⁶International Center for Elementary Particle Physics and Department of Physics, University of Tokyo, Tokyo; Japan.
- ¹⁵⁷Department of Physics, Tokyo Institute of Technology, Tokyo; Japan.
- ¹⁵⁸Department of Physics, University of Toronto, Toronto ON; Canada.
- ¹⁵⁹^(a)TRIUMF, Vancouver BC;^(b)Department of Physics and Astronomy, York University, Toronto ON; Canada.
- ¹⁶⁰Division of Physics and Tomonaga Center for the History of the Universe, Faculty of Pure and Applied Sciences, University of Tsukuba, Tsukuba; Japan.
- ¹⁶¹Department of Physics and Astronomy, Tufts University, Medford MA; United States of America.
- ¹⁶²Department of Physics and Astronomy, University of California Irvine, Irvine CA; United States of America.
- ¹⁶³University of Sharjah, Sharjah; United Arab Emirates.
- ¹⁶⁴Department of Physics and Astronomy, University of Uppsala, Uppsala; Sweden.
- ¹⁶⁵Department of Physics, University of Illinois, Urbana IL; United States of America.
- ¹⁶⁶Instituto de Física Corpuscular (IFIC), Centro Mixto Universidad de Valencia - CSIC, Valencia; Spain.
- ¹⁶⁷Department of Physics, University of British Columbia, Vancouver BC; Canada.
- ¹⁶⁸Department of Physics and Astronomy, University of Victoria, Victoria BC; Canada.
- ¹⁶⁹Fakultät für Physik und Astronomie, Julius-Maximilians-Universität Würzburg, Würzburg; Germany.
- ¹⁷⁰Department of Physics, University of Warwick, Coventry; United Kingdom.
- ¹⁷¹Waseda University, Tokyo; Japan.
- ¹⁷²Department of Particle Physics and Astrophysics, Weizmann Institute of Science, Rehovot; Israel.
- ¹⁷³Department of Physics, University of Wisconsin, Madison WI; United States of America.
- ¹⁷⁴Fakultät für Mathematik und Naturwissenschaften, Fachgruppe Physik, Bergische Universität Wuppertal, Wuppertal; Germany.
- ¹⁷⁵Department of Physics, Yale University, New Haven CT; United States of America.
- ^a Also Affiliated with an institute covered by a cooperation agreement with CERN.
- ^b Also at An-Najah National University, Nablus; Palestine.
- ^c Also at Borough of Manhattan Community College, City University of New York, New York NY; United States of America.
- ^d Also at Center for Interdisciplinary Research and Innovation (CIRI-AUTH), Thessaloniki; Greece.
- ^e Also at CERN, Geneva; Switzerland.
- ^f Also at CMD-AC UNEC Research Center, Azerbaijan State University of Economics (UNEC); Azerbaijan.
- ^g Also at Département de Physique Nucléaire et Corpusculaire, Université de Genève, Genève; Switzerland.
- ^h Also at Departament de Física de la Universitat Autònoma de Barcelona, Barcelona; Spain.
- ⁱ Also at Department of Financial and Management Engineering, University of the Aegean, Chios; Greece.

- j* Also at Department of Physics, California State University, Sacramento; United States of America.
- k* Also at Department of Physics, King's College London, London; United Kingdom.
- l* Also at Department of Physics, Stanford University, Stanford CA; United States of America.
- m* Also at Department of Physics, Stellenbosch University; South Africa.
- n* Also at Department of Physics, University of Fribourg, Fribourg; Switzerland.
- o* Also at Department of Physics, University of Thessaly; Greece.
- p* Also at Department of Physics, Westmont College, Santa Barbara; United States of America.
- q* Also at Hellenic Open University, Patras; Greece.
- r* Also at Imam Mohammad Ibn Saud Islamic University; Saudi Arabia.
- s* Also at Institutio Catalana de Recerca i Estudis Avancats, ICREA, Barcelona; Spain.
- t* Also at Institut für Experimentalphysik, Universität Hamburg, Hamburg; Germany.
- u* Also at Institute for Nuclear Research and Nuclear Energy (INRNE) of the Bulgarian Academy of Sciences, Sofia; Bulgaria.
- v* Also at Institute of Applied Physics, Mohammed VI Polytechnic University, Ben Guerir; Morocco.
- w* Also at Institute of Particle Physics (IPP); Canada.
- x* Also at Institute of Physics, Azerbaijan Academy of Sciences, Baku; Azerbaijan.
- y* Also at Institute of Theoretical Physics, Ilia State University, Tbilisi; Georgia.
- z* Also at National Institute of Physics, University of the Philippines Diliman (Philippines); Philippines.
- aa* Also at Technical University of Munich, Munich; Germany.
- ab* Also at The Collaborative Innovation Center of Quantum Matter (CICQM), Beijing; China.
- ac* Also at TRIUMF, Vancouver BC; Canada.
- ad* Also at Università di Napoli Parthenope, Napoli; Italy.
- ae* Also at University of Colorado Boulder, Department of Physics, Colorado; United States of America.
- af* Also at Washington College, Chestertown, MD; United States of America.
- ag* Also at Yeditepe University, Physics Department, Istanbul; Türkiye.
- * Deceased